UNIVERSITEIT VAN PRETORIA
UNIVERSITY OF PRETORIA
YUNIBESITHI YA PRETORIA

Model predictive suspension control on off-road vehicles

by

Andries Jacobus Peenze

Submitted in partial fulfilment of the requirements for the degree

Master of Engineering (Mechanical Engineering)

in the

Faculty of Engineering, Built Environment and Information Technology (EBIT)

University of Pretoria

Summary

Title: Model predictive suspension control on off-road vehicles

Author: Andries Jacobus Peenze

Supervisor: Prof P.S. Els

Department: Mechanical and Aeronautical Engineering, University of Pretoria

Degree: Master of Engineering (Mechanical Engineering)

Reducing the rollover propensity of off-road vehicles while maintaining good ride comfort and off-road capabilities is a well-known challenge. With controllable suspension systems, the dynamics of the vehicle can be altered to give better performance than passive suspension systems. The semi-active hydro-pneumatic suspension system under consideration can switch between soft spring and a stiff spring, as well as between low and high damping.

In this study, a model predictive controller, based on a linear quadratic regulator and receding horizon theories, was developed to control individual struts of the suspension system.

A combined handing and ride comfort metric was developed to determine the input weights of the model predictive controller based on the driving conditions. The metric discerns between a handling or emergency manoeuvre and normal driving on rough roads. It changes the input weight accordingly to bias the controller towards a handling setting or a ride comfort setting.

A 16 degree of freedom simulation model was validated for both the lateral and vertical dynamics and found to be a close representation of the real Land Rover Defender 110 used for the experiments. The controller was implemented into the simulation model to test and ensure the controller worked as intended. The simulation model was validated at speeds varying from 50 km/h to 80 km/h for severe double lane change handling manoeuvres. The ride validation was performed over a rough Belgian paving track at speeds of 21 km/h and 47 km/h.

The controller was also experimentally validated for the double lane change, Belgian paving and various other handling and ride comfort tests.

In the handling test, the controller performed well keeping the suspension in handling mode and reducing the roll angle as compared to the ride comfort mode. Over the rough tracks, the performance of the controller was not good and the suspension controller did occasionally switch to the handling mode. Although the controller did switch over to the handling mode the vehicle's ride comfort wasn't detrimentally influenced.

Overall key aspects of the controller were identified for improvement to overcome the problem experienced in ride comfort settings and also improve the handling of the vehicle.

Acknowledgements

I would like to thank:

- My supervisor, Prof. Els, for the opportunity and guidance he has given me through the project.
- Dr Hamersma for his help with the vehicle setup and testing.
- My fellow students at the VDG for their friendship, assistance and support.

Table of contents

List of figures

List of tables

List of Symbols and Abbreviations

Roman symbols

Symbol	Description	Units
a	Acceleration or Tyre load sensitivity coefficient	[m/s^2] or [1/rad]
A or $\boldsymbol{A}$	Stiffness matrix	-
b	Distance from the front axle to CG or Tyre load sensitivity coefficient	[m] or [1/Nrad]
B or $\boldsymbol{B}$	Input matrix	-
c	Distance from the rear axle to CG or Coefficient of damping	[m] or [Ns/rad]
$\boldsymbol{C}$	Optimisation function matrix	-
C_α	Cornering stiffness	[N/rad]
E or $\boldsymbol{E}$	Disturbance matrix	-
F	Force	[N]
$\boldsymbol{F}$	Optimisation function matrix	-
g	Gravitational acceleration	[m/s^2]
$\boldsymbol{g}$	Gravitational acceleration vector	[m/s^2]
h	Roll centre height	[m]
$\boldsymbol{H}$	Optimisation function matrix	-
h_{CG}	CG height	[m]
h_1	Distance between CG height and roll centre height	[m]
I	Moment of inertia or Identity matrix	[kgm^2] or -
$\boldsymbol{I}$	Inertia tensor	[kgm^2]
J_0 or J	Cost function	-
k	Spring stiffness	[N/rad]
K	Understeer gradient	[rad]
L	Vehicle wheelbase	[m]
m	Mass	[kg]
M	Moments	[Nm]
$\boldsymbol{M}$	Moments vector	[Nm]
N	Window length	-
n	Index	-
$\boldsymbol{p}$	Zero Moment Point vector	[m]
P	Pressure	[Pa]
P or $\boldsymbol{P}$	Terminal weight matrix	
Q or $\boldsymbol{Q}$	Stage weight matrix	-
$\boldsymbol{r}$	Displacement vector from the origin to the centre of mass	[m]
$\ddot{\boldsymbol{r}}$	Acceleration vector of CG	[m/s^2]
R	Turning circle or Gas constant	[m] or [J/kgK]

R or $\boldsymbol{R}$	Input weight matrix	-
s	Distance between suspension struts	[m]
t	Track width	[m]
T	Temperature or Torque or Timestep	[K] or [Nm] or [s]
u	Input or Force at axle	- or [N]
U	Input vector	-
V	Velocity or Volume	[m/s] or [m^3]
W	Weight	[N]
x	States or x-direction	- or [m]
X	States vector	-
$\dot{x}$	Rate of change in states	-
y	y-direction	[m]
z	Displacement in z direction	[m]
$\dot{z}$	Velocity in z direction	[m/s]

Greek symbols

Symbol	Description	Units
α	Side slip angle	[rad]
$\boldsymbol{\alpha}$	Angular acceleration vector	[rad/s^2]
γ	Adiabatic index	-
$\dot{\gamma}$	Yaw rate	[rad/s]
δ	Steering angle or Controller disturbance	[rad] or -
Δ	Difference	-
ζ	Damping ratio	-
$\dot{\theta}$	Pitch rate	[rad/s]
$\ddot{\theta}$	Pitch acceleration	[rad/s^2]
σ	Standard deviation	-
Σ	Sum of	N/A
v	Specific volume	[m^3/kg]
ϕ	Roll angle	[rad]
$\dot{\phi}$	Roll rate	[rad/s]
$\ddot{\phi}$	Roll acceleration	[rad/s^2]
$\boldsymbol{\omega}$	Angular velocity vector	[rad/s]

Subscripts

Subscript	Description
0	Initial state
add	Additional
CG	About CG
$collinear$	Collinear component
d	Discretised
$d1$ to $d4$	Damper piecewise sections
f	Front
fl	Front left
fr	Front right
g	Gas
i	Inside
k	Index
o	Outside
p	Location for zero moment point
ϕ	Angular component
r	Rear
rl	Rear left
rr	Rear right
s	Sprung mass
x	In the x-direction
y	In the y-direction
z	In the z-direction
xx	Around the x-direction
yy	Around the y-direction
zmp	ZMP location
zz	Around the z-direction

Abbreviations

Abbreviation	Meaning
$4S_4$	Four state semi-active suspension system
AFS	Active Front Steering
a-MPC	Aggressive model predictive control
BS	British Standards
CG	Centre of Gravity
DLC	Double Lane Change
DS	Damper setting
DSF	Damping scaling factor
ESC/ESP	Electronic Stability Control/Program
FBD	Free body diagram
GPS	Global positioning system
GV	Gas volume
IMU	Inertial measurement unit
ISO	International Organisation of Standardisation
KD	Kinetic diagram
LDV	Light duty vehicle
LF	Left front
LR	Left rear
MABX	MicroAutoBox
MPC	Model predictive controller
N/A	Not applicable
NHTSA	National Highway Traffic Safety Administration
RC	Roll centre
RF	Right front
RMS	Root mean square
RMSE	Root mean square error
RR	Right rear
RRMS	Running Root Mean Square
SLC	Single lane change
SS	Spring setting
SUV	Sports Utility Vehicle
VW	Volkswagen
ZMP	Zero Moment Point

1. Background

In a study conducted for the 2015 period by the U.S. Department of Transportation's National Highway Traffic Safety Administration (NHTSA, 2017) it was found that an estimated 11,070,000 vehicles were involved in police-reported traffic crashes in the U.S. with 44,886 of these vehicles involved in crashes leading to fatalities of 22,441 passengers. In these reported fatal accidents 78 per cent of the vehicles were passenger vehicles. From these accidents, rollover crashes were found to be the most fatal, which included 32 per cent of the fatalities in 2015. The Sports Utility Vehicle (SUV) was the most prone to fatalities in the event of a rollover, with 49 per cent of the rollover accidents that occurred resulting in the death of occupants in the vehicle. The study also found that SUV's account for 36 per cent of rollover accidents on rural roads which can be attributed to the uneven and rough nature of these roads.

The SUV is especially prone to rollover due to the relatively high location of the centre of gravity above the ground and the soft and compliant suspension characteristics which best suit ride comfort but lacks handling performance (Consumer Reports, 2014). The SUV's wide and higher field of view also encourages confidence in the driver which may lead to a false sense of control and confidence in the operation of the vehicle.

Since most rollovers happen in emergency or handling manoeuvres an improvement of the SUV's handling performance can help reduce fatalities and aid in the safety of the vehicle. Most vehicles are either designed and optimised through the use of passive systems for either good ride comfort or good handling, but seldom for both, thus there exists a compromise that has to be made by choosing ride comfort or handling. SUVs suspension characteristics, in general, are biased more towards ride comfort.

Various safety systems have been implemented on SUVs in recent years due to an emphasis on safety that has been imposed by the government on vehicle manufacturers. The NHTSA study of the 2015 period also weighed on the improvements of the safety in recent years for SUV's whereby the fatal rollover accidents decreased by 29 per cent from 2006 (2899 fatalities) to 2015 (2065 fatalities). An article published in Forbes (McCarthy, 2015) also showed that safety features in a vehicle ranked as the third highest-selling point for American potential buyers, with 75 per cent of the poll takers indicating that it is an important aspect.

The typical safety systems used in SUVs can include electronic stability control, torque vectoring, lane departure warning systems and many more (Consumer Reports, 2017). These systems are typically optimised for paved road or tar road use and might perform negatively on uneven or rough terrains typically found in rural areas.

This leads to the conclusion that there exists a need for improved handling performance of SUVs where the off-road capabilities and ride comfort of the vehicle is retained and improved handling added in the case of an emergency manoeuvre.

2. Literature Study

The literature study will include the underlying vehicle dynamics including the tyre road interface, yaw-plane analysis, roll-plane analysis and lateral load transfer. Ride comfort evaluation methods, as well as handling and rollover metrics, are discussed including handling measurements, rollover metrics, the zero-moment point and parameters that influence vehicle roll angle. Possible systems that can be used to improve the handling of a vehicle is discussed, with a controllable semi-active suspension system in the form of the $4S_4$ discussed in greater detail. Different suspension control methods are discussed including the model predictive controller. A validated full non-linear vehicle simulation model is discussed as well as different vehicle tests to investigate the ride comfort and handling performance of the vehicle.

2.1. Vehicle dynamics

By investigating the vehicle's underlying dynamics we can identify the major states and parameters that have an effect on the handling of the vehicle which might be leveraged to improve the handling of the vehicle through emergency manoeuvres.

2.1.1. Tyre road interface

Besides aerodynamic forces, all the external forces acting on the vehicle passes through the tyres. Each tyre's contact area on the road surface is approximately the size of the palm of a human hand, thus understanding the tyre road interface for force generation is important. Besides supporting the vertical load of the vehicle, acting as a cushion between the irregularities of the road or developing longitudinal forces for acceleration and braking purposes the tyres also generate lateral forces needed for cornering purposes.

The lateral forces arise from the friction generated by the tyre on the road's surface and the vertical load on the wheel. For a specific road surface, the lateral force is highly dependent on the vertical load and slip angle of the tyre. The slip angle of the tyre is defined as the angle between the wheel heading and the travel direction of the wheel. The slip angle, vertical load and resulting lateral force of the tyre is often represented by the non-linear magic-formula tyre model presented by Bakker (1989). Figure 1 represents a typical lateral force vs. slip angle curves that are produced from this magic-formula tyre model for different vertical loads.

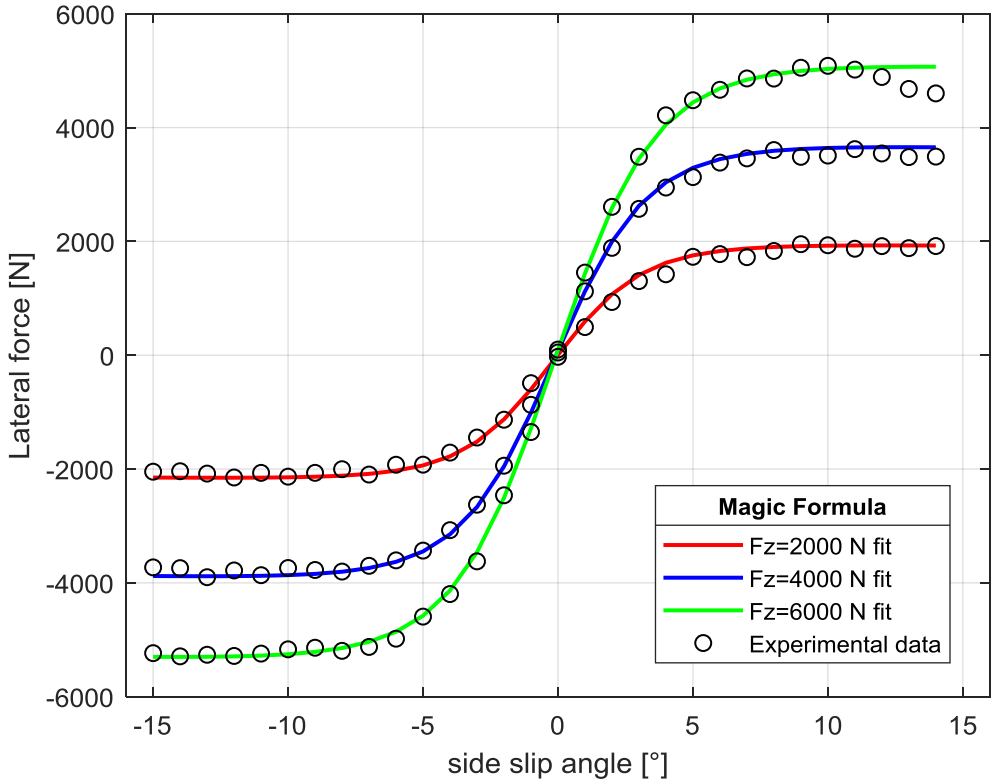

Figure 1: Magic tyre formula lateral force curves for various vertical loads

The tyre cornering stiffness is defined as the gradient of the lateral force slip angle curve at 0° slip angle.

2.1.2. Yaw-plane analysis of handling

A yaw-plane "bicycle" model indicated in figure 2, where the front axle is condensed into one front wheel and the rear axle into one rear wheel, is often used to understand the main underlying handling behaviour of the vehicle neglecting roll and load transfer effects.

For small angles of slip (typically between -3° and 3°), the lateral tyre force can be approximated by the linear function given in equation 1.

$$F_y = C_\alpha \alpha \qquad [1]$$

Here C_α is the combined cornering stiffness of the given axle (i.e. double the cornering stiffness of a single tyre at the load on a single wheel) and an assumption is made that the slip angle is the same for both the wheels on the given axle.

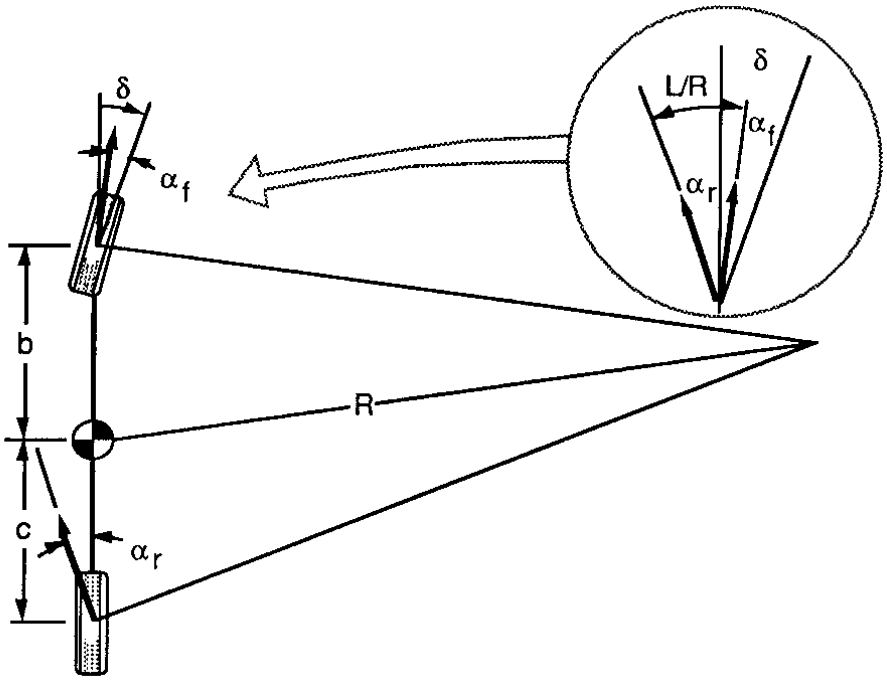

Figure 2: Bicycle model (Gillespie, 1992)

The steering input from the derivation of the yaw-plane model in Appendix A is found to be:

$$\delta = \frac{L}{R} + \left(\frac{W_f}{C_{\alpha f}} - \frac{W_r}{C_{\alpha r}}\right)\frac{V^2}{gR} \qquad [2]$$

Here $(W_f/C_{\alpha f} - W_r/C_{\alpha r})$ is referred to as the understeer gradient arising from only the tyres of the vehicle.

A positive understeer gradient will produce understeer, which is a safe design for passenger vehicles because the front wheels will slip more in a corner than the rear wheels. To develop the necessary lateral forces required to maintain the path at the current speed, the driver needs to increase the steering input angle. Steering more at higher speeds or sharp corners is intuitive for normal drivers.

If the understeer gradient is negative the vehicle will oversteer. The rear wheels slip more than the front wheels. With oversteer characteristics experienced drivers can enjoy drifting or power sliding if they wish to, but since the recovery of an oversteer vehicle is counter-intuitive (less steer angle will result in better turn in) the average driver finds these vehicles difficult to control.

Neutral steer occurs when the understeer gradient is equal to zero, thus the tyres will slip equally at the front and rear of the vehicle. The inputs of the driver will be followed by the vehicle.

This derivation of the bicycle model neglects lateral load transfer from the inner to the outer wheels. The effect of lateral load transfer on the understeer gradient will be discussed in section 2.1.4.

2.1.3. Roll-plane analysis of rollover

By considering the external forces and inertial forces acting on the body of the vehicle during roll the roll-plane equation of motion can be set up and used to analyse which states or parameters have an influence on the roll behaviour of the vehicle.

When a vehicle experiences a lateral acceleration the body of the vehicle tends to roll about its roll centre while the wheels of the vehicle are still in contact with the road. The roll effect is resisted by the suspension forces that act to restore the vehicle body to a horizontal orientation. Figure 3 represents the free body diagram (FBD) and kinetic diagram (KD) of the body of the vehicle during roll.

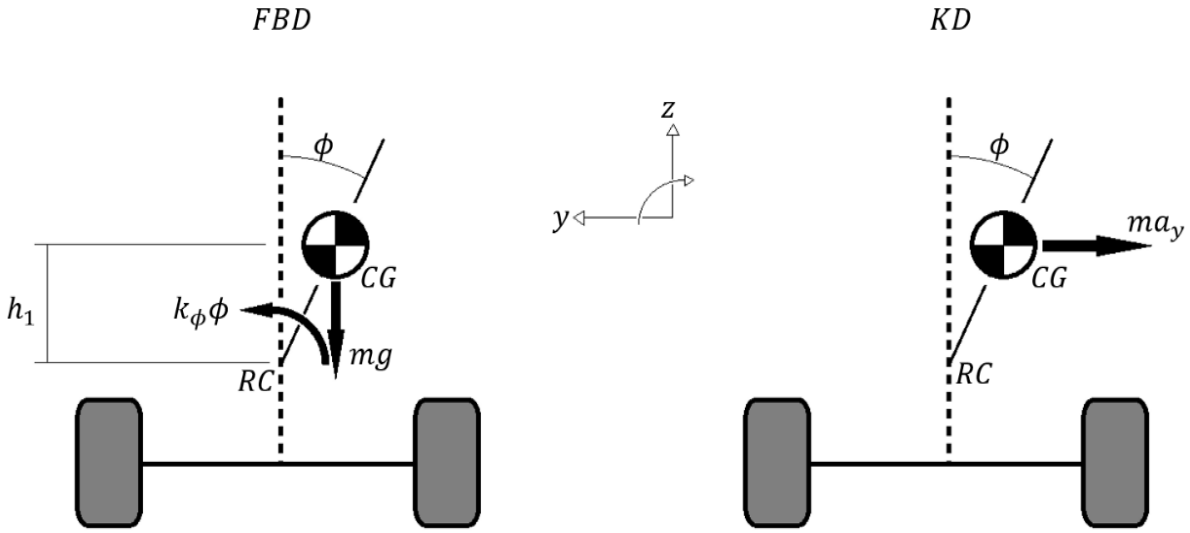

Figure 3: Quasi-static roll plane model (vehicle turning left, viewed from the rear)

The equation that relates the quasi-static roll angle of a suspended vehicle due to a lateral acceleration is (Gillespie, 1992):

$$\phi = \frac{mh_1a_y}{k_{\phi f} + k_{\phi r} - mgh_1} = \frac{mh_1a_y}{k_\phi - mgh_1} \quad [3]$$

Assumptions:

1. Small-angle assumption
    a. $sin\phi = \phi$
    b. $cos\phi = 1$
2. Steady-state behaviour
    a. Roll rate is constant and zero
3. Suspension forces transformed into the equivalent roll torque

Here we can see that for a given linear suspension stiffness and CG height if a lateral acceleration is applied to the vehicle through, for instance, negotiating a turn, the roll angle will increase. More severe manoeuvres will have higher lateral accelerations which will result in higher roll angles. This correlates with the finding of the linear dependence between the roll angle and lateral acceleration described in section 2.3.1.

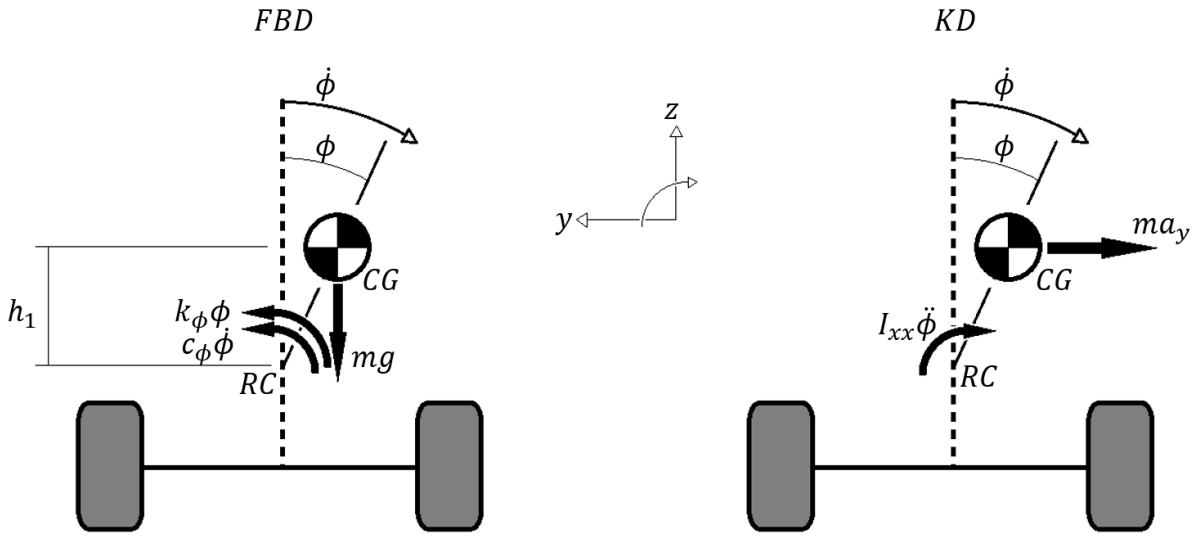

Figure 4: Transient roll-plane model (vehicle turning left, viewed from the rear)

Considering the transient roll-plane analysis in figure 4 where the roll rate and roll acceleration, as well as linear damping characteristics and a constant moment of inertia, is taken into account the state-space equations that describe the transient roll-plane is derived as:

$$I_{xx}\ddot{\phi} = -c_\phi\dot{\phi} - k_\phi\phi + mgh_1\phi + mh_1a_y \quad [4]$$

$$\dot{\phi} = \dot{\phi} \quad [5]$$

Assumptions:

1. Small-angle assumption
    a. $sin\phi = \phi$
    b. $cos\phi = 1$
2. Suspension forces transformed into the equivalent roll torque

Integrating these equations over time with the states being the roll angle and roll rate and with the acting disturbance being the lateral acceleration we can also observe the effects of the transient phenomena to understand the underlying characteristics of the roll-plane. The damping introduced acts as an extra reaction force which slows down the propagation of the roll angle.

2.1.4. Lateral load transfer

By considering a vehicle negotiating a left-hand turn in figure 5 and taking the sum of moments about the roll centre of the vehicle the relation of the suspension springs and dampers, lateral forces and vertical loads can be investigated.

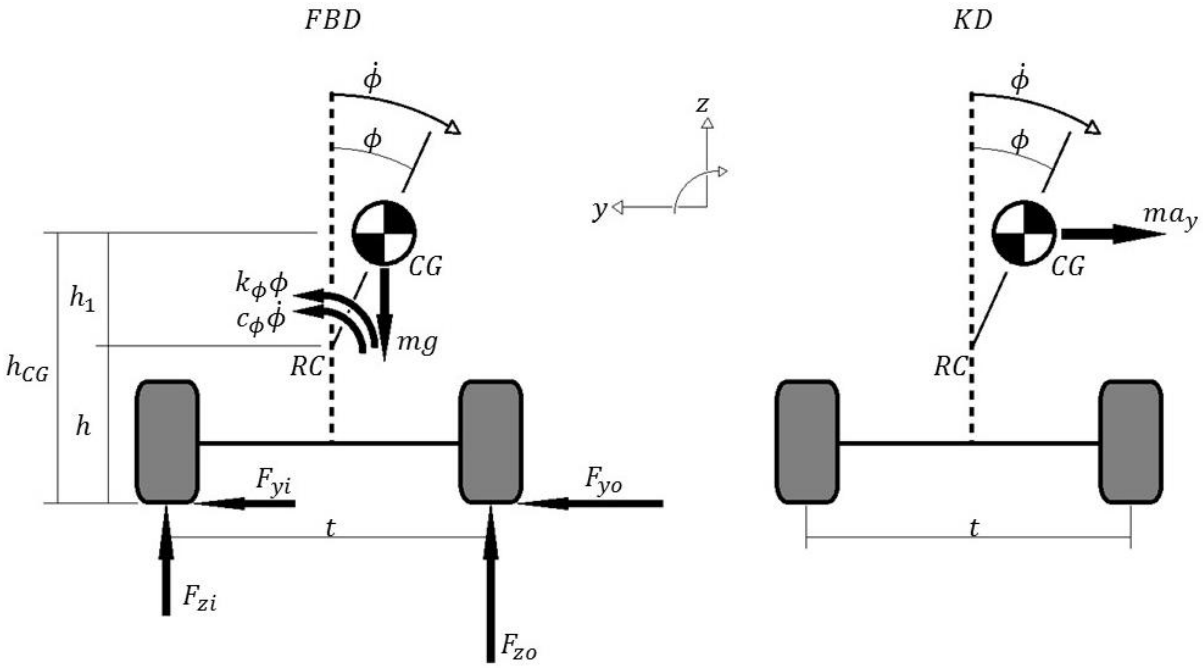

Figure 5: Simple suspended roll-model (vehicle turning left, viewed from the rear)

Newton's second law of forces taken for the model's free body diagram (FBD) and kinetic diagram (KD) in the y and z directions respectively is:

$$\Sigma F_z = ma_{CGz} \quad [6]$$
$$F_{zo} + F_{zi} - mg = 0 \quad [7]$$

$$\Sigma F_y = ma_{CGy} \quad [8]$$
$$F_{yi} + F_{yo} = -ma_y \quad [9]$$

For a given axle with zero roll acceleration the sum of moments about the roll centre is:

$$\Sigma M_{RC} = \cancel{I_{xx}\ddot{\phi}} + ma_{CG}h_1 \quad [10]$$
$$(F_{zi} - F_{zo})\frac{t}{2} + (F_{yi} + F_{yo})h - k_\phi\phi - c_\phi\dot{\phi} + mgh_1\phi = ma_y h_1 \quad [11]$$
$$2\Delta F_z = F_{zo} - F_{zi} = -\frac{2ma_y h_{CG}}{t} - \frac{2k_\phi\phi}{t} - \frac{2c_\phi\dot{\phi}}{t} + \frac{2mgh_1\phi}{t} \quad [12]$$

Assumptions:

1. Small angle assumption
   a. $sin\phi = \phi$
   b. $cos\phi = 1$
2. Zero roll acceleration
   a. $\ddot{\phi} = 0$
3. Suspension forces transformed into the equivalent roll torques

With ΔF_z the difference between the laterally loaded wheel and the static load on the wheel. If the lateral forces increase the load on the outside wheel will increase above the static load and the inner wheel's load will decrease.

Changes in the load will change the cornering stiffness and force characteristics of the tyre as explained in section 2.1.1. A single tyre's cornering stiffness sensitivity to vertical load is represented by a second-order polynomial approximation indicated in figure 6 (Gillespie, 1992).

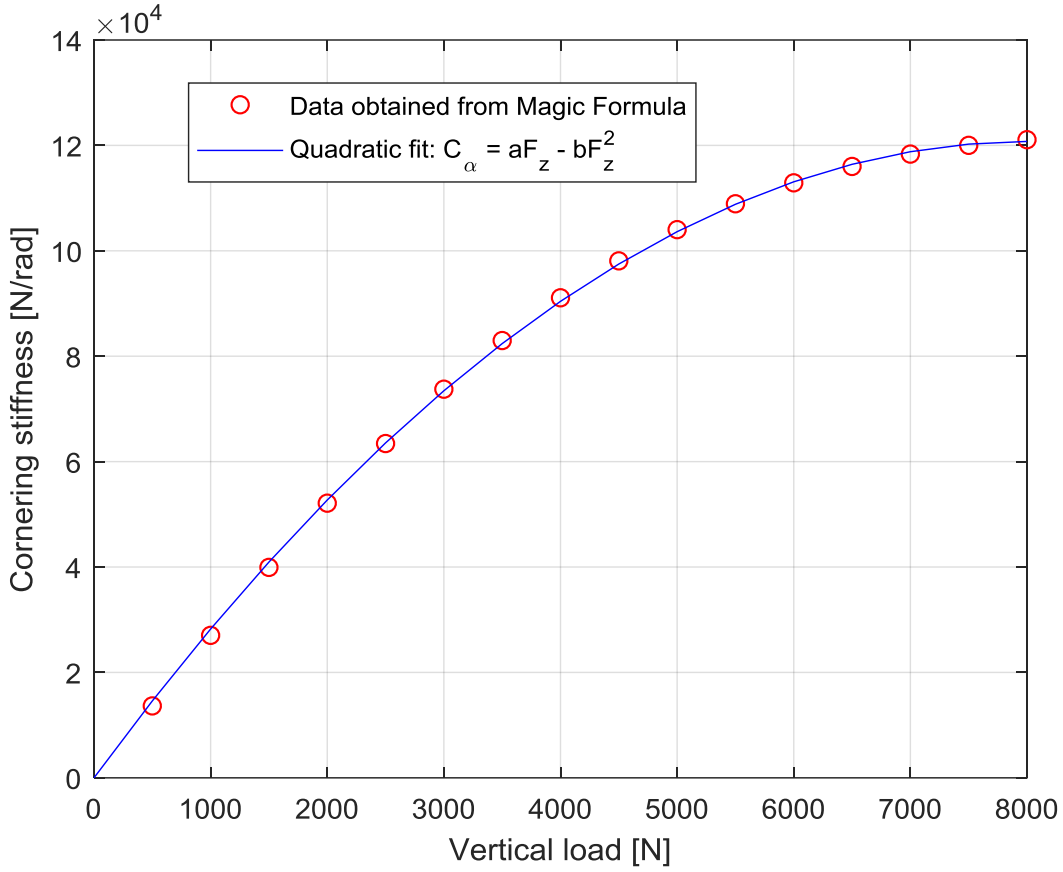

Figure 6: Quadratic fit of cornering stiffness to vertical load sensitivity

This polynomial approximation leads to the tyre lateral force to act in a non-linear fashion dependent on vertical load. The cornering stiffness and ultimately the lateral force developed by the tyre is given by (Gillespie, 1992):

$$F_y' = C_\alpha' \alpha = (aF_z - bF_z^2)\alpha \quad [13]$$

The lateral force for both the tyres on an axle given the load change is given by:

$$F_y = (C_\alpha - 2b\Delta F_z^2)\alpha \quad [14]$$

From equations 12 and 14 we can see that any lateral load transfer will reduce the lateral force that the wheel will produce in a corner.

The steering angle equation (equation 2) described in section 2.1.1 can be adjusted for the lateral load transfer effect. With the tyre cornering stiffness and vertical load sensitivity effect the following equation is found for the steering angle:

$$\delta = \frac{L}{R} + \left(\frac{W_f}{C_{\alpha f} - 2b\Delta F_{zf}^2} - \frac{W_r}{C_{\alpha r} - 2b\Delta F_{zr}^2} \right) \frac{V^2}{Rg} \quad [15]$$

This indicates that the understeer gradient is dependent on the tyre's cornering stiffness and the lateral load transfer experienced. The lateral load transfer, in turn, is affected by the lateral acceleration and the roll stiffness and damping of the suspension.

2.2. Ride comfort evaluation methods

Human response to vibration can be used to objectively evaluate ride comfort of vehicles as they traverse rough off-road terrains and highway roads. The ISO 2631 standard (International Organisation for Standardisation, 1997), British Standard BS 6841 (British Standards Institution, 1987) and Average Absorbed Power or AAP (Pradko & Lee, 1966) is used over the world to objectively evaluate ride comfort of vehicles.

The BS 6841 and ISO 2631 methods make use of frequency weighting functions. The data in the signal is transformed to the frequency domain through a Fast Fourier Transform. The methods weighs the signal magnitudes according to values at a range of frequencies, 0.5-80 Hz for BS 6841 (British Standards Institution, 1987) (see figure 7) and 0.1-80 Hz for ISO 2631 (International Organisation for Standardisation, 1997), which amplifies or attenuates the signal based on the sensitivity of humans at those frequencies. The weighted frequency data is then transformed back to time-domain data and the root mean square (RMS) value is taken of this time-domain data. The root mean square value of a signal is determined as follows:

$$RMS = \sqrt{\frac{1}{N} \sum_{n=1}^{N} a_n^2} \quad [16]$$

Els (2005) investigated the correlation between these objective evaluation methods and subjective inputs from passengers driving in a 14 ton 4x4 military vehicle over different terrains using different speeds and wheel pressures. The terrains were selected to be of typical Southern African terrains and roads which excited the vehicle's body roll, pitch, yaw, lateral, longitudinal and vertical motions. Els concluded that any of the methods can be used to objectively determine ride comfort for the vehicle and terrains used for the purpose of the study. The vertical acceleration gave the best subjective-objective correlation for all of the cases. It was also found that the root mean square value of the vertical acceleration used in the ISO 2631, BS 6841 and unweighted cases were sufficient to define the ride comfort levels of the vehicle.

For this study, the BS 6841 W_b weighting curve is used to weigh the vertical acceleration of the vehicle body where required. The curve is reproduced in figure 7.

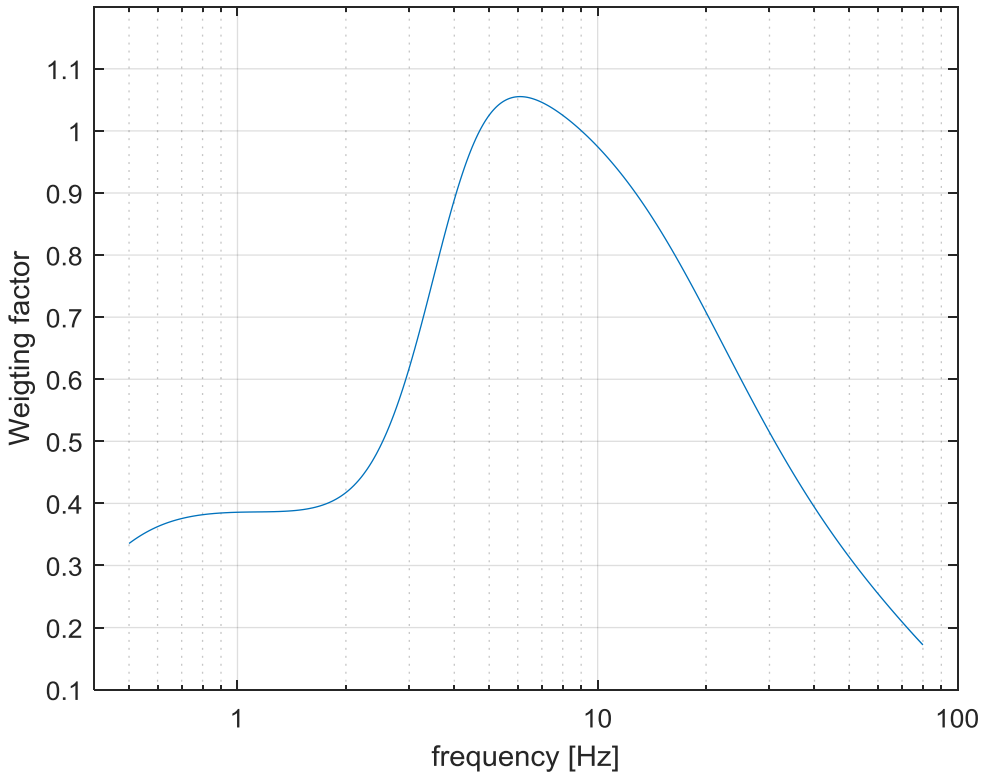

Figure 7: BS 6841 vertical acceleration weighting curve

2.3. Handling and rollover metrics

Objective evaluation of vehicle handling has been a topic of research for many years. A simple measure, which can be used to evaluate objectively the handling characteristics of a vehicle, does not yet exist.

2.3.1. Criteria for handling measurement

In a study performed by Uys et al. (2006) the author presented many methods which have been used in previous studies to find criteria which can be used to evaluate the handling of a vehicle. In the study yaw rate, lateral acceleration, roll angle and steer angle was found to be used the most often to classify the handling characteristics of the vehicle.

The ISO 3888 severe double lane change (International Organisation for Standardisation, 1999) is suggested as a good testing method to evaluate the handling of a vehicle. The test encourages optimised cornering capabilities and limit condition performance. The test also emphasises the handling characteristics of the vehicle in an emergency manoeuvre since the manoeuvre requires 4 major steering inputs in a closed-loop fashion to successfully complete the test. This test is, however, strongly dependant on driver skill and capabilities. Other tests such as the J-turn or Fishhook manoeuvre requires 1 and 2 major steering inputs respectively and are easier to perform repeatedly e.g. by using steering robots.

From the experimental work performed by Uys et al. (2006), a linear dependence is observed for the yaw rate vs. roll angle, yaw rate vs. lateral acceleration and roll angle vs.

lateral acceleration. The tests included different vehicles (Ford Courier LDV, a VW Golf 1 Chico, VW Golf 4 GTi and Land Rover Defender 110), drivers (and driver skills) and test tracks (Gerotek dynamic handling track and ride and handling track (Armscor, 2016)). The difference of the comparison gradients of the vehicles was attributed to the different suspension roll stiffness. The Land Rover's large roll angle was attributed to the relatively high centre of gravity and the soft suspension of the vehicle, something which is prevalent in typical sports utility vehicles. From the study, it is concluded that the roll angle can be used as a suitable metric for handling. If levels of handling acceptance can be determined for the vehicle the roll angle can be used additionally as a metric in a safety system to improve handling.

2.3.2. Rollover metrics

A multitude of different methods, that attempts to solve the detection of rollover and acts to prevent the rollover through improving the handling of the vehicle, exist. In general most of these systems act to change the yaw characteristics, steering input or suspension characteristics to improve handling.

Formally rollover is defined as the instance when the vertical forces of one of the wheels diminish and wheel lift-off has occurred or is about to occur due to the overturning moment of the vehicle's mass around the other side's wheel (Phanomchoeng & Rajamani, 2012).

In general, rollover can be classified as either tripped or un-tripped rollover. A tripped rollover occurs when a vehicle hits an object in the lateral direction while experiencing a lateral acceleration, and the moment induced by this event overturns the vehicle. A un-tripped rollover occurs when the vehicle also experiences a lateral acceleration, but where the outside wheels have enough grip to not slide out and the mass of the vehicle gets overturned around these wheels (Phanomchoeng & Rajamani, 2012).

Static or steady-state rollover metrics are used to determine the rollover event of a vehicle when all of the transients of the system have died out. The static stability factor is a simple measure where quasi-static rollover of a rigid vehicle is assumed and the moments around the outside wheel of the vehicle is solved (see figure 8a)). By assuming that the inside wheel's vertical and lateral force has diminished the sum of moments around the outside wheel is solved for, and the acceleration terms grouped to the one side of the equation. If the surface that the vehicle is traversing is flat and horizontal the equation reduces to an equation that only needs the centre of gravity (CG) height and the track width of the vehicle, which is both vehicle parameters, thus simplifying the method (Gillespie, 1992). This method assumes a rigid vehicle thus it will over-predict rollover.

If a suspended vehicle is used for the steady-state rollover investigation the method becomes less conservative, and more representative of the real rollover threshold (figure 8b)). The method changes since deflection of the suspension and tyres are allowed and the roll angle about the roll centre also effectively lowers the CG height, which improves the rollover threshold. The roll rate (defined in terms of radians per lateral g's) of the vehicle is often an important quantity that is needed in the investigation of this quasi-static rollover of a suspended vehicle (Gillespie, 1992).

All of these methods assume steady-state behaviour i.e. that the roll velocity of the vehicle and roll acceleration is zero. Another approach to finding a rollover metric is to work with a dynamic model. For this approach, the assumption that the roll velocity and acceleration are zero is not made (figure 8c)). Previous research found actual vehicle rollover does not happen in general in a steady-state manner, but rather in a transient manner and at lower lateral accelerations than which might be found for the steady-state metrics (Rakheja & Piche, 1990). In general, it is found that dynamic rollover thresholds can be used rather as a worst-case measure since the lateral acceleration might or might not cause rollover, thus it serves as a necessary condition, but not sufficient to cause rollover. These methods include the roll energy diagram, dynamic stability index and the step acceleration threshold (Bernard, et al., 1989) (Marine, et al., 1999) (Das, et al., 1993).

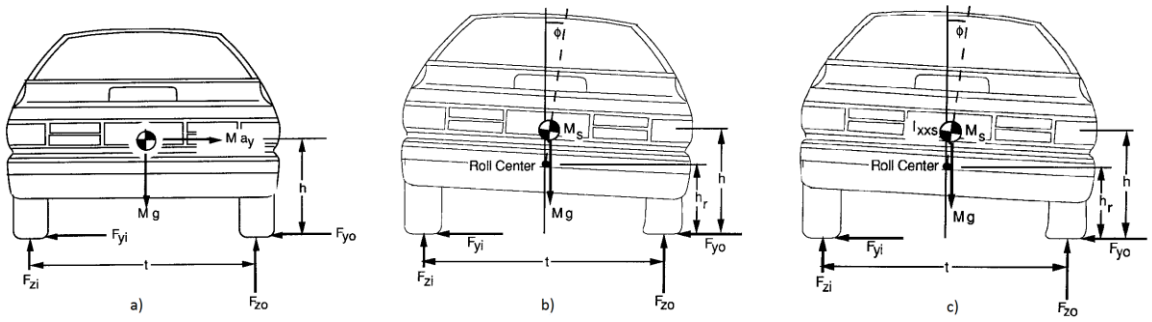

Figure 8: a) Steady-state rigid vehicle rollover b) Steady-state suspended vehicle rollover c) Transient suspended vehicle rollover (Gillespie, 1992)

Although it is quite simple to determine the rollover limits with these methods they are not suitable to predict impending rollover based on the vehicle's current situation. A method to overcome this is with the development of metrics based on the vehicle's current states. These states can be used as a real-time warning of possible dangerous driving situations and may be used by the vehicle's safety systems to act and avoid an imminent rollover situation. These methods make use of the vehicle's current roll velocity, roll angle, lateral acceleration and others to predict rollover (Wielenga & Chace, 2000) (Carlson & Gerdes, 2003) (Yoon, et al., 2007).

Previous work done by Lapapong (2010) showed that the zero-moment point (ZMP) can be used as a real-time metric for rollover due to the fact that the current states of the vehicle are monitored and used to update the ZMP.

In biped robotics, the ZMP is used extensively to determine the stability of walking robots to avoid falling over. The method usually compares the ZMP with a stability region wherein the biped is stable and won't fall over. For walking robots, the stability region is defined as the footprint area, where a ZMP inside this footprint is considered to be safe and stable. If the ZMP moves outside this footprint then external forces or torques can be applied to bring the ZMP back into the stable region, otherwise the robot will fall over (Kim, et al., 2002).

The zero moment point is a metric that can be used as a handling and rollover metric since the metric considers the lateral acceleration of the vehicle (which covers the handling aspect) and the height of the vehicle's centre of gravity (which lends to the rollover aspect since sports utility vehicles tend to have high CGs). The zero moment point is a point on the

ground under the vehicle where about all the inertial forces' moments is equal to zero in the roll and pitch directions. Figure 9 shows a graphical representation of the rigid vehicle used to define the ZMP.

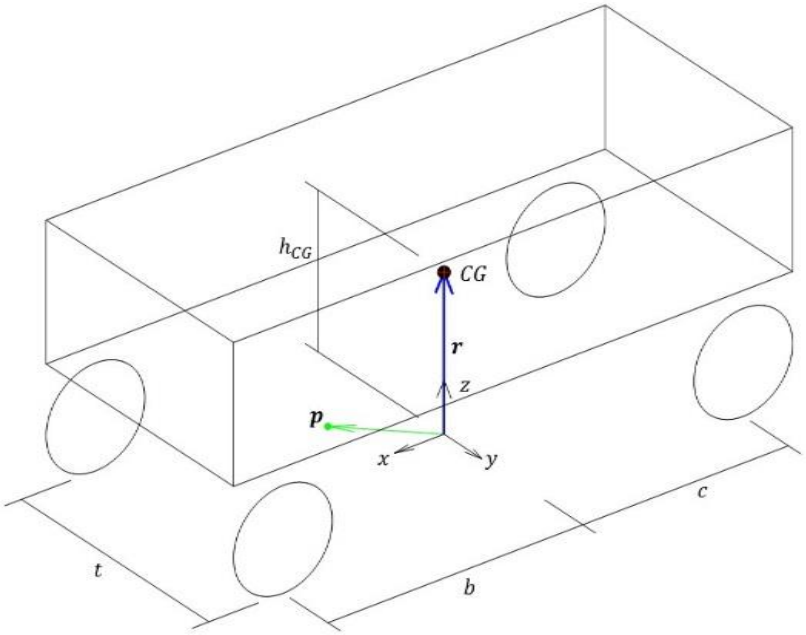

Figure 9: Graphical representation of the zero moment point

By assuming a rigid vehicle and inertial frame of reference on the ground directly below the centre of mass of the vehicle the moments about a point $\boldsymbol{p}$ can be determined by making use of d'Alembert's equation (by assuming no external forces or moments acting on the system).

$$\boldsymbol{M}_p = \sum_i (\boldsymbol{r} - \boldsymbol{p}) \times m(\ddot{\boldsymbol{r}} + \boldsymbol{g}) + \sum_i [\boldsymbol{I} \cdot \boldsymbol{\alpha} + \boldsymbol{\omega} \times \boldsymbol{I} \cdot \boldsymbol{\omega}] \quad [17]$$

By fixing the x and y location of the location vector ($\boldsymbol{r}$) to zero, and setting the roll and pitch moments equal to zero, and zeroing the z location of the point $\boldsymbol{p}$ the x and y location of the point $\boldsymbol{p}$ can be determined. Equations 18 and 19 shows the results of the x and y location of point $\boldsymbol{p}$ or the zero moment point.

$$x_{zmp} = \frac{m a_x h_{CG} + I_{yy}\ddot{\theta} - I_{zz}\dot{\phi}\dot{\gamma} + I_{xx}\dot{\phi}\dot{\gamma}}{m(g - a_z)} \quad [18]$$

$$y_{zmp} = \frac{m a_y h_{CG} - I_{xx}\ddot{\phi} + I_{yy}\dot{\theta}\dot{\gamma} - I_{zz}\dot{\theta}\dot{\gamma}}{m(g - a_z)} \quad [19]$$

Here I_{xx}, I_{yy} and I_{zz} are the moments of inertia of the vehicle around the roll, pitch and yaw axis. For an actual vehicle which regularly gets loaded and unloaded with luggage, fuel or passengers the moments of inertia can vary, but for this study, they are assumed to be constant. The CG height above ground (h_{CG}) is also not constant due to load changes of the vehicle and the rotation about the roll centre, but is considered to be constant for the study due to the rigid vehicle assumption made to derive the equations used to determine the zero moment point. The moments of inertia and location of the CG of the vehicle can be determined through parameter estimation if the effects of loading and unloading of the

vehicle need to be considered or if a non-rigid assumption is made for the derivation of the zero moment point (Kolansky & Sandu, 2013).

2.3.3. Parameters that influence roll angle

In section 2.1 we derived the basic vehicle dynamics equations that include the body roll of the vehicle. These equations were set up for the quasi-static and transient suspended vehicle in the roll-plane.

From the quasi-static analysis from equation 3, we see that vehicle roll can be reduced by increasing the roll stiffness, increasing the stiffness of the suspension, reducing the CG height or reducing the lateral acceleration. Since we want to negotiate a prescribed path at a certain speed the lateral acceleration is predetermined, thus the most viable method to reduce the roll angle is to increase the roll stiffness of the suspension.

From the transient analysis from equations 4 and 5, the damping characteristics and moment of inertia is also taken into account. An increase in the damping characteristics of the suspension also reduced the propagation of the roll angle which, for highly dynamic manoeuvres, reduced the maximum roll angle during the manoeuvre. For slow manoeuvres, the inclusion of the damping resulted in the vehicle reaching the same conditions as which was found in the quasi-static analysis.

By increasing the suspension stiffness and damping characteristics, the lateral load transfer is increased as was found in equation 12, which results in a lower overall lateral force generated by the tyres as seen from equation 14. This decrease in lateral force might cause the vehicle to slide out rather than a rollover. Although the rollover accident is avoided in this circumstance the vehicle may still crash, but from the statistics, an accident due to a sliding vehicle has a lower mortality rate than a rollover, thus sliding is preferred over rollover (NHTSA, 2017).

The load transfer also influences the understeer gradient of the vehicle, thus the roll stiffness and damping should be distributed in a smart manner to both reduce the roll of the vehicle and maintain a desirable understeer gradient so that the vehicle stays predictable for the driver.

2.4. Systems that improve handling

Many different systems have been developed and proven to reduce rollover or improve the handling of vehicles. Some examples of these systems include electronic stability control (ESC), torque vectoring and yaw control, active front steering (AFS) and active and semi-active suspension control.

Electronic stability control (also known as electronic stability program (ESP)) aims to change the vehicle's steerability when the system detects that the vehicle is not moving in the intended direction of the driver. The system applies braking forces to individual wheels to bring the vehicle back under control of the driver. The system does however not serve as a performance system, but rather a safety system for when the driver loses control during an evasive manoeuvre or encounters any form of sliding (van Zanten, 2000).

Although ESC can be seen as a yaw control system it acts only in the interest of safety. Other yaw control systems attempt to improve the directional stability of a vehicle, which in turn improves the handling performance of the vehicle. Torque vectoring is one example of handling performance-based yaw control. Torque vectoring also comes in different packages such as brake-based systems and torque based systems. Brake based systems, as the name implies makes use of the brakes to change the vehicle's yaw rate and yaw angle by applying the brakes to different wheels, causing a turning moment in the yaw plane. Torque based systems are usually employed on electric vehicles, where individual wheel torque can be changed easily, which again changes the vehicles yaw rate and yaw angle by varying the turning moments in the yaw plane. Various manufacturers use different combinations and permutations of these systems to achieve the desired results (Ivanov, et al., 2012). These torque vectoring systems, in general, improves the vehicle's directional stability from a performance perspective but also brings safety aspects which in an emergency manoeuvre will provide the driver with a better handling vehicle that may help prevent accidents.

Another method that can be used to change the vehicle's directional characteristics is that of an active front steering system. These systems detect a lack of steering input from the driver and actively increases the steering angle of the front wheels, to improve the lateral forces that are applied at the wheels to improve directional response. These systems again aim to improve the handling capabilities of the vehicle, which, in an evasive manoeuvre, will help the driver avoid an accident (Fergani, et al., 2016).

Semi-active suspension control aims to change the vehicle's vertical characteristics which in turn, through the tyres change the vehicle's lateral and longitudinal responses. With all passive suspension characteristics, there is a compromise made between the ride comfort of the vehicle and the handling of the vehicle. In terms of ride comfort, a soft and compliant suspension spring and damper is desirable to absorb all the undulations of the road, which is in contrast to the stiff suspension characteristics needed for good handling. With a semi-active suspension setup, the compromise is not needed as different discrete or continuously variable settings for the springs and/or dampers are available. With a good control algorithm, the choice can be made to switch the suspension setting to handling mode when a handling or performance manoeuvre is detected while keeping the suspension in ride comfort mode for the rest of the journey. Since the semi-active suspension system can only change its characteristics it is thought of as a reaction based system, where the system only reacts to other vehicle states, rather than actively change the vehicle's suspension motion (Els, 2006).

Active suspension control is achieved by having actuators in the place of the spring and damper setup to control the vertical movements of the vehicle. An active suspension system is in general equipped with a scanning or computer vision system that measures and monitors the road. These measures are then used to detect road defects and send a signal to the suspension actuators to actuate in the appropriate direction to avoid the impact of the defect in the road. In the case of a handling manoeuvre, the relevant suspension member can be actuated to decrease roll of the vehicle, which will lead to a safer driving experience. One drawback of the active suspension systems is the cost and power

consumption of these systems, which limits them to the upper-class vehicle market (Al-Holou, et al., 1993).

2.5. Four state semi active suspension system ($4S_4$)

Els (2006) designed and implemented a semi-active suspension system on a test Land Rover Defender 110. The semi-active suspension system was characterised and optimised by Thoresson (2007) and Uys et al. (2007) for the best possible ride comfort when the suspension is switched to a soft setting and the best possible handling performance when the suspension is switched to a hard setting. The suspension system has two discrete spring settings and two discrete damping settings, hence four states that the suspension can be in. The name of the suspension system stems from the working method: 4 State Semi-active Suspension System or $4S_4$. The system has two gas chambers with different gas volumes (GV) to act as two springs with different characteristics for the suspension. The damping is controlled with bypass valves, where oil can be passed through a low resistance channel in the low damping setting but is forced through an orifice once the valve is closed for high damping. Figure 10 shows a schematic of the $4S_4$ suspension strut.

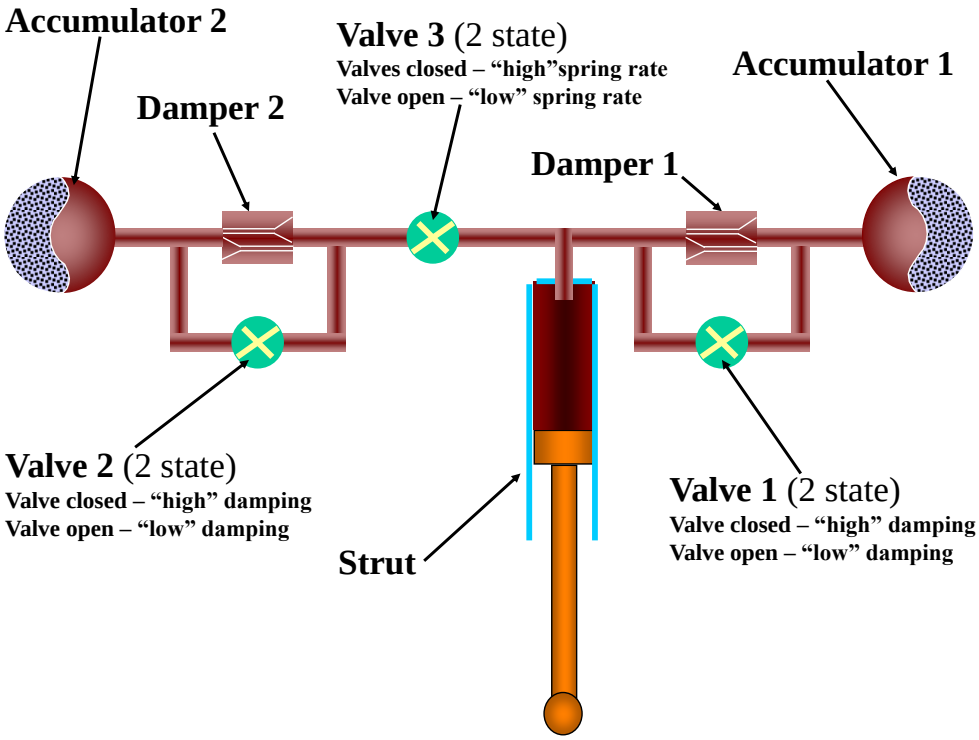

Figure 10: Schematic representing the $4S_4$ suspension system (Els, 2006)

If valve 3 is closed the oil can only pass to accumulator 1 which has a small gas volume and acts like a stiff spring. With valve 3 open the oil can pass to both accumulators which then has a large total gas volume which acts as a soft spring. Valve 1 and 2 acts as the low resistance bypass valves, which, when closed, forces the oil to pass through the high flow resistance damper packs 1 and 2 to achieve high damping, and when open will bypass these damper packs and have a low flow resistance and low damping. The delays for opening and closing of the valves and the dynamics of the flow the characteristic changes can have a cumulative delay between 40 to 100 milliseconds over the pressure range of interest (Els, 2006).

The 4S4 suspension system prototype was extensively characterised and modelled by Els (2006) with further refinement by van der Westhuizen (2015) for the spring and Thoresson (2003) for the damping.

2.5.1. Hydro-pneumatic spring model

Van der Westhuizen (2015) compared different models including ideal gas, real gas and energy equations. The spring model makes use of an ideal gas model (nitrogen gas) and an adiabatic compression assumption to iteratively update the gas pressure (Van Der Westhuizen & Els, 2015). The ideal gas approach is:

$$P = \frac{RT_g}{v} \quad [20]$$

$$P_k V_k^{\gamma} = P_{k-1} V_{k-1}^{\gamma} \quad [21]$$

The mass of the gas in the gas accumulator stays constant and is determined based on the static pressures and volumes. The change in displacement is the input to the model changing the gas volume. With the gas volume of the previous sample time and the current sample time known and under the assumption of an adiabatic process the pressure can be updated for each iteration by making use of the adiabatic index $\gamma = 1.4$ for the nitrogen gas used in the gas accumulator. With the pressure known and the piston area of the strut rod, the force due to the gas spring can be determined and fed back to the simulation model. A force-displacement figure of the front left suspension strut is shown in figure 11 for both the large gas accumulator volume and the small gas accumulator.

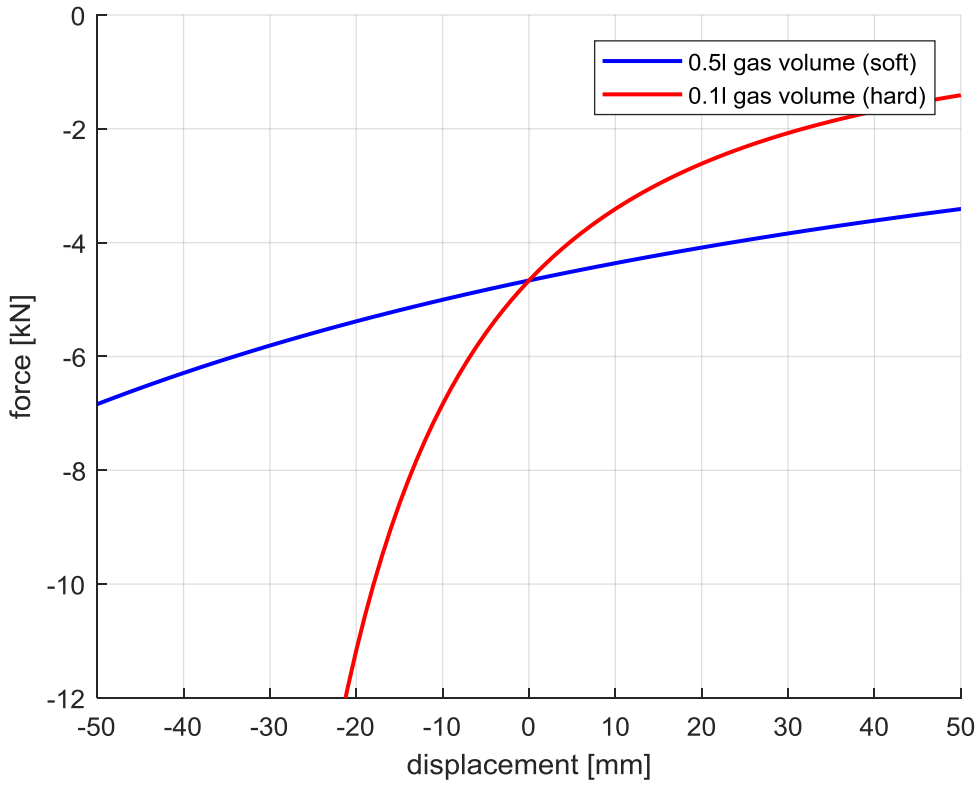

Figure 11: Force-displacement curves for gas springs

2.5.2. Damper model

The damper model is presented as a piecewise fit of polynomial equations (Thoresson, 2003). The piecewise fit of the equations was selected to closely resemble the damper force curves from experimental tests. The damping curves (figure 12) have a scaling factor (DSF) that increases or decreases the standard curve to represent the high and low damping in the suspension strut. The polynomials that represent the damping curves are given in equations 22 to 25:

$$F_{d1} = 5000 \times \dot{z} \times (-2000 \times \dot{z}^2 + DSF)^{0.9} - 100 \times DSF - 700 \quad [22]$$

$$F_{d2} = -50000 \times \dot{z}^2 + 14000 \times \dot{z} \quad [23]$$

$$F_{d3} = 40000 \times \dot{z}^2 + 10000 \times DSF^{0.3} \times \dot{z} \quad [24]$$

$$F_{d4} = 5000 \times (\dot{z} - 0.05)^2 + 7000 \times DSF^{1.3} \times (\dot{z} - 0.05) + 200 \times DSF + 800 \quad [25]$$

F_{d1} and F_{d2} represents the negative velocity section of the force curves whereby for a specific damping scaling factor the larger positive force value of the two equations is returned ($\max(F_{d1}, F_{d2})$). F_{d3} and F_{d4} represents the positive velocity section of the force curves where the smaller positive force value is returned between the two equations for a specific damping scaling factor ($\min(F_{d3}, F_{d4})$).

The hard damper setting has a scaling factor of 2, while the low damper setting has a scaling factor of 0.25. The damper curves are shown in figure 12.

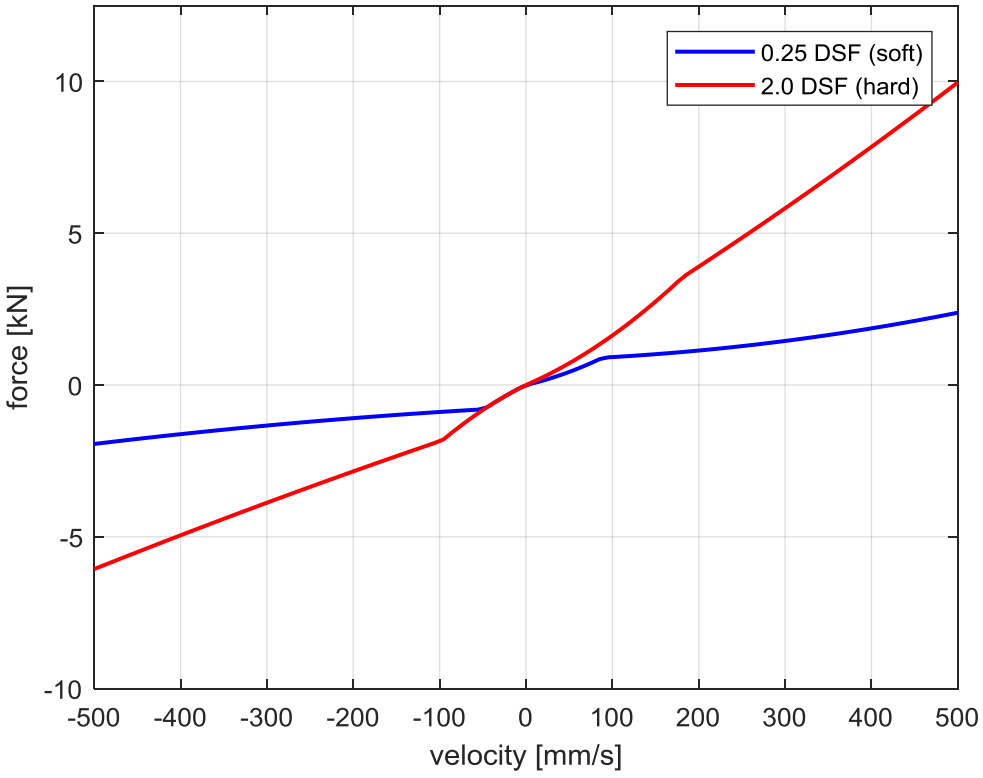

Figure 12: Force velocity curves for dampers

2.5.3. Baseline $4S_4$ control strategy

Els (2006) developed a novel semi-active suspension switching strategy that works well to keep the $4S_4$ suspension on the Land Rover Defender 110 in a ride comfort mode while traversing a rough road and switches the suspension (all four suspension struts) to a handling mode when a handling or emergency manoeuvre is encountered.

The method uses the vertical and lateral acceleration root mean square values over a fixed-length moving window to determine the state in which the suspension should be. The root mean square calculation over this window is termed as the running root mean square value, or RRMS of the signal. Els (2006) used an RRMS value for 1 second worth of signal sampled at 100 Hz, recalculated after each sample, to compare the RRMS value of the vertical and lateral accelerations. The RRMS (at sample N+k-1) over a specific window (with length N) is calculated as follow:

$$RRMS = \sqrt{\frac{1}{N}\sum_{n=k}^{N+k-1} a_n^2} \quad , k = 1,2,3 \ldots \qquad [26]$$

If the lateral acceleration RRMS value is below 0.05g the suspension will stay in ride comfort mode. If the lateral acceleration RRMS value is above 0.3g the suspension will switch to and stay in handling mode. In between these lateral acceleration RRMS values, the suspension will switch to handling mode when the lateral acceleration RRMS value is larger than the vertical acceleration RRMS value or stay in ride comfort mode when the vertical RRMS value is larger than the lateral RRMS value.

With this strategy, if the vehicle experiences a rough road, a high vertical acceleration RRMS value will be calculated and the suspension will stay in ride comfort. The vertical acceleration RMS was found in section 2.2 to be a good metric for ride comfort. At large lateral accelerations, which is one of the metrics discussed in section 2.3 for handling, the lateral acceleration RRMS value will increase indicating that the vehicle experiences a handling manoeuvre and the suspension will switch to a handling mode.

Els (2006) found that the Land Rover with the semi-active suspension system and RRMS switching strategy has significantly improved handling capabilities as compared to the baseline Land Rover passive suspension system through comparing the absolute and relative roll angle through a double lane change handling manoeuvre. At higher speeds and thus higher lateral accelerations, the suspension system stayed in handling mode throughout the handling manoeuvre but the strategy had a short delay to switch over to the handling mode (between 0.4 and 0.8 seconds depending on the speed). The vehicle with the semi-active suspension system showed similar ride comfort levels as the baseline vehicle when traversing rough roads.

2.6. Suspension control

To overcome the compromise of passive suspension systems, namely, ride comfort of vehicles and handling characteristics, a form of controllable suspension can be used. With

the addition of actuation or control to a system, the operation conditions need to be defined in detail and the control objective set in such a way such that the control input may bias the system according to a preferred trajectory. The optimisation of this control strategy may find the best control to achieve the objective (Sharp & Peng, 2011).

2.6.1. Skyhook-, Groundhook-, and Hybrid control

Skyhook control consists of the idea that an ideal damper can be attached to the sprung mass of the vehicle and a fictitious reference in the sky to limit the vertical motion of the body of the vehicle. The controller is designed from a ride comfort standpoint. The ideal skyhook suspension control is realised in practice by adding a semi-active continuously varying damper between the sprung mass and un-sprung mass of the vehicle at each strut. The continuously varying damper's characteristics are varied based on the suspension deflection velocity and sprung mass velocity to match the damper force of the ideal skyhook damper (Strydom, 2013).

With the groundhook control approach, the un-sprung mass of the vehicle is attached to a fictitious reference on the ground through an ideal groundhook damper which minimises the vertical displacement change of the un-sprung mass of the vehicle with respect to the ground. In doing so the vertical deflection of the tyre is minimised which minimises the variation in vertical loads which increases the handling of the vehicle. Again the continuously variable damper is added in between the un-sprung mass and sprung mass where the controllable damping characteristic is varied such that the damping force mimics that of the ideal groundhook damper (Strydom, 2013).

Hybrid control makes use of a combination of skyhook and groundhook control to overcome the compromise between ride comfort and handling of the skyhook and groundhook control respectively. Biasing the hybrid controller to either ride comfort or handling is achieved by weighing the skyhook or groundhook controller respectively (Strydom, 2013).

2.6.2. H_∞ (H infinite) control

H_∞ control is a form of robust control theory where the optimal control prioritises low sensitivity to variations in the parameters and disturbances of the inputs. It applies to linear uncertain systems and involves minimizing the maximum gain of input-related frequency response functions of the closed-loop system. Loop shaping is a common feature of robust control designs, making it possible to improve stability without prejudice to responses (Sharp & Peng, 2011).

H_∞ control for suspension systems is usually limited to quarter car models whereby vertical accelerations are limited for ride comfort purposes and suspension and tyre deflections minimised for handling performance (Sammier, et al., 2003).

2.6.3. Sliding mode control

Sliding mode control is another robust control technique which works well with modelling mismatch and unknown disturbances. The main advantages of sliding mode control include

the robustness properties to uncertainty, finite-time convergence, and reduced-order compensated dynamics (Shtessel, et al., 2014).

Sliding mode control has been used in the past for suspension control in the form of an active anti-roll bar (Chu, et al., 2015). The authors presented the controller results from simulation work done whereby the additional roll torque was applied to the vehicle CG whenever a predetermined rollover threshold value was exceeded during severe handling manoeuvres. No results were presented for ride comfort analysis.

In general, the sliding mode controller will work best for continuously variable control systems or active control systems because of the smooth control output the controller gives.

2.7. Model predictive control

Model predictive control of a linear system makes use of the formulation of the dynamics of the problem in the state space form, whereby linear-quadratic optimal control methods can be used to formulate the optimal inputs over a finite or infinite horizon, and the receding horizon control law to determine the input to the system to stabilise or track a certain trajectory. A good controller will attempt to keep the state or trajectory as small as possible for good regulation and the input as small as possible for efficient control efforts.

Model predictive control has been used in the past on active and semi-active suspension systems. Göhrle, et al. (2012) used a variable damper model in their model predictive controller to minimise vertical body acceleration and roll and pitch accelerations in simulation. In this study the authors aimed at increasing the ride comfort and didn't present any results for handling. Nguyen, et al. (2016) also used a model predictive controller and a semi-active suspension model to improve ride comfort over different simulated road roughness by minimising vertical acceleration and roll angles. No handling results were presented to confirm handling improvements. Brezas, et al. (2015) used a clipped-optimal linear quadratic regulator for a semi-active suspension to improve ride comfort through the minimisation of the bounce/pitch dynamics and improve handling through the minimisation of the roll/warp dynamics. Canale, et al. (2006) used a "fast" model predictive controller to control a continuous variable damping suspension system to improve the ride comfort of the vehicle.

2.7.1. Linear quadratic regulator

A linearized state-space formulation of the dynamics of the system that needs to be controlled needs to be formulated with full state feedback. The state-space formulation and quadratic cost function are given as follows:

$$\dot{x} = Ax + Bu \qquad x \in \mathbb{R}^n, u \in \mathbb{R}^n, x_o \; given$$
$$J = \frac{1}{2}\int_0^T (x^T Q x + u^T R u)\, dt + \frac{1}{2} x^T(T) P x(T)$$

where $Q \geq 0, R > 0, P \geq 0$ are symmetric, positive (semi-) definite matrices used to tune the controller with state weighting, input weighting and terminal state weighting respectively (Borrelli, et al., 2017).

This problem can be solved via the maximum principle from which the Riccati ordinary differential equation can be derived and solved backwards in time to find an input vector which will control the system optimally based on the tuning of the weighting matrices. This method is generally referred to as a dynamic programming effort to solve the control problem (Borrelli, et al., 2017).

The batch approach can also be used to solve the problem where each subsequent state can be related to the initial state and a large linear algebra problem can be solved to determine the optimal control input vector. If the model used to define the state space system is the same as the actual system then both methods will regulate to the same final state (Borrelli, et al., 2017).

2.7.2. Receding horizon control

Since the linear quadratic regulator calculates the future control efforts based on the current initial state, the controller is thought of as an open-loop controller. If the model used to create the state-space system deviates from the actual system's dynamics then the regulation will not proceed as expected in the control effort of the problem.

One method to attempt to make the controller a closed-loop controller is by introducing the concept of receding horizon control, where a fixed length preview horizon is used at the beginning of typically each sample instance. The control effort is then determined by using the linear quadratic regulator and the first entry of the control vector is applied to the system. This is done at typically each sample instance for the duration of the use of the system. The length of this fixed length preview horizon affects the control effort and state regulation (Borrelli, et al., 2017).

The combination of receding horizon control and the linear quadratic regulator results in a model predictive controller.

2.8. Validated full non-linear vehicle model

A Land Rover Defender 110 is used as the vehicle in this study. The multibody dynamics software package MSC Adams (MSC Software, 2018) was used to create a fully non-linear validated model with 16 degrees of unconstrained freedom of the vehicle which can be used for simulation work. The Adams model was developed and extensively validated experimentally by Thoresson (2007), Uys, et al. (2007) and Cronje (2008) to be a close representation of the true test vehicle. The basic information of the model is shown in Table 1. The model included a validated FTire (cosin scientific software, 2018) tyre model of the Michelin LTX AT2 tyre (Bosch, et al., 2016) used on the vehicle. The body of the vehicle is represented by two rigid bodies connected with a torsional spring to capture the torsional stiffness of the vehicle chassis in the roll direction. The $4S_4$ suspension model (section 2.5) is incorporated into the Adams model through co-simulation with Simulink (MathWorks, 2018). The suspension of the vehicle is attached to a solid axle with the suspension struts

mounted vertically. Non-linear bump stops and bushings are also added in the model to improve the validity of the model.

Botha (2011) and Hamersma (2014) developed a driver model used for path following and longitudinal demand forces respectively for the simulation model.

Through co-simulation between the multibody dynamics software package MSC Adams and Matlab & Simulink, various scenarios and vehicle tests can be investigated.

Table 1: Vehicle parameters used in simulation model

Parameter	Value	Unit
Total vehicle mass	2047	kg
Vehicle sprung mass	1582	kg
Total mass moment of inertia around the longitudinal axis (roll)	839	kgm^2
Total mass moment of inertia around the lateral axis (pitch)	2471	kgm^2
Total mass moment of inertia around the vertical axis (yaw)	2057	kgm^2
Longitudinal distance from the front axle to CG	1.55	m
Longitudinal distance from the rear axle to CG	1.25	m
Track width front and rear	1.49	m
Distance between front suspension struts	1.01	m
Distance between rear suspension struts	0.97	m
Vehicle width	1.86	m

2.9. Vehicle tests

To evaluate the handling and ride comfort of the vehicle and control strategies, simulations and physical tests need to be performed. The different tests considered for this study are presented here.

2.9.1. Handling tests

The ISO3888 severe double lane change (International Organisation for Standardisation, 1999) is used to determine the dynamic handling behaviour of a vehicle. The test mimics the evasive manoeuvre that a driver might experience on a highway. The course layout is defined in the standard and included in figure 13.

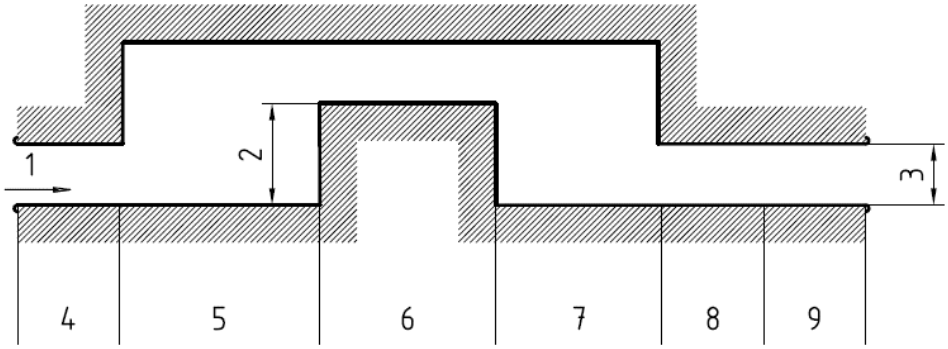

Figure 13: DLC course layout (International Organisation for Standardisation, 1999)

The width of the track is related to the vehicle's width and as such Table 2 can be followed to create the correct layout for the test.

Table 2: Double lane change dimensions

Section	Length [m]	Width [m]	Description
1	-	-	Entry direction
2	-	3.5	Lane offset
3	-	-	Exit
4	15	1.1 x vehicle width +0.25 = 2.296	Enter first lane
5	30	1.2 x vehicle width +3.75 = 5.982	Turn towards second lane
6	25	1.2 x vehicle width +0.25 = 2.482	Drive in second lane
7	25	1.2 x vehicle width +3.75 = 5.982	Turn back towards first lane
8	15	1.3 x vehicle width +0.25 = 2.668	Drive in first lane
9	15	1.3 x vehicle width +0.25 = 2.668	Exit test

An image of the vehicle performing a double lane change is shown in figure 14. For this study, the double lane change (figure 13) is mirrored to make the evasive manoeuvre to the right of the first lane instead of towards the left, because the vehicle is right-hand drive.

Figure 14: Land Rover performing a double lane change manoeuvre at Gerotek

The dynamic handling track at Gerotek (Armscor, 2016) is designated for the testing of the handling characteristics of light vehicles at high speeds. The track consists of multiple high and low-speed corners which tests a wide range of the handling of the vehicles. A schematic of the track is given in figure 15. For this study, the outermost routes were followed (i.e. the trapezium curve and spiral curve).

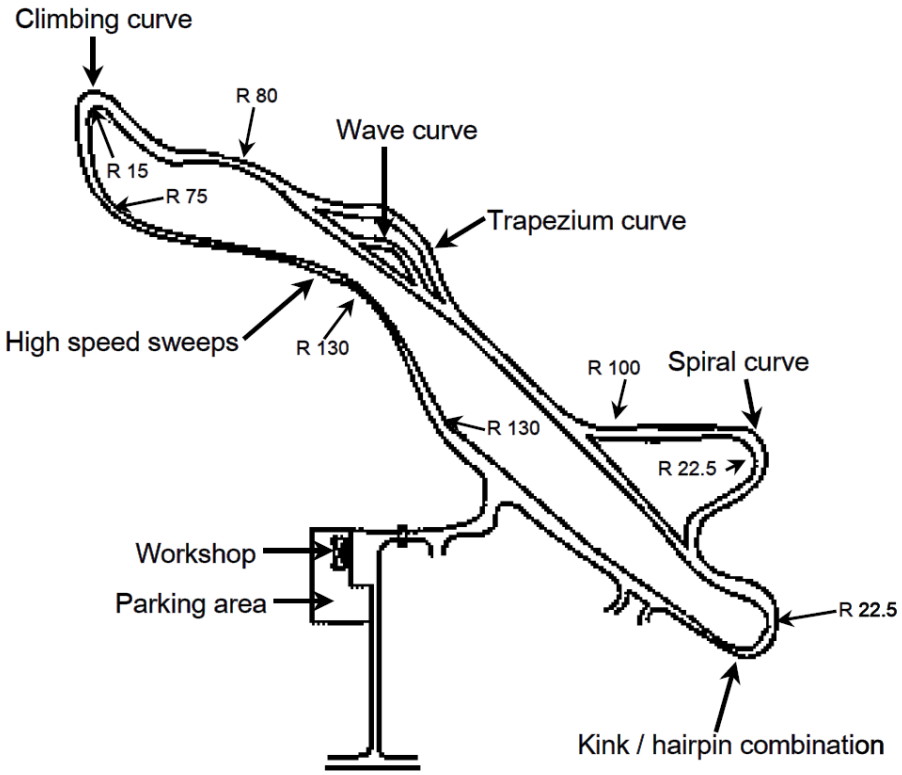

Figure 15: Dynamic handling track at Gerotek (Els, 2006)

2.9.2. Ride comfort test

The Belgian paving track is used to test the vehicle's ride comfort. Usually, a vehicle with good handling oriented passive suspension system will perform exceptionally poorly on this road. The track is made from cast concrete blocks in the shape of cobblestones. An image of the Belgian paving track at Gerotek is shown in figure 16.

Figure 16: Belgian paving track at Gerotek (Hamersma & Els, 2014)

2.9.3. Combined ride and handling test

An 800m section of the rough track at Gerotek, consisting of a hairpin and many road camber changes as well as dips and climbs were used to experimentally evaluate a situation where both ride comfort and handling are required simultaneously. The rough track is a concrete cast track with many undulations in the road. The track is a good representation of a real off-road track that might be negotiated by a typical SUV with off-road capabilities. A plan view of the track is shown in figure 17 and a photo of the track in figure 18.

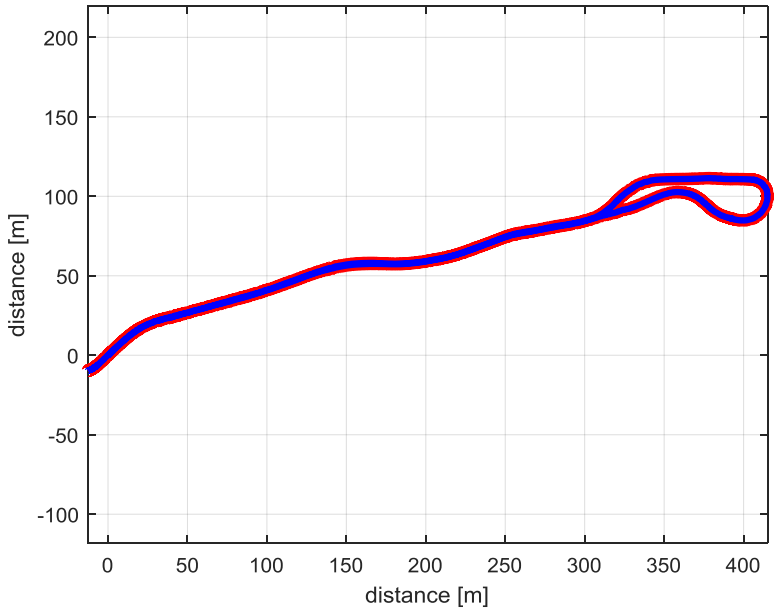

Figure 17: Rough track top plateau with a hairpin at Gerotek

Figure 18: Photo of the rough track at Gerotek (Els, 2006)

2.10. Conclusion

From the literature study, the underlying vehicle dynamics were investigated which influence the handling characteristics of a vehicle. The yaw-plane analysis was used to determine the influence the tyre forces had on the steering characteristics of the vehicle and to derive the understeer gradient of the vehicle. A roll-plane analysis was used to discern which parameters of the vehicle had an influence on the roll angle and propagation of the roll angle. The load transfer effect and the influence it has on the understeer gradient was also investigated.

Ride comfort evaluation methods were investigated and it was found that the vertical acceleration of the vehicle body gave a good indication of the ride comfort levels of the vehicle over a certain terrain. Specifically, the RMS value of the vertical acceleration can be used as a suitable ride comfort metric.

Different handling and rollover metrics were investigated with the vehicle roll angle and lateral acceleration giving a good indication of limit handling of SUVs. The zero moment point gave a good indication on the rollover stability of the vehicle, specifically the y location of the zero moment point, with the vehicle CG height and lateral acceleration forming part of the metric.

Increased vehicle roll stiffness and damping characteristics (through the suspension system of the vehicle) were found to be good candidates to reduce the roll angle propagation of the vehicle. With harder suspension members the lateral load transfer of the vehicle in a handling manoeuvre will be higher, thus the distribution of the increased spring and damper characteristic is important for a stable understeer gradient.

Different systems used to improve handling were discussed including semi-active suspension systems which can be used to vary the spring and/or damper characteristics of a given suspension member. The $4S_4$ hydro-pneumatic suspension system installed on the Land Rover Defender was discussed and a model presented which can be used to vary the spring and damper characteristics in simulation.

Different suspension control strategies were presented wherefrom the model predictive controller was selected for the control method used in this study. The model-based design approach of the controller with the possible addition of constraints to perform optimal or clipped-optimal control gave promising results for ride comfort and/or handling improvements in previous work.

A validated full non-linear simulation model of the Land Rover Defender is presented whereon controller development, simulation and validation will be done through co-simulation.

Lastly, vehicle tests are presented to investigate the performance of the controller in a simulation environment and experimentally. Handling tests will be performed with the ISO3888 severe double lane change to quantify handling performance of the controlled suspension. Tests on the Belgian paving will be used to determine ride comfort levels and controller fidelity to stay in ride comfort mode over rough terrains. Additional tests are also investigated to determine further performance comparisons in ride comfort and handling, as well as combined ride comfort and handling tests.

2.11. Project plan

The purpose of this study is to find an answer to the research question: Can a controller be developed to change the spring and damping characteristics of individual suspension struts to reduce body roll, maintain the desired understeer gradient and maintain the course of the vehicle in an emergency manoeuvre while still ensuring good ride comfort for normal driving or rough terrain driving. If this question can be answered then the ride comfort versus handling compromise of passive suspension systems can be circumvented to ensure fewer rollover accidents and better handling characteristics for high CG vehicles

The controller will be developed through a model-based design methodology by making use of a validated fully non-linear multibody dynamics simulation. The semi-active suspension system implemented on the test vehicle is also extensively modelled for the validated simulation model and will be used to test the controller.

Finally, the controller will be implemented on the test vehicle where real tests will be conducted to validate the performance of the controller for both the handling performance and the ride comfort fidelity.

The deliverables of the study will thus be to:

- Validate the lateral and vertical dynamics of the simulation vehicle against experimental tests in case of any vehicle, suspension or tyre parameter changes due to age or use.
- Develop a semi-active suspension controller that will improve the handling characteristics in an emergency manoeuvre while maintaining good ride comfort for normal or rough terrain driving. The controller should be developed for discrete control.
- Implement the discrete semi-active suspension controller on the Land Rover Defender 110 test vehicle available at the University, test and validate the performance of the implemented controller.

3. Validation of vehicle simulation model

The simulation work serves as the first step for proof of concept, where many simulations can be run sequentially without the initial need for physical testing of the concepts. This process reduces the cost of testing and can be easily changed to investigate different ideas without risk. The simulation work can also be used after testing to validate the correct or expected performance of the controls of the system designed. Since the proposed MPC will initially be developed using simulation and later tested on the real vehicle, it is imperative that confidence in the simulation model be established. Although the simulation modal has been validated many times in the past, it was considered essential for the current work to establish a baseline in case any vehicle, suspension or tyre parameters have changed due to age and use.

3.1. Vehicle instrumentation

For this study, a MicroAutoBox II (MABX) (dSPACE, 2018) is used to process the signals and record the data of the vehicle states. A VBox 3i differential GPS (VBOX automotive, 2018) integrated with the IMU04 (VBOX automotive, 2018) inertial measurement unit is used to capture the vehicle's roll, pitch and yaw rates, the vertical, longitudinal and lateral accelerations and GPS location, vehicle speed and heading. The integrated Kalman Filter in the VBox is used to determine the roll angle. This roll angle will later be used in the controller. The suspension switching is controlled by a Coremodule 420 computer (PC-104 (PC/104 Consortium, 2018) form factor) from AMPRO with analogue inputs measured with a Diamond Systems MM-16-AT 16-bit analogue to digital converter card with the input to the PC-104 coming from the MABX and the outputs, controlling the solid-state relays, are provided by a Diamond Systems Onyx-MM-DIO card which switches the valves on the suspension strut to change the damping or spring characteristics. Relative strut displacements are measured using ICS-100 In-Cylinder Sensors from Penny & Giles. A schematic diagram of the unit is provided in figure 19.

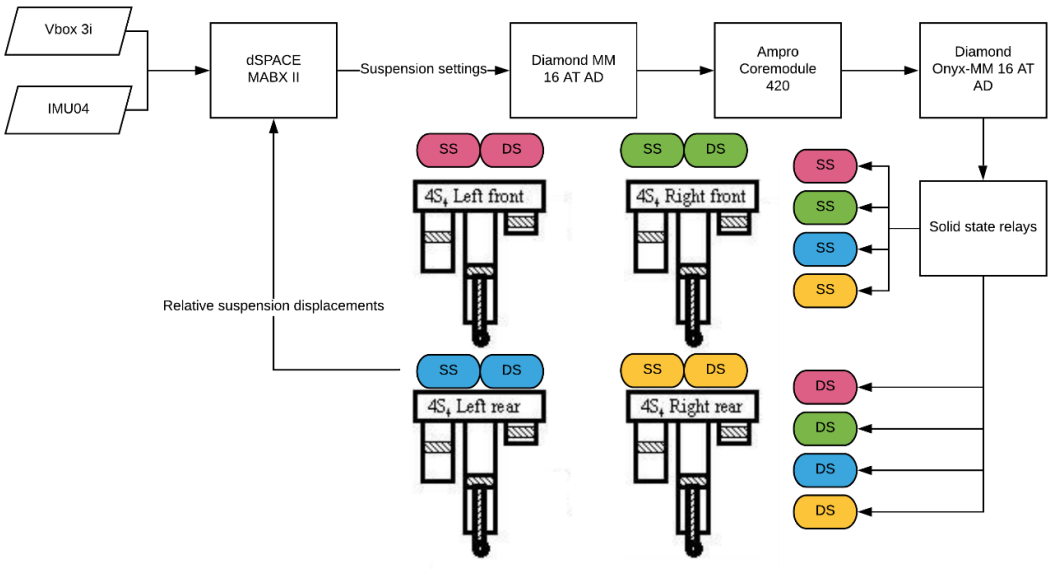

Figure 19: Suspension measurement and control schematic

The specific parameters used for the controller or validation purposes is shown in Table 3 together with the sensor that supplies the data.

Table 3: Parameter and corresponding measurement device

Parameter	Sensor/Actuator	Purpose
Yaw rate	VBox/IMU	Validation
GPS location		Validation
Speed		Validation
Roll angle		Validation and control
Roll rate		Validation and control
Vertical acceleration		Validation and control
Lateral acceleration		Validation and control
Relative suspension displacement	ICS-100 In-Cylinder Sensors	Validation
Main control unit	DSpace MABX	Control
Suspension control unit	PC-104	Control
Suspension switching	$4S_4$ Hydraulic valves	Control

3.2. Lateral dynamics validation

For the validation of the lateral dynamics, the experimental results of a double lane change for speeds of 50 km/h, 60 km/h, 70 km/h and 80 km/h are compared to the simulation results of the same manoeuvre for both the ride comfort and handling suspension settings. The roll angle, roll rate, lateral acceleration, yaw rate and longitudinal speed results are compared, with the roll angle, roll rate, lateral acceleration and yaw rate used for the validation. In figure 20, the soft suspension double lane change results are presented for a speed of 70 km/h. The longitudinal speed of the vehicle was maintained by the driver who attempted to keep it as constant as possible throughout the test. Also, in simulation, steering input is determined by the driver model and can vary substantially from the steering input during tests. Figure 21 presents the results for the hard suspension at a speed of 70 km/h.

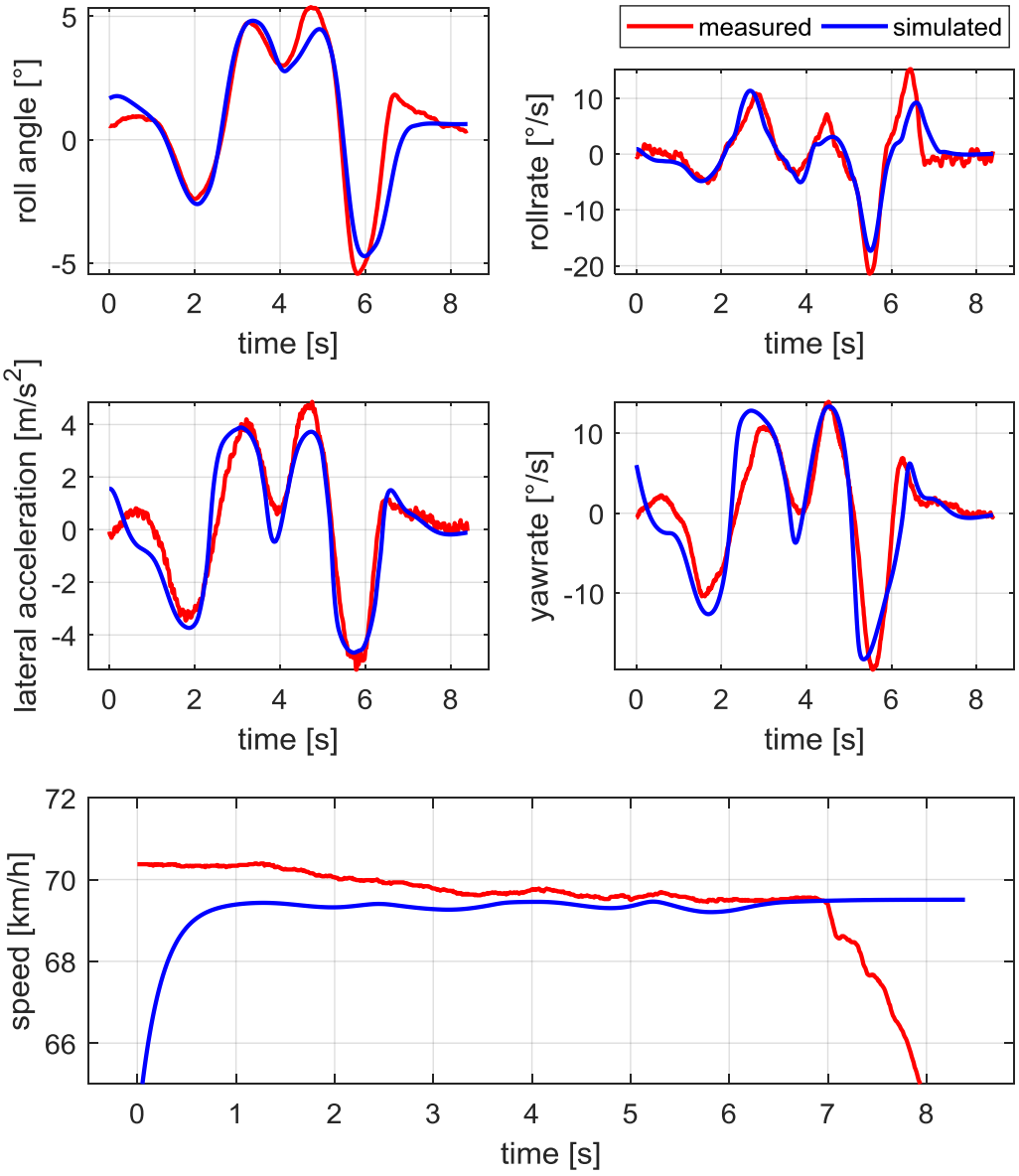

Figure 20: 70 km/h DLC soft suspension validation

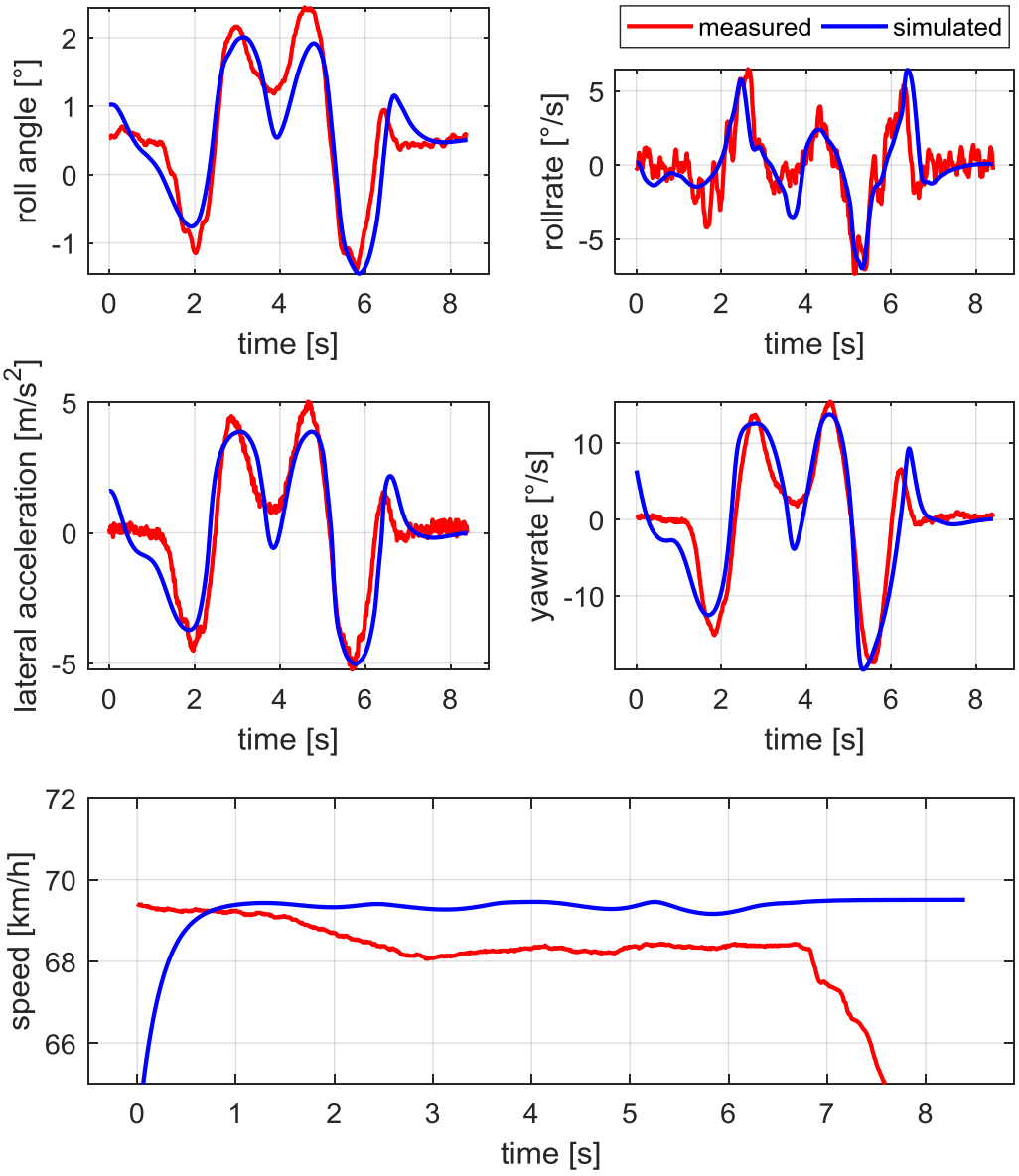

Figure 21: 70 km/h DLC hard suspension validation

To quantitatively compare the results the root mean square error (RMSE) and percentage of the absolute of the errors below the root mean square error is reported in Table 4. From this measure the lower the RMSE value is the better the correlation between the two data sets. This RMSE value and the magnitude of the data set should be considered together to determine whether the differences in the data is acceptable or not. The larger the percentage of absolute errors below the RMSE the better the correlation is as well.

Table 4: RMSE (%below) lateral simulation validation results

	RMSE (%below)				
Vehicle speed [km/h]	Suspension setting	Roll angle $[deg]$	Roll rate $[deg/s]$	Lateral acceleration $[m/s^2]$	Yaw rate $[deg/s]$
50	Soft	0.65 (68%)	1.76 (81%)	0.73 (73%)	3.41 (76%)
	Hard	0.25 (67%)	1.01 (70%)	0.53 (70%)	2.51 (71%)
60	Soft	0.81 (74%)	2.45 (80%)	0.82 (74%)	3.77 (77%)
	Hard	0.34 (82%)	1.45 (79%)	0.84 (80%)	3.48 (76%)
70	Soft	0.92 (78%)	2.55 (75%)	0.87 (66%)	3.57 (75%)
	Hard	0.40 (67%)	1.56 (77%)	1.00 (69%)	3.38 (71%)
80	Soft	1.49 (70%)	4.66 (72%)	1.40 (57%)	4.64 (65%)
	Hard	0.74 (68%)	2.67 (72%)	1.72 (67%)	5.48 (68%)

From the results, we can see that visually the simulated and experimental results correlate well. The small differences in the figures can be attributed to many different reasons such as un-modelled friction in the suspension which came to be over the years of service or the fact that a non-perfect driver model was used to perform the simulation path following. The fact that the speed of the vehicle was not perfectly constant throughout the test can also add to the discrepancies between the data sets, especially the difference between the magnitude and time lag of some of the peaks. From the RMSE values and percentages, we can see that the biggest portion of the error between the simulation and experimental results are below the RMSE. The large RMSE values seen for the roll rate can be attributed to the oscillations seen in the data that might be due to noise in the measurements. The large RMSE values of the yaw rate can be attributed to the lag in time of the simulated and experimental work. Overall the trends of the data sets agree well. The lateral dynamics of the simulation model is deemed suitable for the development of the suspension control system.

3.3. Vertical dynamics validation

The vertical dynamics of the simulation model is validated by comparing the unweighted running root mean square values (0.25 seconds window size sampled at 2000 Hz and 100 Hz for the simulation and experimental work respectively) of the vertical acceleration to the experimental data for the runs over the Belgian paving in the soft suspension setting at speeds of 21 km/h (figure 22) and 47 km/h (figure 23). The speed of the vehicle was kept constant throughout the test by driving the vehicle against the governor in low range in second gear and high range in second gear for the 21 km/h and 47 km/h speeds respectively. A histogram with the spread of the vertical accelerations for the simulation and experimental data is also shown. The mean of the running root mean square (RRMS) values of the vertical acceleration and the standard deviations of the vertical acceleration is given in Table 5 for comparison.

Table 5: Vertical simulation validation results

	Data set	21 km/h	47 km/h
Mean of vertical acceleration RRMS [m/s²]	Simulation	1.36	2.12
	Experimental	1.57	2.21
Standard deviation of vertical acceleration [m/s²]	Simulation	1.47	2.24
	Experimental	1.62	2.28

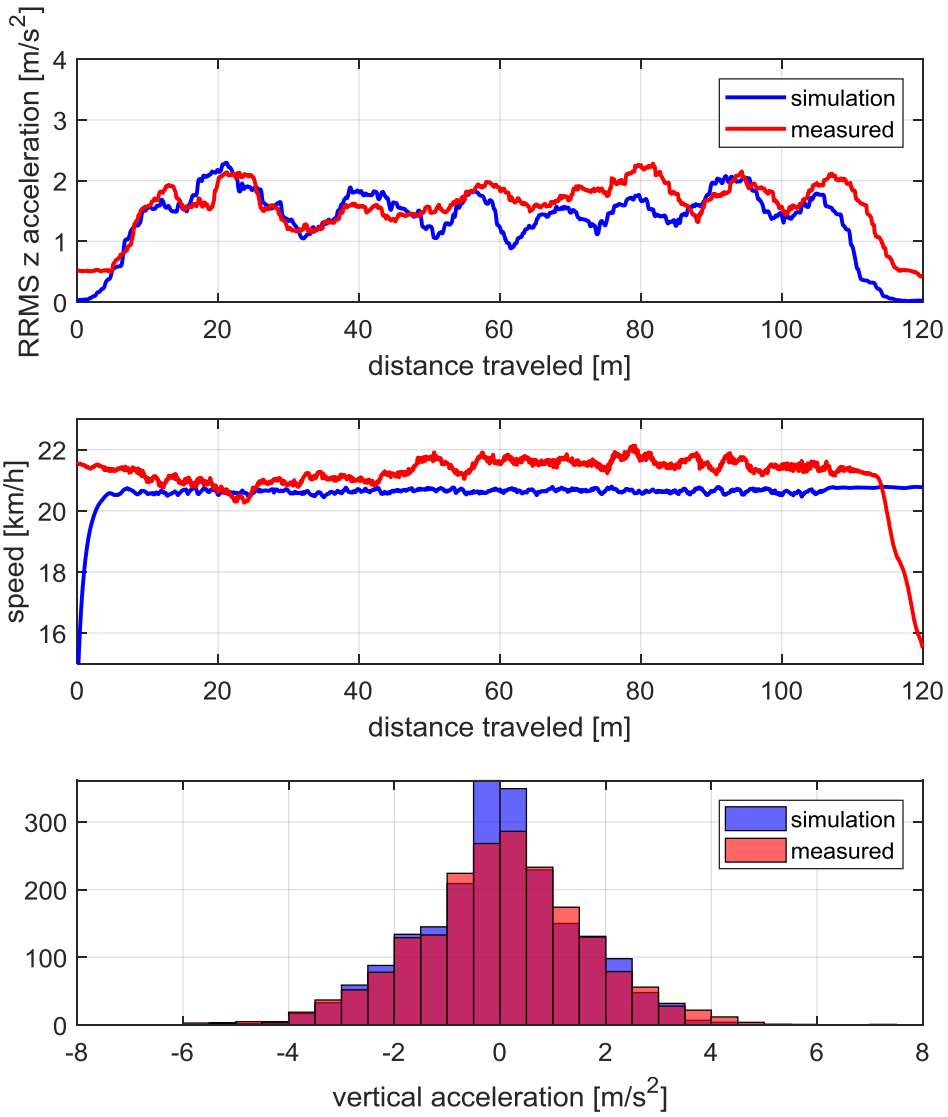

Figure 22: 21 km/h Belgian paving run vertical validation

The vertical dynamics of the simulation model follows the experimental results quite well visually. From the histograms we can see that the spread of the vertical accelerations is similar, considering that the large peaks in the simulation data close to zero can be due to the simulation model having an exceptionally smooth road just before and after the Belgian paving, which would lead to a larger concentration of low vertical accelerations around zero. The mean of the vertical acceleration RRMS and standard deviation of the vertical acceleration is also close between the simulation and experimental data. The vertical

dynamics of the simulation model is captured well and is deemed suitable for the development of the control of the suspension system.

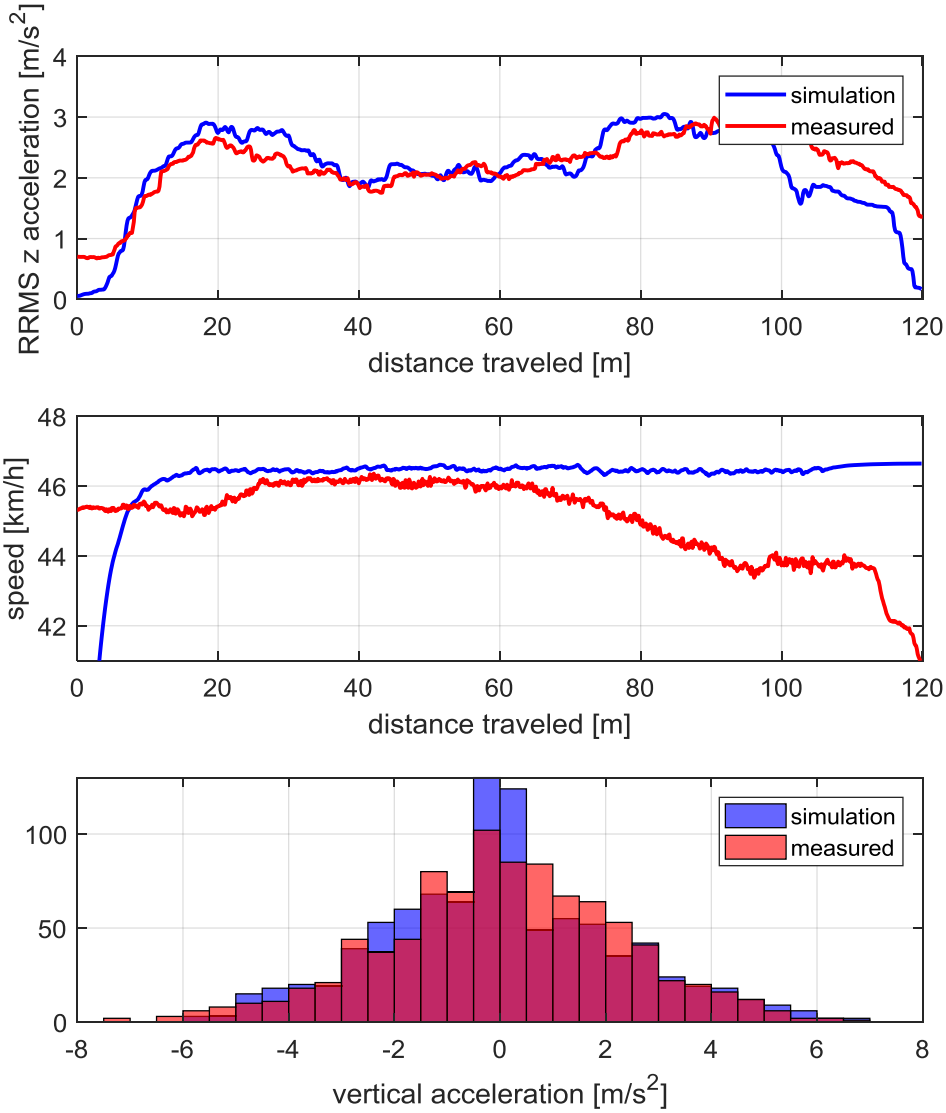

Figure 23: 47 km/h Belgian paving run vertical validation

3.4. Conclusion

From the results, we can see that the lateral and vertical dynamics of the simulation model is well captured. Although there are some visual differences in the lateral validation this can be attributed to friction in the physical system that has not been accounted for in the simulation model and the driver model used in simulations that did not follow the same path which was followed in experimental tests.

Overall the trend of the lateral dynamics in simulation and experiments are the same with acceptable error and thus we can say that the lateral dynamics has been captured well. The vertical dynamics also correlate well between the simulations and experimental work, thus the ride comfort of the simulation vehicle is properly validated.

With this reassurance, the controller to switch the semi-active suspension can be developed and implemented on the simulation model to fine-tune the control parameters.

4. Development of control system

In this section, the development of a semi-active suspension controller, based on MPC properties, is discussed in detail. The roll dynamics of the vehicle is used to predict the future states of the vehicle. Both a continuously variable controller and discrete sub-optimal controller are presented. The controller makes use of a model predictive controller based on the theories of the linear quadratic regulator and receding horizon control. Through the control of individual suspension struts' spring and damper settings, it is anticipated that the semi-active suspension system can reduce the roll angle of the vehicle in a handling manoeuvre while maintaining good ride comfort on rough roads or non-severe handling manoeuvres.

4.1. Vehicle dynamic equations concerning rollover

To maintain computational efficiency of the controller and reduce the complexity of the problem, the vehicle dynamics equations of only the roll plane analysis is considered for the model predictive controller. A simplified model, as included in figure 24, is thus used for controller development.

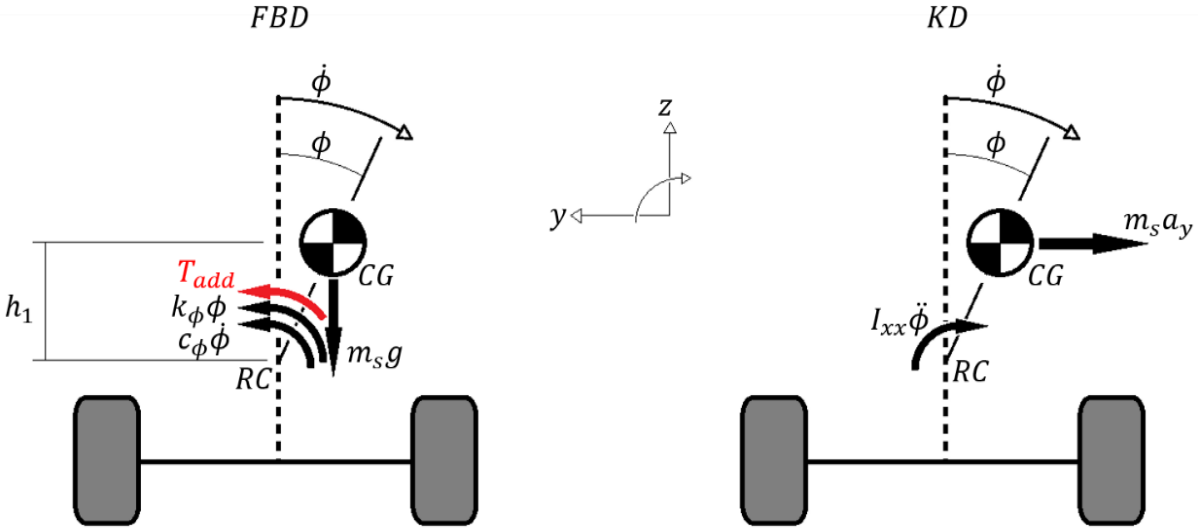

Figure 24: Roll plane of a simple suspended vehicle (vehicle turning left, viewed from the rear)

Taking the moments about the roll centre (RC) of the vehicle (as in the transient analysis of section 2.1.3) and assuming small angles the following equation is found:

$$I_{xx}\ddot{\phi} = -c_\phi\dot{\phi} - k_\phi\phi + m_s g h_1\phi + m_s h_1 a_y + T_{add} \quad [27]$$

T_{add} is the additional torque needed, as the controller input, to achieve the desired roll dynamics.

Since spring stiffness and damping coefficients of automobiles are usually presented assuming collinear motions the conversion from collinear to rotational coefficients are:

$$k_\phi = k_{collinear}\frac{s^2}{4} \quad [28]$$

$$c_\phi = c_{collinear}\frac{s^2}{4} \quad [29]$$

With s the distance between the suspension struts on the front or rear axles. Seeing that the suspension's collinear displacement and velocities aren't used in the equation of the roll moment, a relation is made based on the small angles assumption. The equation that relates the roll angle to each strut's collinear displacement is:

$$\Delta z_{fl} = \phi \frac{s_f}{2} \quad [30]$$

$$\Delta z_{fr} = -\Delta z_{fl} \quad [31]$$

$$\Delta z_{rl} = \phi \frac{s_r}{2} \quad [32]$$

$$\Delta z_{rr} = -\Delta z_{rl} \quad [33]$$

For the strut's collinear velocity the relation is extended to the roll rate of the vehicle through:

$$\dot{z}_{fl} = \dot{\phi} \frac{s_f}{2} \quad [34]$$

$$\dot{z}_{fr} = -\dot{z}_{fl} \quad [35]$$

$$\dot{z}_{rl} = \dot{\phi} \frac{s_r}{2} \quad [36]$$

$$\dot{z}_{rr} = -\dot{z}_{rl} \quad [37]$$

The correlation between the suspension displacements, measured with the ICS-100 In-Cylinder Sensors, and the calculated suspension displacements from the roll angle, measured with the integrated Kalman Filter of the VBox 3i and IMU04, is shown in figure 25 for the front struts for a DLC at 80 km/h on the soft suspension setting. These measurements were obtained during the model validation tests described in chapter 3. The comparison shows excellent correlation indicating that equations 30 to 37 are adequate.

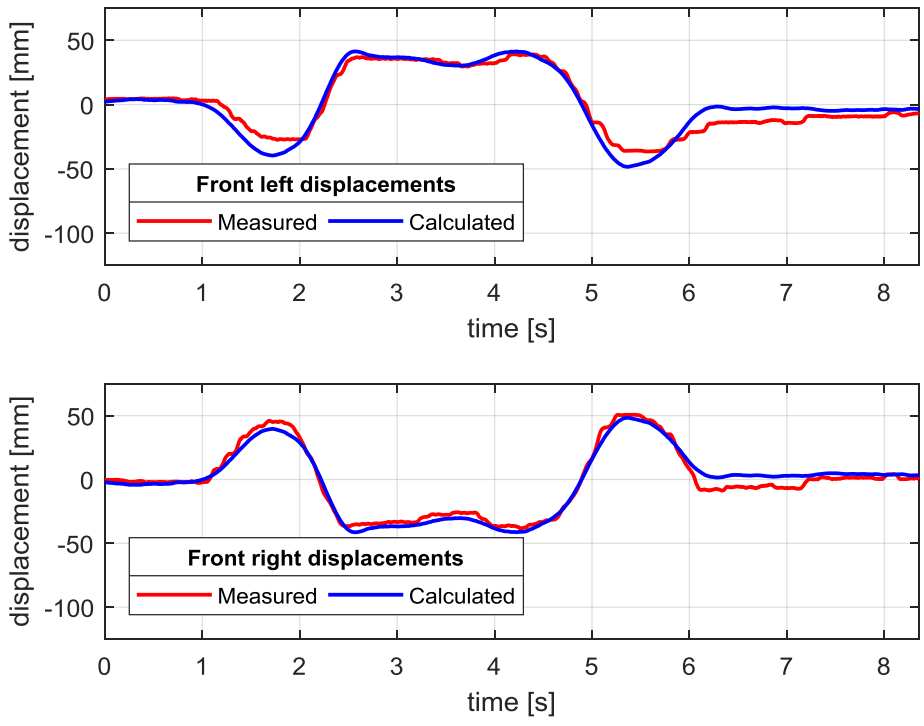

Figure 25: Roll angle to suspension displacement correlation 80 km/h DLC soft suspension setting

The spring and damper characteristics presented in figure 11 and 12 are highly nonlinear. For equation 27 to be linear the spring and damper are linearized around the current state, which is necessary for the linear quadratic regulator which will be discussed later. The following assumptions are made to create the state space equations which will be used in the controller later on:

- The spring and damper characteristics are linearized around the current state of the vehicle to determine the spring stiffness and damping coefficient.
- The linearization of the spring and damper is valid as long as the prediction horizon is sufficiently short.
- The lateral acceleration is assumed to act as an external disturbance and will be treated as a constant throughout the controller's preview horizon.
- The vertical acceleration is also assumed to be constant throughout the preview horizon.
- The suspension's displacement is assumed to be related to the roll angle by equations 30 to 33.
- The suspension's velocity is assumed to be related to the roll velocity by equations 34 to 37.

With these assumptions the following state-space equation is created:

$$\begin{Bmatrix} \ddot{\phi} \\ \dot{\phi} \end{Bmatrix} = \begin{bmatrix} \frac{-c_\phi}{I_{xx}} & \frac{-k_\phi + m_s g h_1}{I_{xx}} \\ 1 & 0 \end{bmatrix} \begin{Bmatrix} \dot{\phi} \\ \phi \end{Bmatrix} + \begin{Bmatrix} \frac{m_s h_1}{I_{xx}} \\ 0 \end{Bmatrix} \{a_y\} + \begin{Bmatrix} \frac{1}{I_{xx}} \\ 0 \end{Bmatrix} \{T_{add}\} \quad [38]$$

This is simplified to

$$\dot{x} = Ax + E\delta + Bu \quad [39]$$

with

$$A = \begin{bmatrix} \frac{-c_\phi}{I_{xx}} & \frac{-k_\phi + m_s g h_1}{I_{xx}} \\ 1 & 0 \end{bmatrix}; \quad B = \begin{Bmatrix} \frac{1}{I_{xx}} \\ 0 \end{Bmatrix}; \quad E = \begin{Bmatrix} \frac{m_s h_1}{I_{xx}} \\ 0 \end{Bmatrix}$$

$$x = \begin{Bmatrix} \dot{\phi} \\ \phi \end{Bmatrix}; \quad u = \{T_{add}\}; \quad \delta = \{a_y\}$$

These equations are discretised with Eulerian discretisation for the time steps (T_s) that will be used in the linear quadratic regulator as follows:

$$A_d = e^{A \cdot T_s}; \quad B_d = A^{-1}((A_d - I)B); \quad E_d = E$$

This leads to a discrete state space equation in the form of:

$$x_{k+1} = A_d x_k + E_d \delta_k + B_d u_k \quad [40]$$

With these equations, the model predictive controller can be designed through the linear quadratic regulator and receding horizon theories.

4.2. Model predictive controller design

The model predictive controller used in this study makes use of the linear quadratic regulator theory such that a discretised linear system can be used to control the states of the system through receding horizon control. This discrete-time optimal control scheme calculates an optimal input to the system over a finite time horizon based on the minimisation of an objective function. This control is applied to a system with a given initial state $x(0)$.

In the broader sense of the control method, the objective function is defined as the minimisation of the sum of stage costs and a terminal cost (in the case of finite-horizon control) while the states should satisfy the system dynamics or any state or input constraints as imposed by the designer.

For this study a linear discrete time-invariant system as defined in 4.1 is used with a quadratic objective function of the form:

$$J_0(x_0, U) \triangleq \min_{U_0} \sum_{k=0}^{N-1} [x_k' Q x_k + u_k' R u_k] + x_N' P x_n \qquad [41]$$

Subject to: $x_{k+1} = A_d x_k + E_d \delta_k + B_d u_k,\ k = 0, \dots, N-1$

$x_0 = x(0)$

With:

- The terminal weight P being positive semidefinite and symmetric
- The stage weight Q being positive semidefinite and symmetric
- The input weight R being positive definite and symmetric
- N the horizon length
- $x_0, \dots, x_N$ and $u_0, \dots, u_{N-1}$ the state and input optimisation variables
- $U \triangleq [u_0, \dots, u_{N-1}]$ the vector of inputs that minimises the objective function

This controller does not consider state or input constraints and the states, namely the roll rate and roll angle, are regulated towards the origin.

A batch approach is followed where the input vector, which represents the optimal control over the time horizon of the controller, to minimise the objective function is found by numerically solving a larger linear algebra problem. The batch approach makes use of the fact that all of the subsequent states can be represented by just the initial state x_0 and the inputs $u_0, \dots, u_{N-1}$.

Beginning with $x_0 = x(0)$

we can find $x_1 = A_d x_0 + E_d \delta + B_d u_0 = A_d x(0) + E_d \delta + B_d u_0$

and $x_2 = A_d x_1 + E_d \delta + B_d u_1 = A_d^2 x(0) + A_d B_d u_0 + A_d E_d \delta + E_d \delta + B_d u_1$

And so forth by substituting the previous state in the current state's calculation up to x_N. This results in:

$$\begin{Bmatrix} x_0 \\ x_1 \\ x_2 \\ \vdots \\ \vdots \\ x_N \end{Bmatrix} = \begin{Bmatrix} I \\ A_d \\ A_d^2 \\ \vdots \\ \vdots \\ A_d^N \end{Bmatrix} x_0 + \begin{bmatrix} 0 & \cdots & \cdots & \cdots & 0 \\ B_d & 0 & \ddots & \ddots & \vdots \\ A_d B_d & B_d & 0 & \ddots & \vdots \\ \vdots & \ddots & \ddots & \ddots & \vdots \\ \vdots & \ddots & \ddots & \ddots & 0 \\ A_d^{N-1} B_d & A_d^{N-2} B_d & \cdots & A_d B_d & B_d \end{bmatrix} \begin{Bmatrix} u_0 \\ u_1 \\ u_2 \\ \vdots \\ \vdots \\ u_{N-1} \end{Bmatrix} + \begin{Bmatrix} 0 \\ E_d \\ (A_d + I)E_d \\ \vdots \\ \vdots \\ \sum_{i=0}^{N-1} A_d^i E_d \end{Bmatrix} \delta \quad [42]$$

Or simplified as:

$$X = \boldsymbol{A} x_0 + \boldsymbol{B} U + \boldsymbol{E} \delta \quad [43]$$

The objective function as defined in equation 41 can also be simplified into the following form:

$$J = X' \begin{bmatrix} Q & 0 & \cdots & \cdots \\ 0 & \ddots & \ddots & \vdots \\ \vdots & \ddots & Q & \ddots \\ \vdots & \cdots & \ddots & P \end{bmatrix} X + U' \begin{bmatrix} R & 0 & \cdots & \cdots \\ 0 & \ddots & \ddots & \vdots \\ \vdots & \ddots & \ddots & \ddots \\ \vdots & \cdots & \ddots & R \end{bmatrix} U \quad [44]$$

Or

$$J = X' \boldsymbol{Q} X + U' \boldsymbol{R} U \quad [45]$$

To solve for the problem in an efficient manner a quadratic optimisation problem of the form:

$$J = \frac{1}{2} U' \boldsymbol{H} U + \boldsymbol{F} U + \boldsymbol{C} \quad [46]$$

needs to be solved, where the variable of the quadratic problem U is the optimal input to the system to recover the vehicle in the event of a handling manoeuvre. Equation 43 is substituted into equation 45 and manipulated into the form of equation 46 which is presented below, whereby with coefficient comparison the $\boldsymbol{H}, \boldsymbol{F}$ and $\boldsymbol{C}$ matrices and vectors can be found.

$$J = x_0' \boldsymbol{A}' \boldsymbol{Q} \boldsymbol{A} x_0 + x_0' \boldsymbol{A}' \boldsymbol{Q} \boldsymbol{B} U + x_0' \boldsymbol{A}' \boldsymbol{Q} \boldsymbol{E} \delta + x_0' \boldsymbol{A}' \boldsymbol{Q} \boldsymbol{B} U + U' \boldsymbol{B}' \boldsymbol{Q} \boldsymbol{B} U + \delta' \boldsymbol{E}' \boldsymbol{Q} \boldsymbol{B} U$$
$$+ \delta' \boldsymbol{E}' \boldsymbol{Q} \boldsymbol{A} x_0 + \delta' \boldsymbol{E}' \boldsymbol{Q} \boldsymbol{B} U + \delta' \boldsymbol{E}' \boldsymbol{Q} \boldsymbol{E} \delta + U' \boldsymbol{R} U$$

$$\boldsymbol{H} = 2\boldsymbol{B}' \boldsymbol{Q} \boldsymbol{B} + 2\boldsymbol{R}$$
$$\boldsymbol{F} = 2x_0' \boldsymbol{A}' \boldsymbol{Q} \boldsymbol{B} + 2\delta' \boldsymbol{E}' \boldsymbol{Q} \boldsymbol{B}$$
$$\boldsymbol{C} = x_0' \boldsymbol{A}' \boldsymbol{Q} \boldsymbol{A} x_0 + 2x_0' \boldsymbol{A}' \boldsymbol{Q} \boldsymbol{E} \delta + \delta' \boldsymbol{E}' \boldsymbol{Q} \boldsymbol{E} \delta$$

Note that $\boldsymbol{H}$ is positive definite since $\boldsymbol{B}' \boldsymbol{Q} \boldsymbol{B}$ is positive semidefinite and $\boldsymbol{R}$ is positive definite, thus $\boldsymbol{H}^{-1}$ always exists. Since the problem is unconstrained and the objective function J is a positive definite quadratic function of U we can find the optimal control input U by setting the gradient of the quadratic optimisation function with regards to U equal to zero and solve for U.

$$\nabla_U J = \boldsymbol{H}U + \boldsymbol{F} = 0 \quad [47]$$

$$U = -\boldsymbol{H}^{-1}\boldsymbol{F} \quad [48]$$

The output of the controller U is a roll torque vector that should recover the vehicle in a finite horizon. When the first entry of the roll torque vector $U(0) = u_0$ is used to perform the input to the physical system the controller is said to be a receding horizon controller. Due to the fact that no input or state constraints are added to the problem, the controller will work in a sub-optimal manner, but for the purposes of this study, the inputs are deemed to be sufficiently good to control the vehicle's body roll.

At each sampling time, the initial state of the controller is reset to the current sample, the state space equations are setup again through time discretisation and linearization and the controller is run again to determine a new control input vector, where the first entry in the vector is used to control the system.

For this study, the terminal weight and state weight was selected to be the same. The weight on the error of both the roll rate and roll angle was chosen to tend towards unity of the state squared multiplied to the respective weight as shown below ($max_{roll\,rate} = 10\ °/s$ for roll rate and $max_{roll\,angle} = 3.55°$ for the roll angle, all converted to radians):

$$P = Q = \begin{bmatrix} \frac{1}{max_{roll\,rate}^2} & 0 \\ 0 & \frac{1}{max_{roll\,angle}^2} \end{bmatrix} = \begin{bmatrix} 33 & 0 \\ 0 & 260 \end{bmatrix} \quad [49]$$

These maximum values were selected to be approximately half of the maximum roll angle and roll velocity that the vehicle will experience in a severe double lane change at 80 km/h with the suspension in the ride comfort setting. These values are also tuning parameters that can be varied to change the performance of the controller. The weighting of the input is discussed in section 4.3.1.

After initial simulations, a preview horizon of 100 ms and discretised time step of 10 ms (100 Hz calculation speed) produced desirable results from the controller. This agrees with work done by Els (2006) who found that the roll velocity and relative suspension displacement (which correlates well with the vehicle roll angle as seen in section 4.1) has a natural frequency at approximately 2 Hz, which is well below the 100 Hz calculation speed of the controller and will show up adequately in the 100 ms preview horizon.

4.3. Metric to decide between ride or handling

As discussed in section 4.2 the weighting of the input of the model predictive controller needs to be determined. This weighting determines how hard the input should try to force the states back to the origin, based on the objective function defined in section 4.2. This means that a higher weighting value will force the input to be a smaller numeric value, while a smaller weighting value will force the input to be a larger value to force the states to the origin and counteract the disturbances imposed on the vehicle.

As discussed in section 2.2 a metric to determine the ride comfort of a vehicle is the RMS value of the vertical acceleration. With changing road inputs the RRMS of the vertical acceleration can be used to monitor the ride comfort levels of the vehicle.

For this study, only the y coordinate of the ZMP is used as a handling metric, since this value gives information about the lateral stability of the vehicle. Since the y_{zmp} uses the height of the vehicle's CG above the ground the method works well for vehicles with high rollover propensity due to the height of the CG. Strauss (2016) found that the $\ddot{\phi}$, $\dot{\gamma}$ and $\dot{\theta}$ states in equation 19 contribute to less than 1 per cent of the y_{zmp} value if these states are changed by 10%, thus a simplified y_{zmp} of

$$y_{zmp} = \frac{ma_y h_{CG}}{m(g - a_z)} \quad [50]$$

can be used.

The running root mean square value (0.25 seconds window size sampled at 2000 Hz and 100 Hz for the simulation and experimental work respectively) of the vertical acceleration can be used to determine the standard deviation of the vertical acceleration, with the mean around the 9.81 m/s^2 downwards direction. This root mean square value is calculated as previously discussed in section 2.2. The standard deviation is then:

$$\sigma_{a_z} = RRMS_{a_z} \quad [51]$$

Seeing that any excessive vertical vibrations make the vehicle unstable, the following equation is used to determine the modified y_{zmp} location

$$y_{zmp} = \frac{a_y h_{CG}}{g - \sigma_{a_z}} \quad [52]$$

A vehicle can be seen as stable if the y_{zmp} value lies within a predefined polygon underneath the vehicle. If the ZMP location moves outside of this polygon then rollover may occur. The vehicle is thus stable if the ZMP lies within the track width of the vehicle (i.e. the stable polygon is bounded in the y direction within the track width of the vehicle). For the vehicle considered in this study the maximum value of the y_{zmp} is ±0.743 m, or half the track width of the vehicle.

4.3.1. Combined ride comfort and handling metric

With the metrics set out above a combined metric can be made that considers both ride and handling. The metrics can be plotted with the x-axis being the absolute value of the ZMP value, and the y-axis the RRMS value of the vertical acceleration. A surface can be created from this that based on the x, y coordinates give a high, low or value in between that can be used to change the input weight R (which needs to be a positive value) in section 4.2 equation 41 to bias the controller.

With some manual tuning in the simulation environment, the surface indicated in figure 26 was created which gave desirable results.

From this, we can see that at high vertical RRMS values the input weight will be high for a larger range of ZMP values. This will ensure that the suspension stays in ride comfort mode

when traversing a rough road with low to moderate handling manoeuvres. Sometimes the vehicle will have to negotiate a handling manoeuvre even on a rough road, thus the weight will decrease if the y-location of the zero moment point nears 0.6 m location, which is close to the critical 0.743 m location, where after rollover might occur. This ensures that the vehicle on a rough road will be as comfortable as possible up until the vehicle gets close to a critical handling scenario.

On the lower side of the RRMS values the input weight decreases earlier for the range of ZMP values. The point where the weight decreases is approximately 0.27 m of the y-location of the zero moment point. This value corresponds to the 0.3g limit lateral acceleration proposed by Els (2006) for when the suspension should switch to the handling mode. This ensures that the controller steers to handling mode quickly when a handling manoeuvre is experienced with little vertical acceleration inputs.

From the BS 6841 standard guide used to evaluate human exposure to whole-body vibration (British Standards Institution, 1987) a 0.5-1.0 m/s^2 weighted root mean square vertical acceleration signal is deemed as fairly uncomfortable, which was used to determine the transition point on the map for the weighting at the lower side of the vertical RRMS accelerations. Also, a 1.25-2.5 m/s^2 weighted root mean square vertical acceleration signal is deemed as very uncomfortable, which correlates to the area on the map where, above those vertical RRMS accelerations, the weighting will favour ride comfort on the map.

With this metric, the input roll torque of the controller can be determined, but since the torque can't be applied directly to the vehicle, this roll torque needs to be analysed to determine what the suspension settings on each individual strut need to be to 'generate' this torque with an optimal distribution between the different suspension struts.

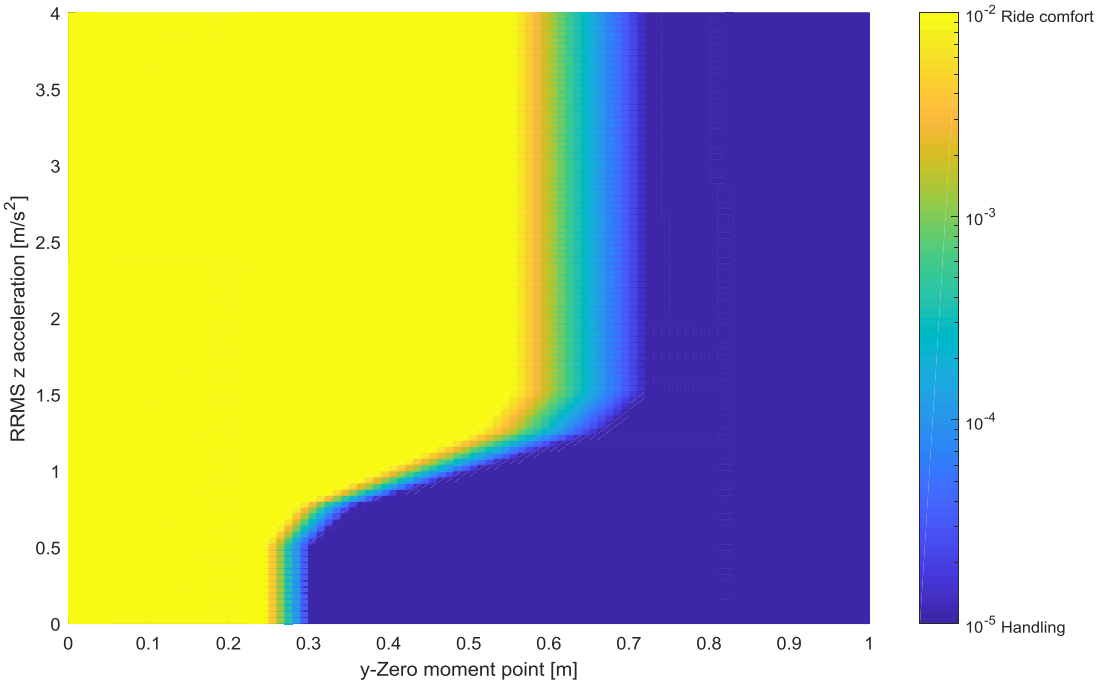

Figure 26: Combined ride comfort and handling metric weighting function for input

4.4. Roll moment distribution

Since the roll torque from the controller needs to be distributed between the front and rear axle the roll moment distribution can be made such that the vehicle can produce as close to neutral steer as possible. The understeer gradient which arises from the tyre's cornering stiffness (from the linear lateral tyre force assumption made in section 2.1.2, although this assumption does not hold at large lateral accelerations it is deemed to be satisfactory for this application) and the lateral load transfer is defined as:

$$K = \left(\frac{W_f}{C_{\alpha f}} - \frac{W_r}{C_{\alpha r}}\right) + \left(\frac{W_f}{C_{\alpha f}}\frac{2b\Delta F_{zf}^2}{C_{\alpha f}} - \frac{W_r}{C_{\alpha r}}\frac{2b\Delta F_{zr}^2}{C_{\alpha r}}\right) \quad [53]$$

Here the ΔF_{zf} and ΔF_{zr} values, which represents the lateral load transfer, can be changed by changing the spring and damping characteristics of the suspension. The soft suspension settings are selected as the baseline spring and damper characteristics. The change in the load can be shown to be:

$$\Delta F_{zf} = \frac{m_f h_f}{t_f} a_y + \frac{k_{\phi f}}{t_f}\phi + \frac{c_{\phi f}}{t_f}\dot{\phi} + u_f \quad [54]$$

$$\Delta F_{zr} = \frac{m_r h_r}{t_r} a_y + \frac{k_{\phi r}}{t_r}\phi + \frac{c_{\phi r}}{t_r}\dot{\phi} + u_r \quad [55]$$

With

$$T_{add} = u_f t_f + u_r t_r \quad [56]$$

By setting equation 53 equal to zero (neutral steer), and substituting equation 56 into equation 55, and then substituting equation 54 and equation 55 into equation 53, then solving for u_f we determine the additional force on the front axle, and the other axle if we substitute u_f into equation 56 and solving for u_r. To remove unnecessary suspension switches for low additional torque requirements from the controller a low cut off value was added such that absolute torque values under 5 Nm would be treated as zero.

From this, we know the additional vertical forces that need to be added to the wheels to obtain the desired understeer gradient over and above the forces due to the lateral load transfer from the lateral acceleration and the soft suspension members.

The additional spring and damping forces are determined by making the assumption that the damping ratio for the associated coefficients is constant at ζ= 0.5 for both the front and rear axle. The force is related to the spring and damping through:

$$u_f = \frac{k_{\phi f,add}}{t_f}\phi + \frac{c_{\phi f,add}}{t_f}\dot{\phi} \quad [57]$$

and

$$u_r = \frac{k_{\phi r,add}}{t_r}\phi + \frac{c_{\phi r,add}}{t_r}\dot{\phi} \quad [58]$$

The damping ratio is determined as:

$$\zeta_f = \frac{c_{\phi f,add}}{2\sqrt{k_{\phi f,add} I_{xx,f}}} \quad [59]$$

and

$$\zeta_r = \frac{c_{\phi r,add}}{2\sqrt{k_{\phi r,add} I_{xx,r}}} \quad [60]$$

By substituting equation 59 and equation 60 into equation 57 and equation 58 respectively $c_{\phi,add}$ and $k_{\phi,add}$ can be found for the front and rear axles.

By adding the additional spring stiffness and damping values to the baseline soft suspension's stiffness and damping the total values required for each axle can be determined.

4.5. Individual suspension spring and damper settings

Since we now know what the distribution of the spring stiffness and damping needs to be for the front and rear axles of the vehicle, the left and right strut's settings can be determined per axle. This is done by considering the sign of the y_{zmp} for the spring stiffness and the roll rate for the damping.

Both the left hand and right-hand strut's gas volumes start at the soft spring's gas volume. If the sign of the y_{zmp} is positive then the right-hand strut's gas volume is decreased until the stiffness of the hydro-pneumatic spring of the right hand and left-hand strut (the equivalent roll stiffness) is equal to or just greater than the desired stiffness as determined in section 4.4. If, after reducing the gas volume of the right-hand side's strut to the minimum, the desired roll stiffness is not met, the left-hand strut's gas volume is decreased until the desired stiffness is found. If after this both the left and right struts are at the lowest gas volume and the desired stiffness is not met the gas volumes for both sides are kept at the minimum gas volume. The same method is followed for both the front and rear axle's hydro-pneumatic springs separately, and the opposite side is started if the y_{zmp} is negative. The process is illustrated in figure 27.

A similar method as for the hydro-pneumatic spring's gas volume is followed for the dampers. All the dampers start at the lowest damper scaling factor. If the roll rate of the vehicle is positive, the right-hand side's damper scaling factor is increased until the equivalent roll damping coefficient is equal to or just larger than the required damping coefficient as determined in section 4.4. If the right-hand side's damper scaling factor reached its maximum value then the left-hand side is increased until the required roll damping is found. If both sides reach the maximum damper scaling factor then the damping is kept high for the left and right struts. This is done for both the front and rear axles separately, and the opposite side is started if the roll rate is negative.

With this method, it is also possible to control a continuously variable suspension system, such as a continuously variable damper or spring. Since the model predictive controller does not take into consideration the explicit hard constraints of the suspension system, this method is classified as a sub-optimal controller, although the results may still be satisfactory.

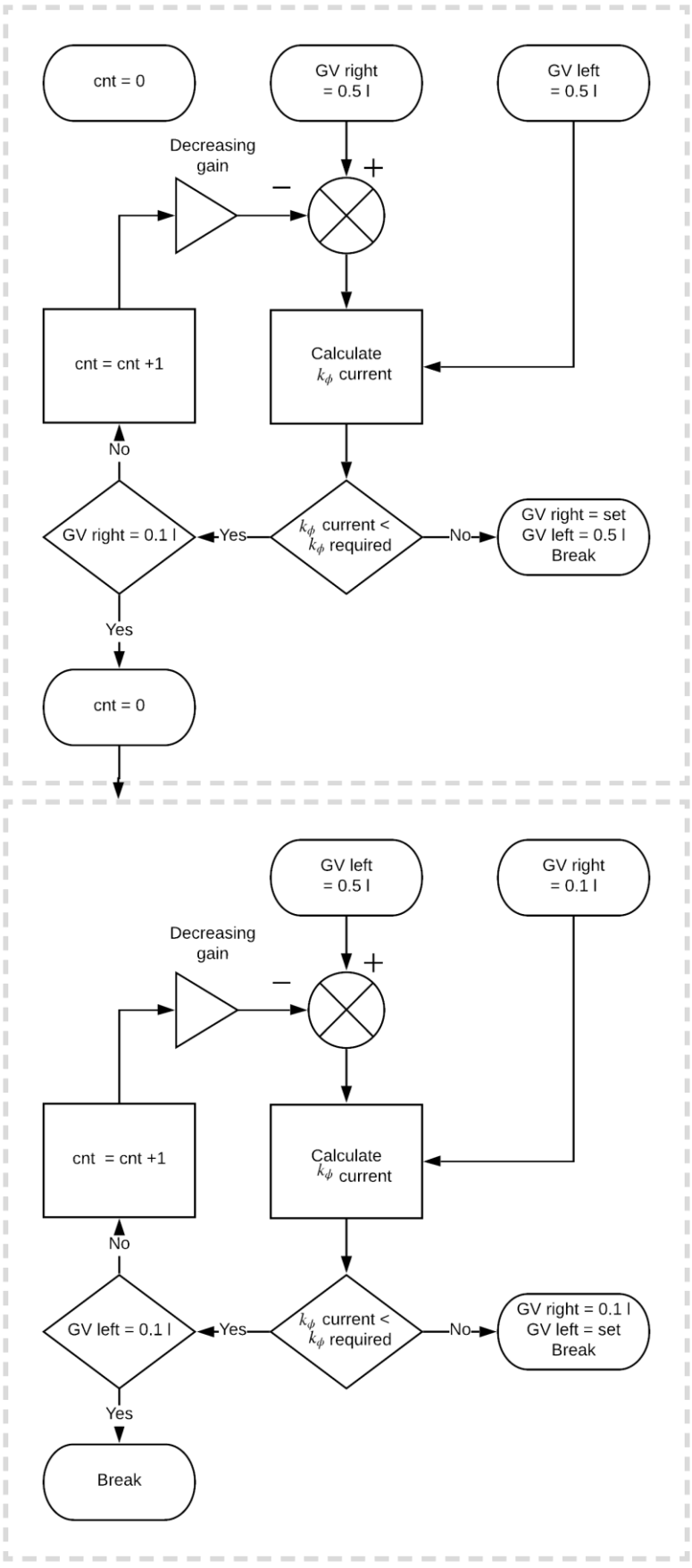

Figure 27: Determining gas volume spring setting for a left-hand turn

4.6. Simulink implementation

For the simulation work co-simulation between the multibody dynamics software MSC Adams (MSC Software, 2018) and Matlab and Simulink (MathWorks, 2018) is used to simulate the validated fully non-linear model of the vehicle. The controller is implemented in Simulink by making use of Matlab function blocks.

Since the physical semi-active suspension system used on the vehicle has two discrete damping and two discrete spring settings the controller needs to be further simplified. This was done in the Simulink model after the spring and damper characteristics have been calculated as described in section 4.5 by passing these settings through a Simulink relay block.

The relay block switches the spring setting (SS) to high (SS=1)(stiff spring with 0.1l accumulator gas volume) when the calculated gas volume decreased below 50% (or 0.25l) of the original 0.5l soft spring accumulator volume. The spring then only switches back to the soft spring setting (SS=0) until the calculated gas volume increases above 70% (or 0.35l) of the 0.5l. The relay block used for the damper setting (DS) was set to high (DS=1)(high damping with a scaling value of 2.0) when the calculated damping setting increased above a setting of 1.2. The damper setting is then only returned to the soft setting (DS=0) (low damping with a scaling value of 0.25) when the calculated damper scaling factor decreases below 0.8. These high and low values are used to change the characteristics of the functions that are used in the simulation to represent the spring and damper forces. A schematic of the process is shown in figure 28.

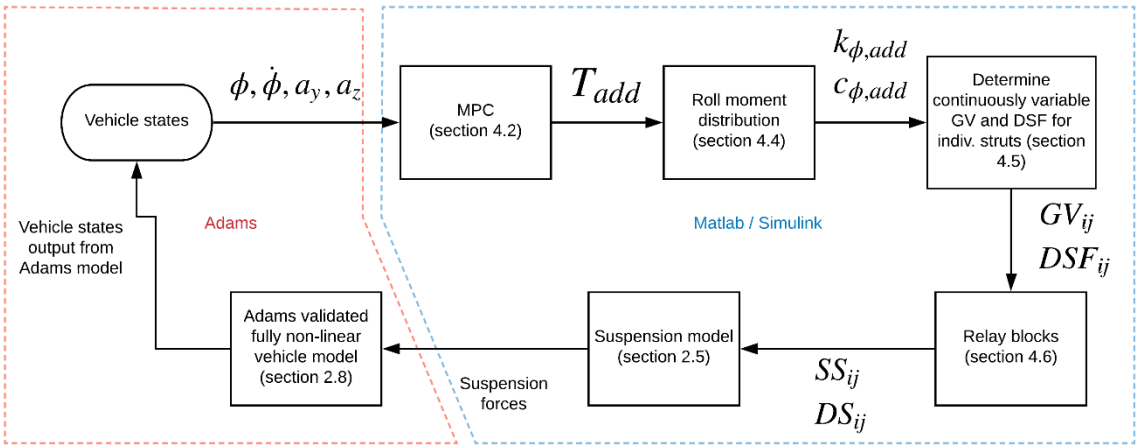

Figure 28: Simulation process schematic

4.7. Conclusion

By setting up the vehicle's dynamic equations to consider the roll dynamics, a discretised linearized time-invariant state-space equation is developed. The state-space model is used in the model predictive controller through the batch approach by making use of the linear quadratic regulator and receding horizon theories to determine the torque input needed for the vehicle to make the system stable. A combined rollover and ride comfort metric was used to determine the input weighting for the controller. By making use of the roll moment

distribution and considering the understeer gradient of the vehicle the individual suspension spring and damper settings were found and used to switch the individual suspension struts. The controller needs to be validated through simulation and experimental testing to confirm the performance in handling manoeuvres and ride comfort scenarios.

5. Controller validation in simulation

The performance of the designed controller can be validated through simulations. The handling manoeuvres were simulated through the double lane change at speeds of 50 km/h, 60 km/h, 70 km/h and 80 km/h. The robustness of the controller to not switch to the handling mode while traversing over a rough track such as the Belgian paving is also simulated. The performance of the controller is also compared to the existing baseline RRMS control strategy of Els (2006) as discussed in section 2.5.3.

5.1. Handling manoeuvres

We expect the roll angle and roll rate of the MPC controlled suspension to be lower than the soft suspension but still higher than the hard suspension in simulation. This is due to the fact that the controller stays in ride comfort mode for the low dynamic parts of the manoeuvres and only once the dynamics get more severe the controller switches to handling mode in an attempt to minimise the propagation of the roll angle and roll velocity. Figures 29 and 30 show the difference between the roll angle and roll rates of the different runs and the switching commands for each of the springs and dampers respectively. A switch value of 1 corresponds to a harder spring setting or higher damper setting. The results for the 60 km/h DLC, superimposed on the rollover and ride comfort metric map is shown in figure 31. The rest of the maps for the other runs are included in appendix B.

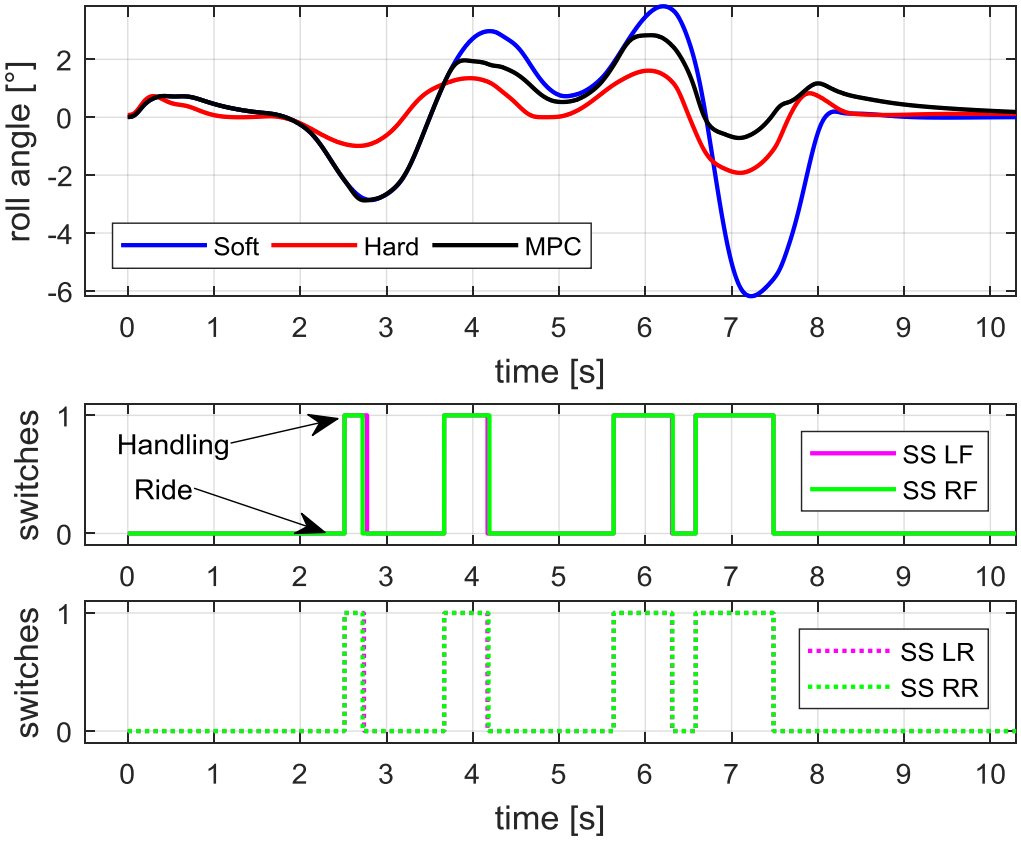

Figure 29: 60 km/h DLC roll angle and spring setting switching simulation data comparison

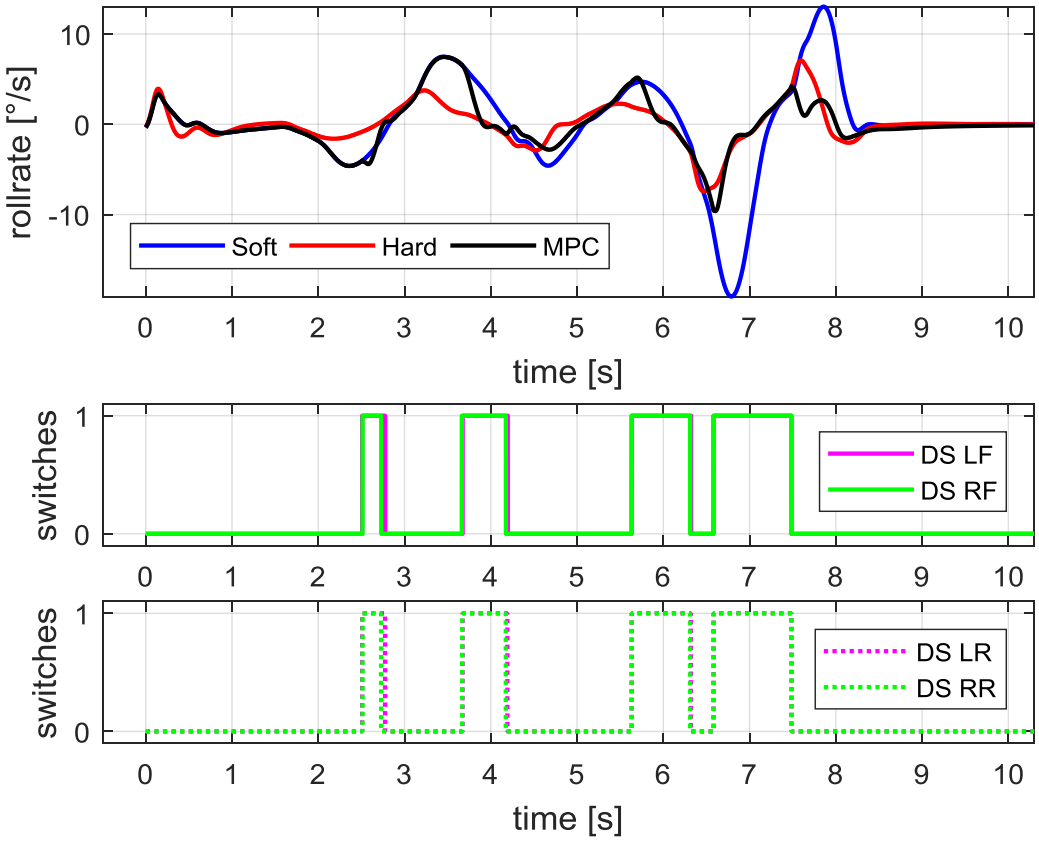

Figure 30: 60 km/h DLC roll rate and damper switching simulation data comparison

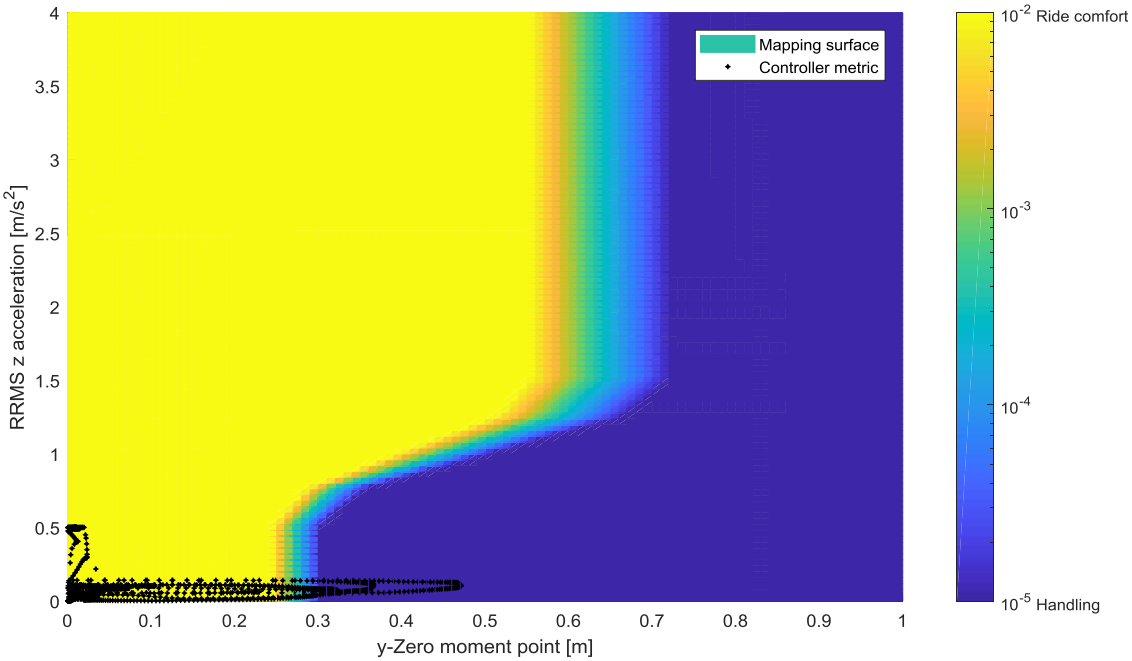

Figure 31: 60 km/h DLC simulation rollover metric

From the results, we can see that the MPC controller did, in fact, reduce the maximum roll angle as compared to the soft suspension setting. The maximum peak of the roll rate is also reduced as compared to the roll rate of the soft suspension. It is interesting to see that the

suspension only switches to a harder setting once the vehicle is in the most critical parts of the manoeuvre for the 60 km/h DLC. The results for the 80 km/h DLC is presented in figures 32 and 33 and here we can see that the suspension stays in the handling mode for longer.

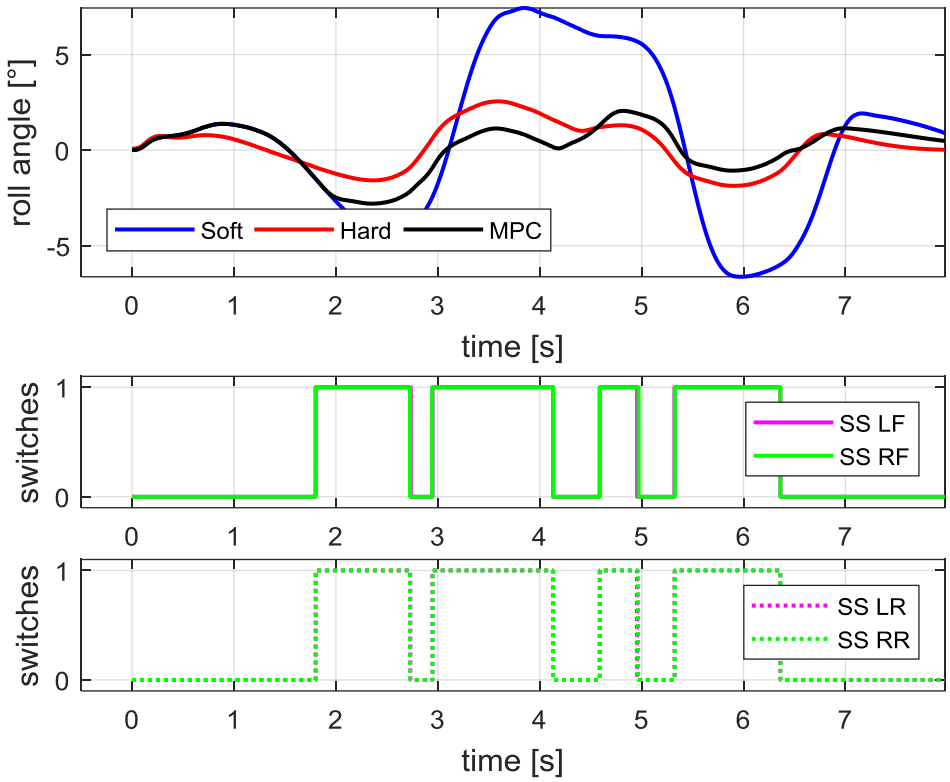

Figure 32: 80 km/h DLC roll angle and spring setting switching simulation data comparison

It's also interesting to see that for the lower speed 60 km/h handling manoeuvre just before 3 seconds only the left-hand side's suspension spring setting is set to the handling mode as the controller determines that switching only those to a harder setting will be sufficient to keep the vehicle safe. On the other hand, for the higher speed 80 km/h run both the left and right-hand side's springs are set to the handling mode at the same time, which makes sense since the high dynamics of the vehicle would ask of the controller to deploy all the effort to reduce the rollover.

The additional roll torque required from the MPC controller calculation is presented graphically in appendix C for the double lane change at different speeds. The maximum available additional roll torque from the suspension system, the achievable additional roll torque from a continuously variable suspension system and achievable roll torque from the discrete system are presented which shows the sub-optimality of the controller described in section 4.5.

For all the runs the percentage of decrease in the RMS of the roll angle and roll rate of the controlled suspension as compared to the soft suspension for all of the speeds are shown in Table 6. Also in Table 7 the percentage of time in handling mode for the manoeuvre for each of the springs and dampers are shown. The time in handling shows the controller's level of effort where we can see that for more severe handling manoeuvres a higher effort is required from the controller.

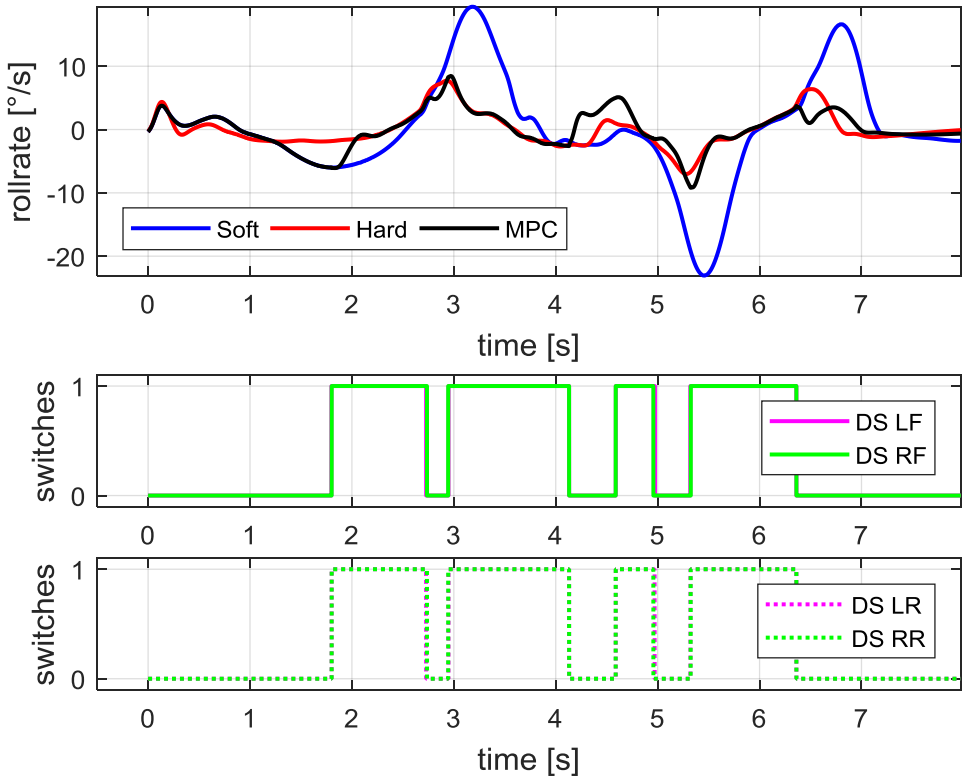

Figure 33: 80 km/h DLC roll rate and damper switching simulation data comparison

Table 6: DLC simulation roll angle and roll rate improvements with the controller

Speed [km/h]	Suspension setting	Roll angle RMS [°]	% roll angle RMS improvement	Roll rate RMS [°/s]	% roll rate RMS improvement
50	Soft	1.51	20.6	3.00	20.0
	Controlled	1.20		2.40	
60	Soft	2.22	41.9	5.05	45.8
	Controlled	1.29		2.74	
70	Soft	2.53	51.7	5.15	46.6
	Controlled	1.22		2.75	
80	Soft	4.13	69.3	7.97	62.5
	Controlled	1.27		2.99	

Table 7: Time spent in handling through DLC for the simulated controller

	% Time SS LF	% Time SS RF	% Time SS LR	% Time SS RR	% Time DS LF	% Time DS RF	% Time DS LR	% Time DS RR
50	9.9	9.7	9.8	9.7	9.8	9.8	9.8	9.8
60	22.8	22.5	22.4	22.4	23.1	22.4	23.1	22.3
70	33.0	33.4	32.9	33.3	33.5	33.2	33.4	33.1
80	44.2	44.3	44.1	44.2	44.4	44.2	44.3	44.3

5.2. Rough roads

To determine if the controller acts as expected on rough roads the simulation is performed over the Belgian paving track at speeds of 21 km/h and 47 km/h. The running root mean square of the vertical accelerations are used to compare the soft suspension and the controlled suspension simulations in figures 34 and 36. For this test, the controller should ideally stay in ride comfort mode for the entire duration. Again the maps that indicate the rollover and ride comfort metric are shown in figures 35 and 37.

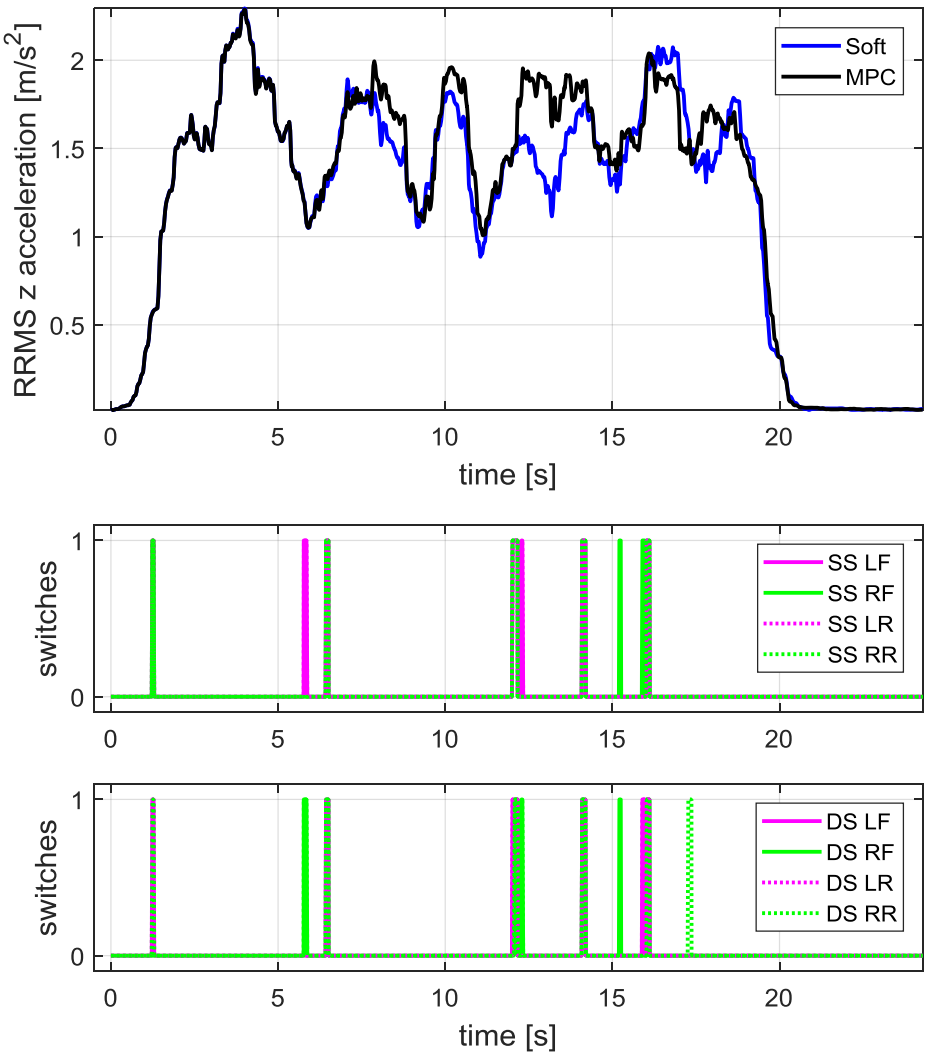

Figure 34: 21 km/h Belgian paving vertical acceleration RRMS with simulated MPC controller

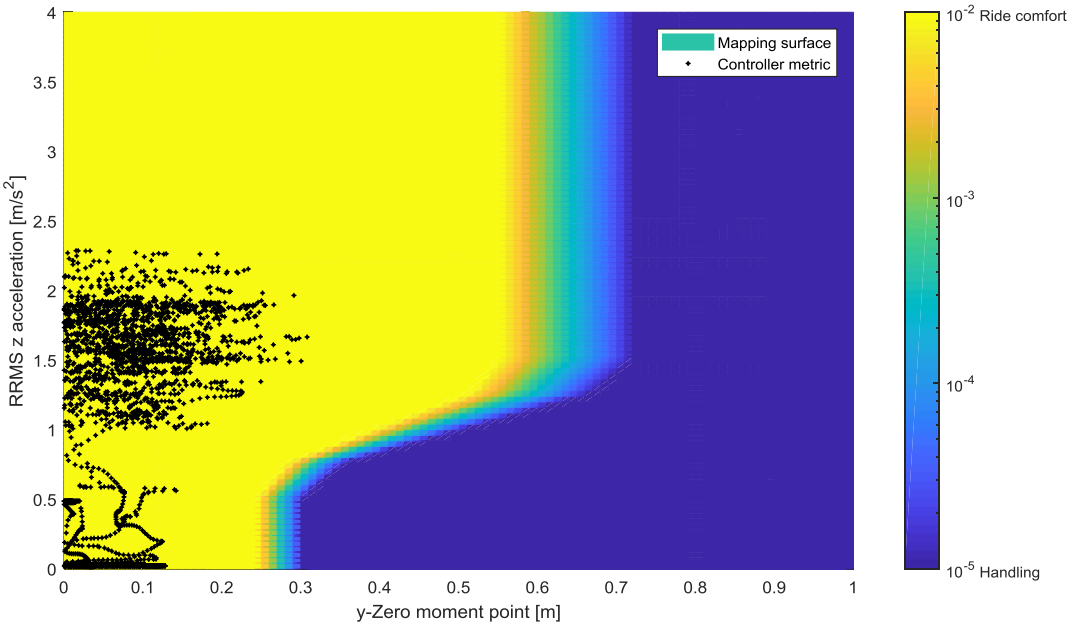

Figure 35: 21 km/h Belgian paving simulation rollover metric

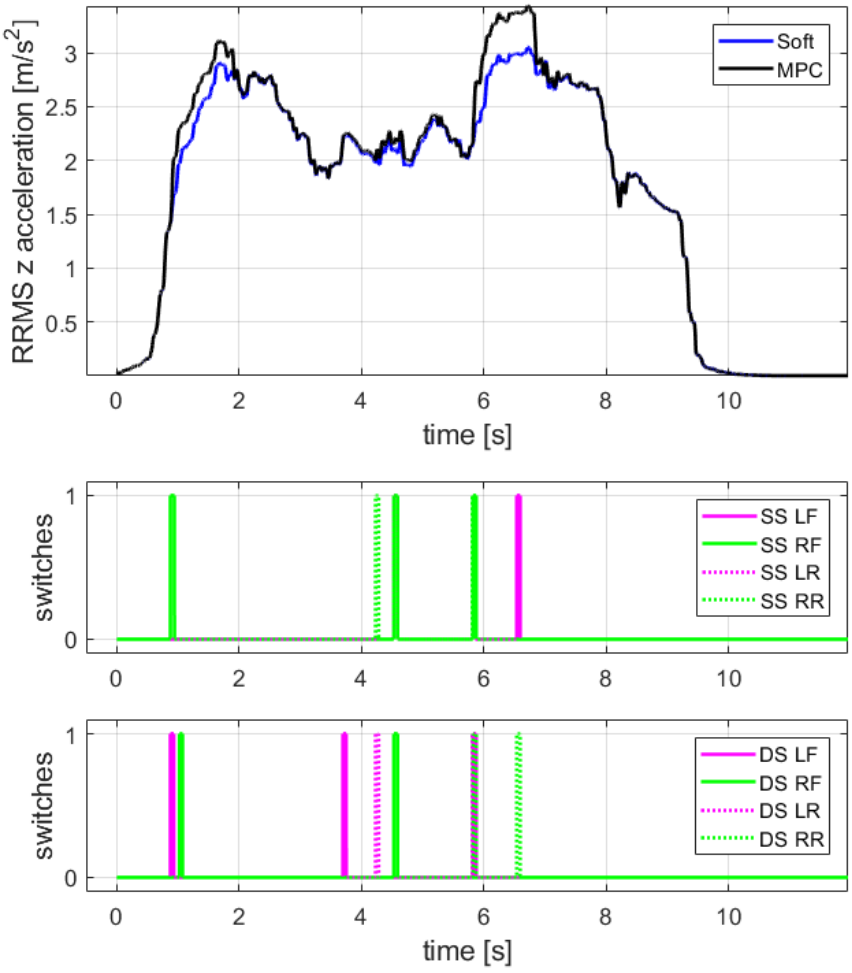

Figure 36: 47 km/h Belgian paving vertical acceleration RRMS with simulated MPC controller

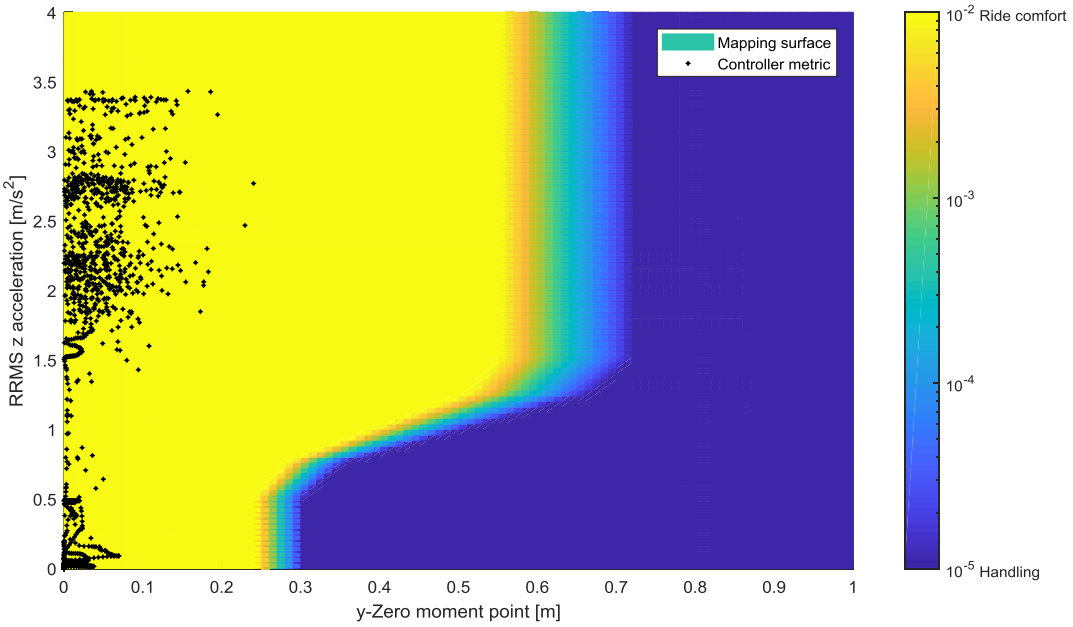

Figure 37: 47 km/h Belgian paving simulation rollover metric

The BS6841 vertical acceleration weighted RMS (British Standards Institution, 1987) and unweighted RMS values are also reported in Table 8 as well as the time spent in handling mode in Table 9.

Table 8: Percentage difference in vertical acceleration RMS values on Belgian paving in simulation

Speed [km/h]	Controller	Unweighted vertical acceleration RMS [m/s^2]	% difference unweighted	Weighted vertical acceleration RMS [m/s^2]	% difference weighted
21	Soft	1.36		1.10	
	MPC	1.42	4.2	1.15	4.3
47	Soft	1.98		1.81	
	MPC	2.07	4.3	1.87	3.2

Table 9: Time spent in handling on Belgian paving for simulated controller

Speed [km/h]	Controller	% Time SS LF	% Time SS RF	% Time SS LR	% Time SS RR	% Time DS LF	% Time DS RF	% Time DS LR	% Time DS RR
21	MPC	2.7	2.6	2.6	2.1	2.4	2.4	2.4	2.8
47	MPC	1.4	1.5	1.0	2.0	1.4	0.9	1.9	1.8

From these results, we can see that the controller experience some challenges in keeping the suspension in ride comfort mode when a rough road is traversed. From the rollover maps, we can confirm that the metric worked well in stating that the suspension should stay in ride comfort mode. For the speeds, it seems that for a higher speed the suspension switches less frequently to the handling mode, which also results in the smaller percentage difference in the vertical acceleration RMS values at higher speeds.

5.2.1. Rough road controller problem identification

After the same switching to handling mode was found in the experimental results (discussed later in section 6) while the vehicle is traversing a rough road it was found that the low cut off torque requirement of 5 Nm was far too small. Even though the input weight of the MPC controller is set so that the suspension should have stayed in ride comfort the output of the controller's torque was higher than the 5 Nm low cut off value and resulted in the switching of the suspension.

In figure 38 the output torque requirement (taken as the absolute value in the figure) of the MPC is plotted with a horizontal line representing the low cut of torque value of 5 Nm for the 47 km/h Belgian paving simulation results, as well as the collective spring setting suspension switches.

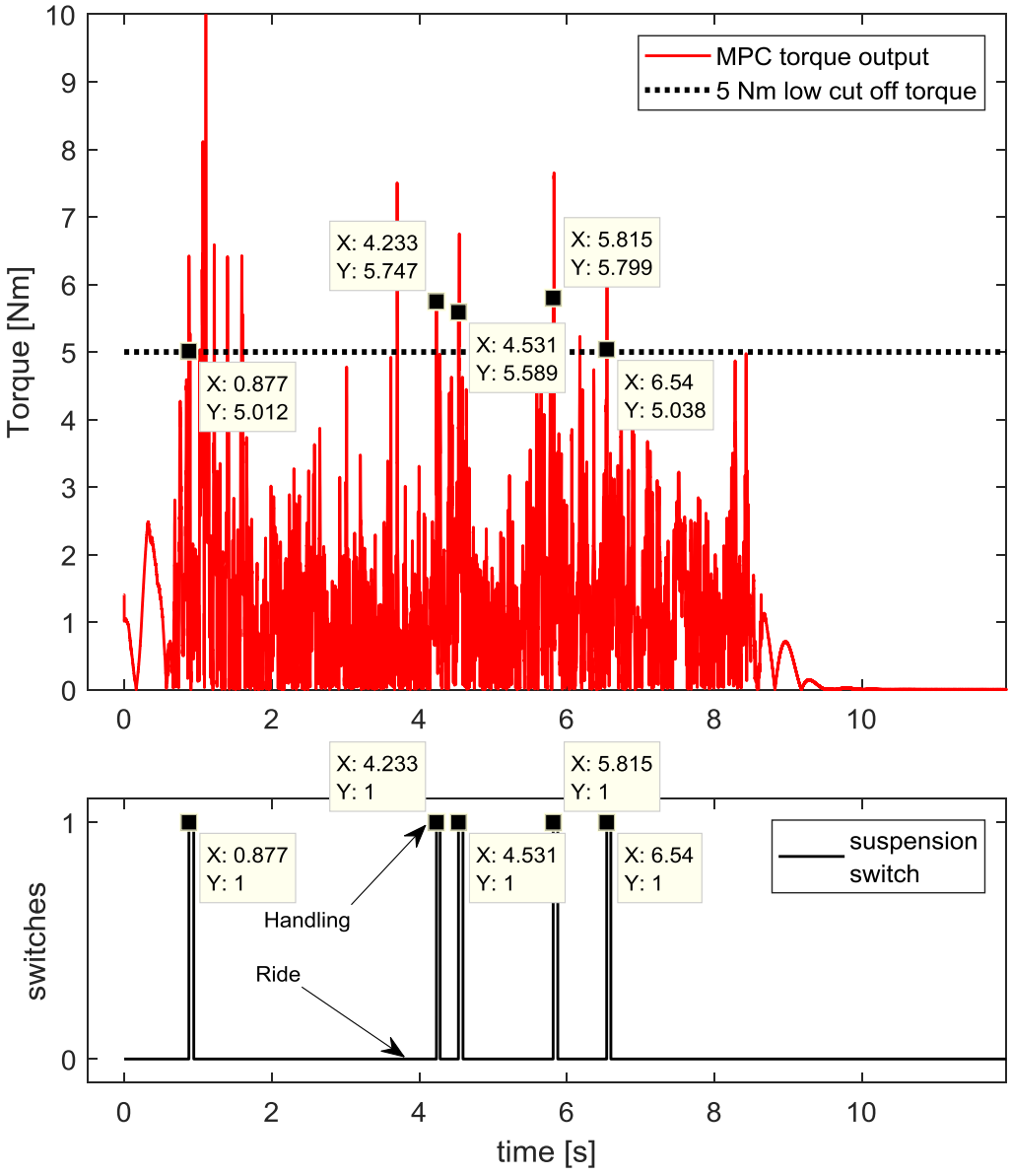

Figure 38: low cut off torque controller issue

In figure 38 we can see that the suspension switches correspond to locations on the MPC torque output where the torque is above 5 Nm. There are other locations where the torque output is higher than the 5 Nm cut off value where the suspension did not switch to the handling mode. This can be attributed to the spring or damper setting being below the buffer value used in the relays in the Simulink model as described in section 4.6, thus the suspension member's spring or damper setting never had to change.

5.3. Comparing MPC controller to baseline RRMS strategy

The roll angle and time spent in handling is used to compare the handling performance of the proposed MPC controller and baseline RRMS strategy, while the vertical RMS acceleration is used to compare the ride comfort performance.

5.3.1. Handling comparisons

In figure 39 the roll angle for the soft, hard, MPC controlled and RRMS strategy controlled suspension setups are shown for the double lane change at 70 km/h. The y zero moment point and vertical and lateral RRMS accelerations are shown as the handling metrics for the MPC and RRMS strategy respectively as well as the suspension spring setting switches. From the figure, we can see that the RRMS strategy switched the suspension to a handling mode earlier, due to the high lateral RRMS acceleration as compared to the vertical RRMS acceleration, and stayed in handling mode throughout the manoeuvre. The MPC controller switched to handling only when the y location of the zero moment point exceeded the predefined limits of +/- 0.27m as explained in section 4.3. If we consider the roll angle we can see that the RRMS strategy kept the roll angle very close to the hard suspension's roll angle throughout the handling manoeuvre, while the MPC controlled suspension's roll angle was larger. For a comparison at 50, 60 and 80 km/h double lane changes see appendix D.

The results of the RMS roll angle and RMS roll rate and per cent improvement over the soft suspension is shown in Table 10 for the double lane change at speeds of 50, 60, 70 and 80 km/h. The time spent in handling mode (for the spring settings) is also shown in Table 11.

Table 10: DLC simulation roll angle and roll rate improvements with controller and baseline controller

Speed [km/h]	Suspension setting	Roll angle RMS [°]	% roll angle RMS improvement	Roll rate RMS [°/s]	% roll rate RMS improvement
50	Soft	1.51		3.00	
	MPC	1.20	20.6	2.40	20.0
	RRMS strategy	0.58	61.7	1.42	52.6
60	Soft	2.22		5.05	
	MPC	1.29	41.9	2.74	45.8
	RRMS strategy	0.81	63.4	2.11	58.3
70	Soft	2.53		5.15	
	MPC	1.22	51.7	2.75	46.6
	RRMS strategy	1.08	57.3	2.33	54.9
80	Soft	4.13		7.97	
	MPC	1.27	69.3	2.99	62.5
	RRMS strategy	1.36	67.0	2.67	66.4

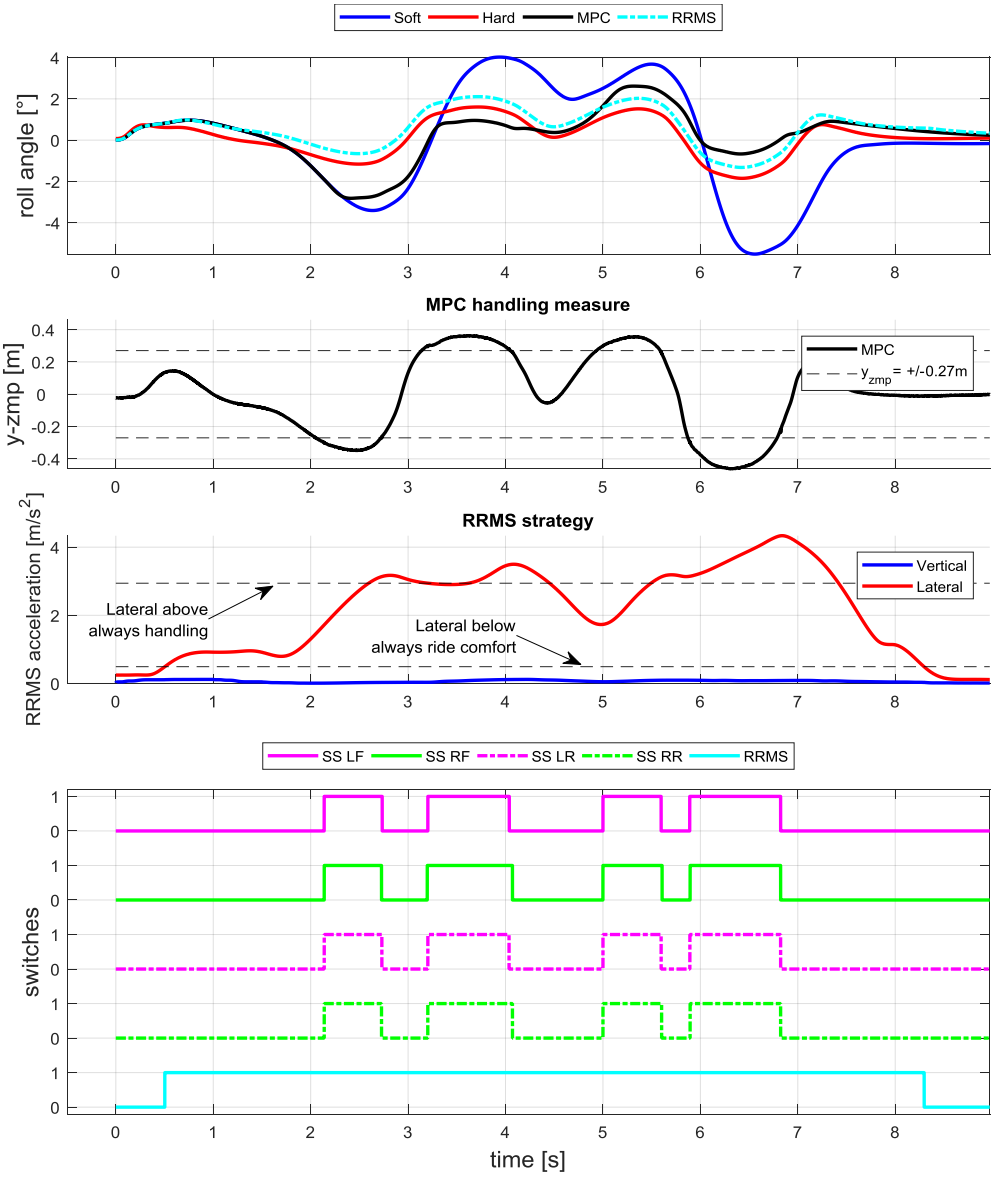

Figure 39: MPC vs baseline RRMS 70 km/h DLC handling comparison

Overall the RRMS strategy performed better in the roll angle and roll rate aspects, especially at low speeds. At higher speeds and higher lateral forces, the two controllers performed similarly. Although the MPC controller performed worse than the RRMS strategy at low-speed handling manoeuvres the controller still performed as expected and designed seeing that the suspension was set to a handling mode when the y location of the zero moment point crossed the defined point used in the handling metric of +/-0.27m for low vertical acceleration inputs.

Table 11: Time spent in handling through DLC for the simulated controller and baseline controller

	Suspension setting	% Time SS LF	% Time SS RF	% Time SS LR	% Time SS RR
50	MPC controlled	9.9	9.7	9.8	9.7
	RRMS strategy controlled	54.9	54.9	54.9	54.9
60	MPC controlled	22.8	22.5	22.4	22.4
	RRMS strategy controlled	76.8	76.8	76.8	76.8
70	MPC controlled	33.0	33.4	32.9	33.3
	RRMS strategy controlled	86.9	86.9	86.9	86.9
80	MPC controlled	44.2	44.3	44.1	44.2
	RRMS strategy controlled	93.6	93.6	93.6	93.6

5.3.2. Ride comfort comparisons

In figure 40 we can see the RRMS z acceleration as the vehicle traversed the Belgian paving at 47 km/h for the soft, MPC and RRMS suspension control strategy as well as the metrics used in the RRMS strategy to decide between the handling or ride comfort. The spring setting switches are also presented to indicate the switching of the suspension for both the controllers. From the figure, we can see that the RRMS strategy stayed in ride comfort mode for the whole run over the Belgian paving, whereas the MPC controller did switch for a few instances to handling mode based on the issues identified in section 5.2.1. The figure for the 21 km/h run over the Belgian paving is added in appendix D.

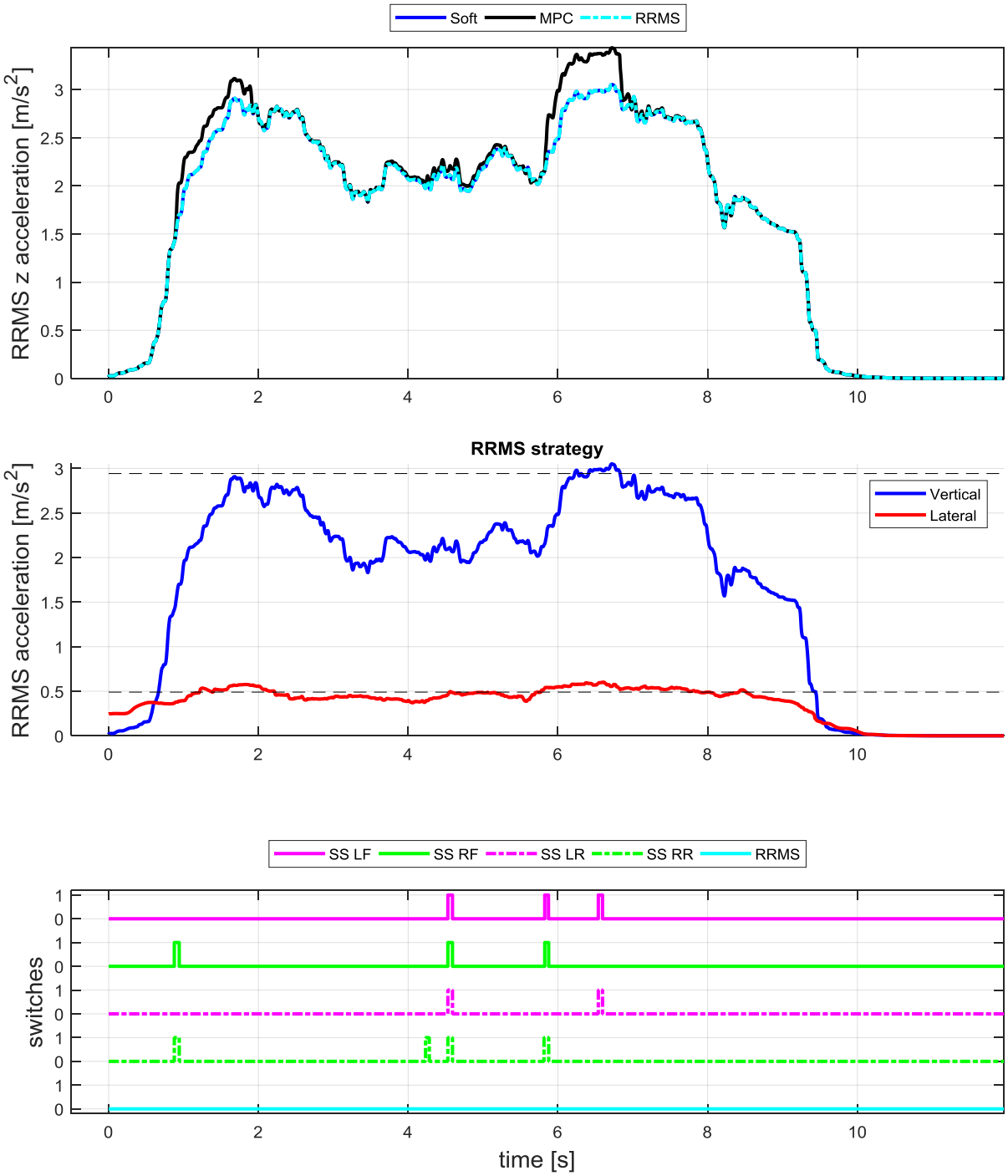

Figure 40: MPC vs baseline RRMS 47 km/h Belgian paving ride comfort comparison

From this, we can conclude that the RRMS strategy to control the ride comfort of the suspension over a rough road is better than the proposed MPC controller.

5.4. Conclusion

From the simulations, we can conclude that the handling aspect of the controller works well with the controller decreasing the roll angle the vehicle experience by 20% to 69% and decreasing the roll rate by 20% to 62% as compared to the soft suspension. It's also noted that the rollover and ride comfort metric worked well in establishing the presence of an emergency manoeuvre.

The controller's performance over the rough Belgian paving was not as good since the suspension switched multiple times to the handling mode, which in the simulation environment resulted in a decrease of the ride comfort which is observed through the weighted and unweighted vertical acceleration RMS values. If we considered again the rollover and ride comfort metric we can see that the vehicle didn't find itself in a handling manoeuvre at all and that the suspension should have stayed in ride comfort through the simulation.

The performance of the MPC controller is similar to the performance of the RRMS control strategy used by Els (2006) at high-speed handling manoeuvres with higher lateral accelerations. At lower speeds and lateral accelerations, the RRMS strategy switched the suspension system more often to the handling mode than the MPC controller. The RRMS strategy also performed better on rough roads by keeping the suspension in ride comfort mode over the Belgian paving, whereas the MPC controller had instances when the suspension switched to handling mode.

6. Experimental controller validation

With the controller performing as expected in simulation (section 5) the controller can be implemented on the test vehicle with the necessary measurement instrumentation and the semi-active suspension system to validate the real performance of the system. For this, the double lane change was again used to test handling performance in a severe handling manoeuvre. The Belgian paving was used to validate the reliability of the controller to stay in ride comfort mode.

Additional tests were performed on the Belgian paving track such as driving with one side of the vehicle on the smooth road and the other side on the Belgian paving track as well as a single lane change from the Belgian paving track on to the smooth road. The dynamic handling track was also used to investigate the dynamics of the vehicle in a performance-oriented environment while a section of the rough track at Gerotek was driven to represent a more real-life rough road driving experience with some handling manoeuvres included.

Experimental tests need to be performed to validate the performance of the controller in controlled real-world conditions. The effects of measurement noise, varying valve response times and friction in the suspension system is not present in the simulation environment and need to be tested against to ensure the controller will work under real-world conditions.

6.1. Handling manoeuvres

For this section, the handling of the vehicle is compared to the soft and hard suspension settings. Two maps for the rollover and ride comfort metric is used here, with the first (referred to as the MPC controller) being the same as the one described in section 5, and the second more aggressive (referred to as the a-MPC controller) map shown in figure 41, overlaid on top of the MPC controller. All the metric maps for all the runs are included in appendix E if not presented in this chapter.

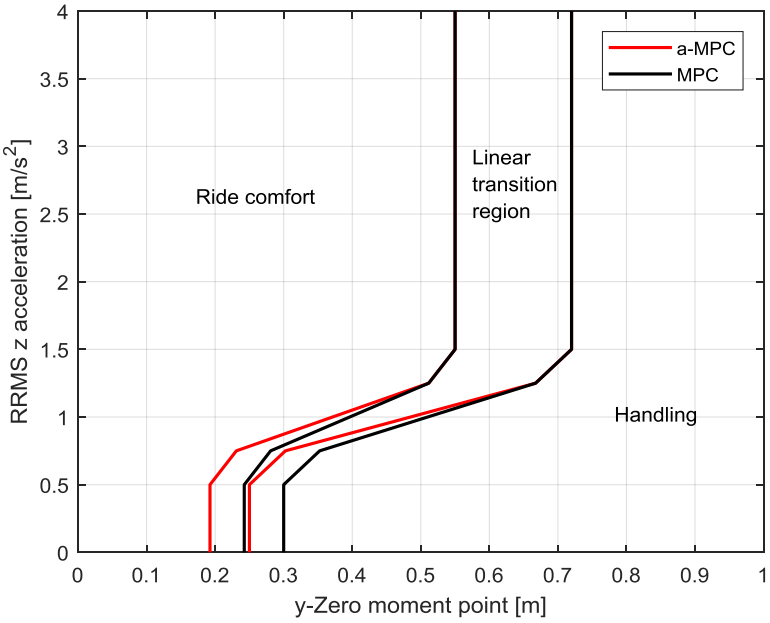

Figure 41: MPC vs a-MPC rollover and ride comfort metric map comparisons

6.1.1. Double lane change

The roll angle and roll rate is used to compare the performance of the normal MPC controller against the hard and soft suspension settings directly at 70 km/h in figures 42 and 43 together with the switching of the suspension's damper and spring. In figure 44 the rollover ride comfort metric map is shown for the MPC controller.

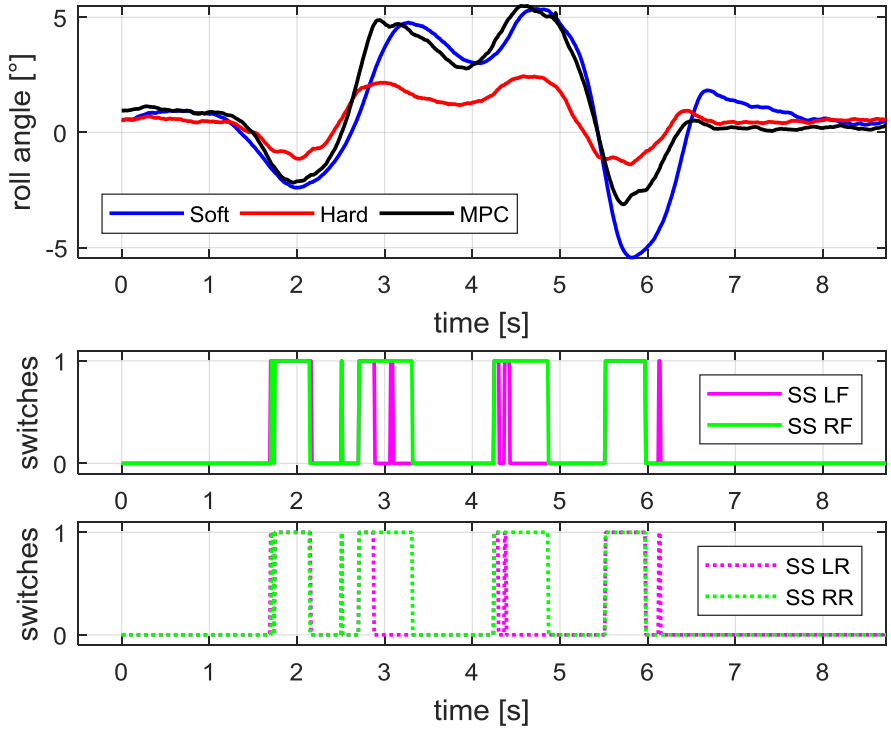

Figure 42: 70 km/h DLC roll angle experimental MPC data comparison

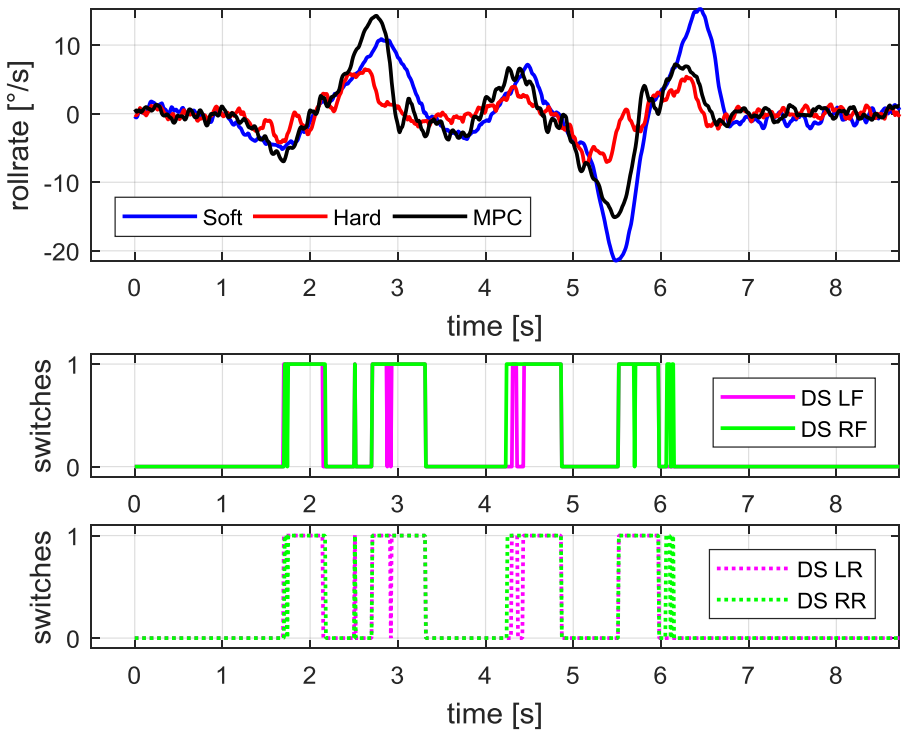

Figure 43: 70 km/h DLC roll rate experimental MPC data comparison

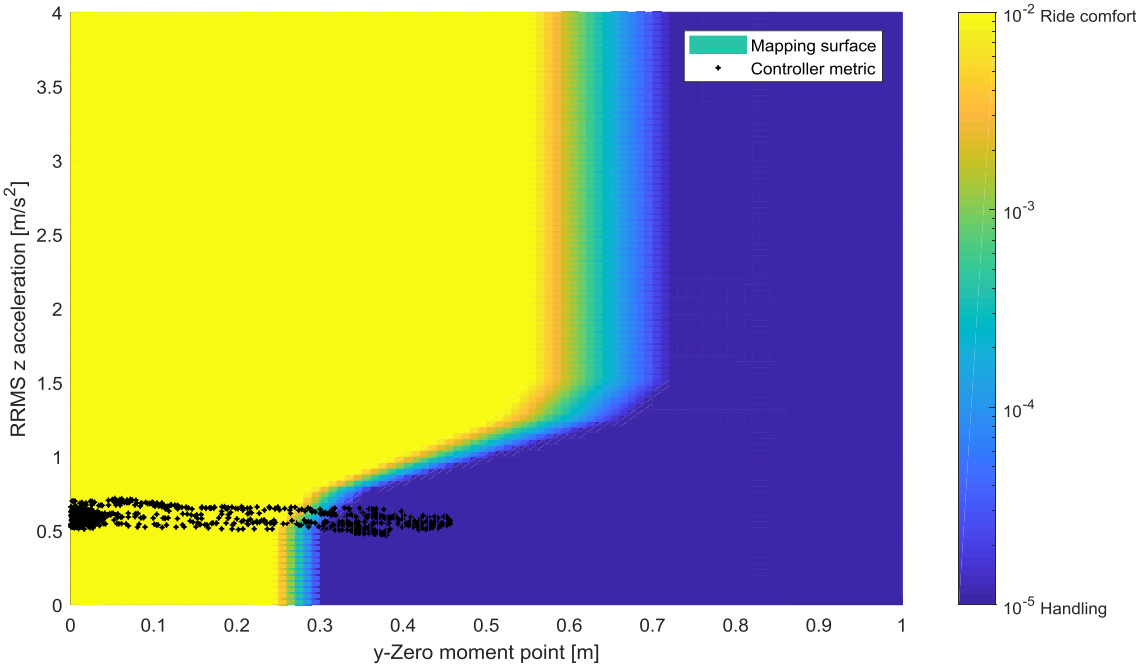

Figure 44: 70 km/h DLC MPC experimental metric map

From the figures, we can see that the normal MPC controller failed to reduce the roll angle of the vehicle significantly as compared to the soft suspension setting at 70 km/h. The roll rate was reduced by a small amount. We can also see that the crossover region from ride comfort to handling on the rollover ride comfort metric map was at a higher vertical acceleration RRMS value as compared to the simulation results shown in figure 44.

Table 12: DLC experimental roll angle and roll rate improvements with controllers

Speed [km/h]	Suspension setting	Roll RMS [°]	% roll RMS improvement	Roll rate RMS [°/s]	% roll rate RMS improvement
50	Soft	1.69		2.21	
	Hard	0.82	51.3	1.18	46.5
	Controlled MPC	1.48	12.7	2.16	2.1
	Controlled a-MPC	1.25	26	1.98	10.1
60	Soft	2.29		4.42	
	Hard	0.82	64.1	1.71	61.2
	Controlled MPC	1.74	24.2	2.96	33
	Controlled a-MPC	1.5	34.4	2.46	44.4
70	Soft	2.65		5.81	
	Hard	1.09	59.1	2.23	61.6
	Controlled MPC	2.48	6.4	4.83	16.9
	Controlled a-MPC	1.79	32.7	3.45	40.7
80	Soft	3.43		7.34	
	Hard	1.33	61.3	3.7	49.6
	Controlled MPC	3.07	10.3	5.87	20
	Controlled a-MPC	2.26	34	4.2	42.8

The per cent RMS roll angle and roll rate improvements are shown in Table 12 for all the runs where the hard setting, normally controlled MPC and more aggressively controlled a-MPC results are compared to the soft suspension results. The time spent in the handling mode for the MPC controlled test for each of the strut's springs and dampers is also reported in Table 13.

Table 13: Time spent in handling through DLC for experimental MPC controller

MPC	% Time SS LF	% Time SS RF	% Time SS LR	% Time SS RR	% Time DS LF	% Time DS RF	% Time DS LR	% Time DS RR
50	1.5	1.6	1.5	1.5	1.5	1.6	1.5	1.6
60	11.3	11.2	9.6	11.1	11.4	11.2	11.4	11.3
70	14.8	24.4	13.5	24.4	22.8	25.4	23.3	25.5
80	17.3	28.7	17.2	28.4	25.9	31.0	26.6	31.0

The more aggressive a-MPC controller's roll angle and roll rate comparisons are shown in figures 45 and 46 again at 70 km/h, together with the suspension switching. In figure 47 the rollover ride comfort metric map is shown for the a-MPC controller.

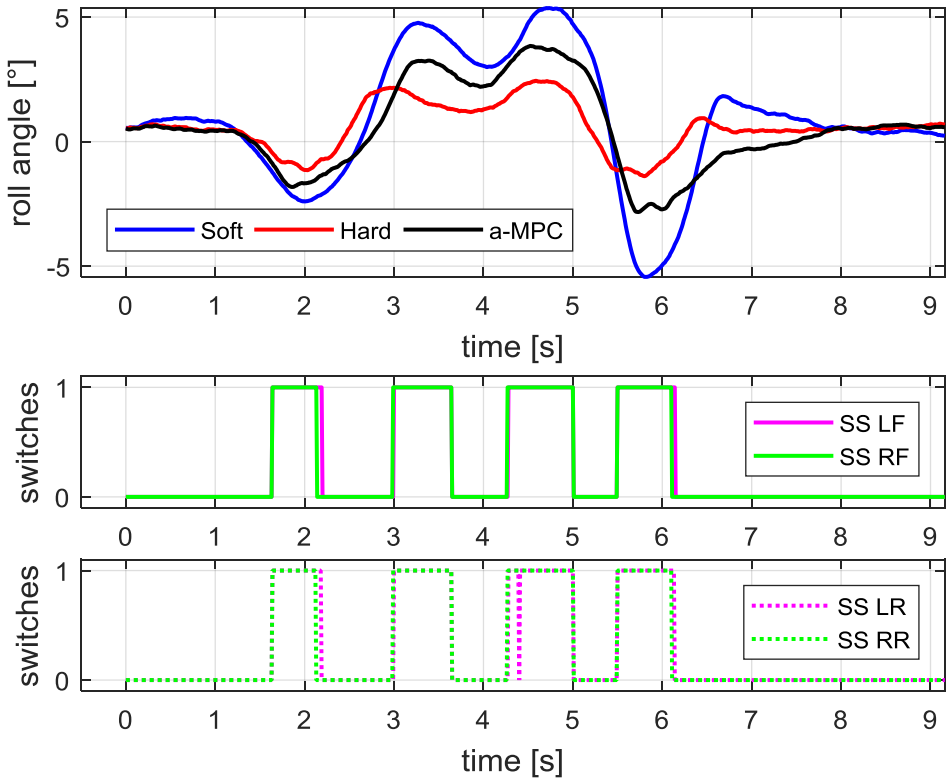

Figure 45: 70 km/h DLC roll angle experimental a-MPC data comparison

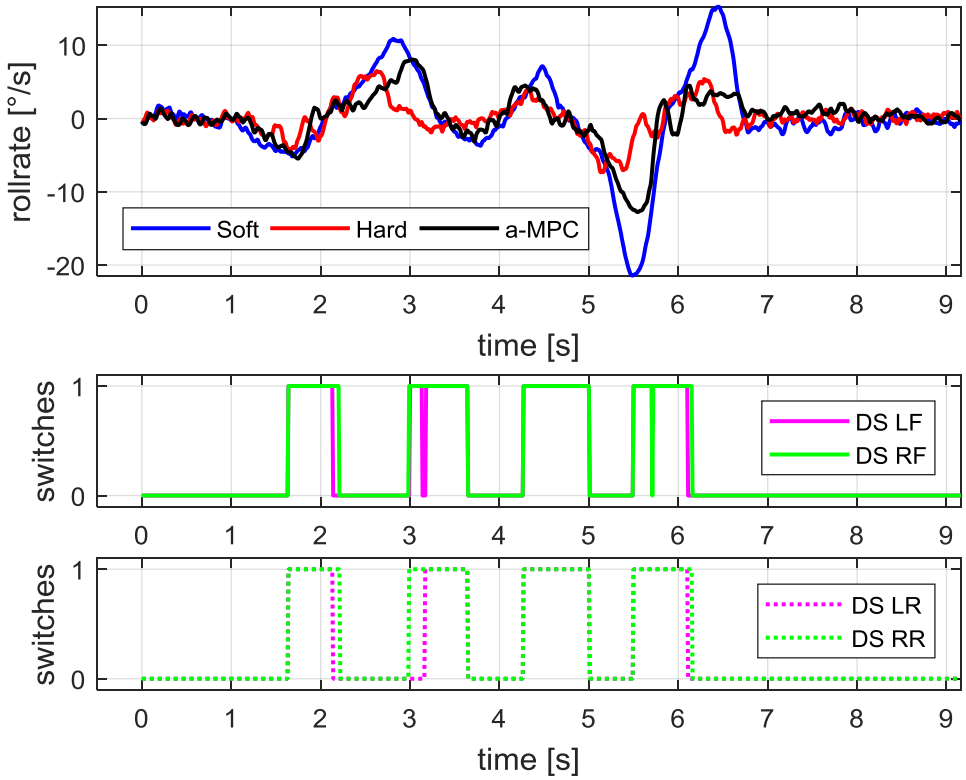

Figure 46: 70 km/h DLC roll rate experimental a-MPC data comparison

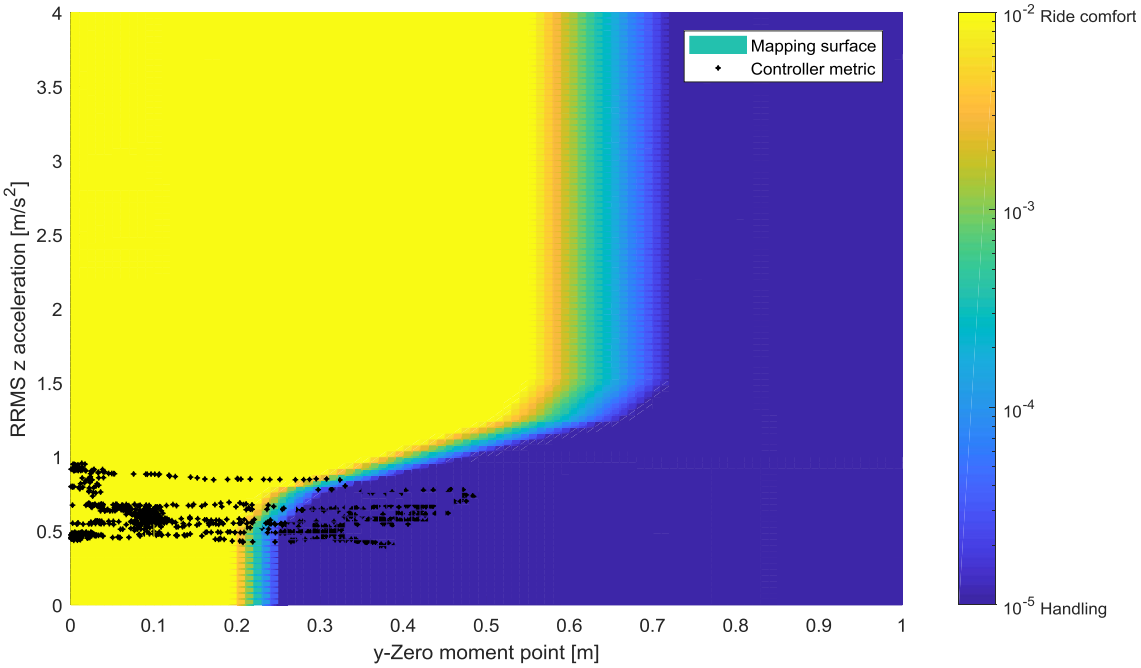

Figure 47: 70 km/h DLC a-MPC experimental metric map

From the results, we can see that the a-MPC controller provides a larger reduction of the roll angle and roll rate over the soft suspension between the two MPC control strategies. Also, from figure 47, we can see that the a-MPC crossed deeper into the handling part of the

metric map which explains the longer times spent in handling mode for the suspension settings. Figure 48 shows the RMS results of Table 12 graphically.

The time spent in the handling mode for each of the strut's springs and dampers for the a-MPC controller is reported in Table 14.

Table 14: Time spent in handling through DLC for experimental a-MPC controller

a-MPC	% Time SS LF	% Time SS RF	% Time SS LR	% Time SS RR	% Time DS LF	% Time DS RF	% Time DS LR	% Time DS RR
50	5.8	5.7	5.8	5.7	5.8	5.7	5.8	5.8
60	20.6	20.1	20.2	20.1	20.1	21.2	20.1	21.4
70	28.2	27.4	27.9	27.3	26.8	28.6	25.4	28.8
80	26.4	32.2	18.5	32.1	32.1	32.6	32.0	32.6

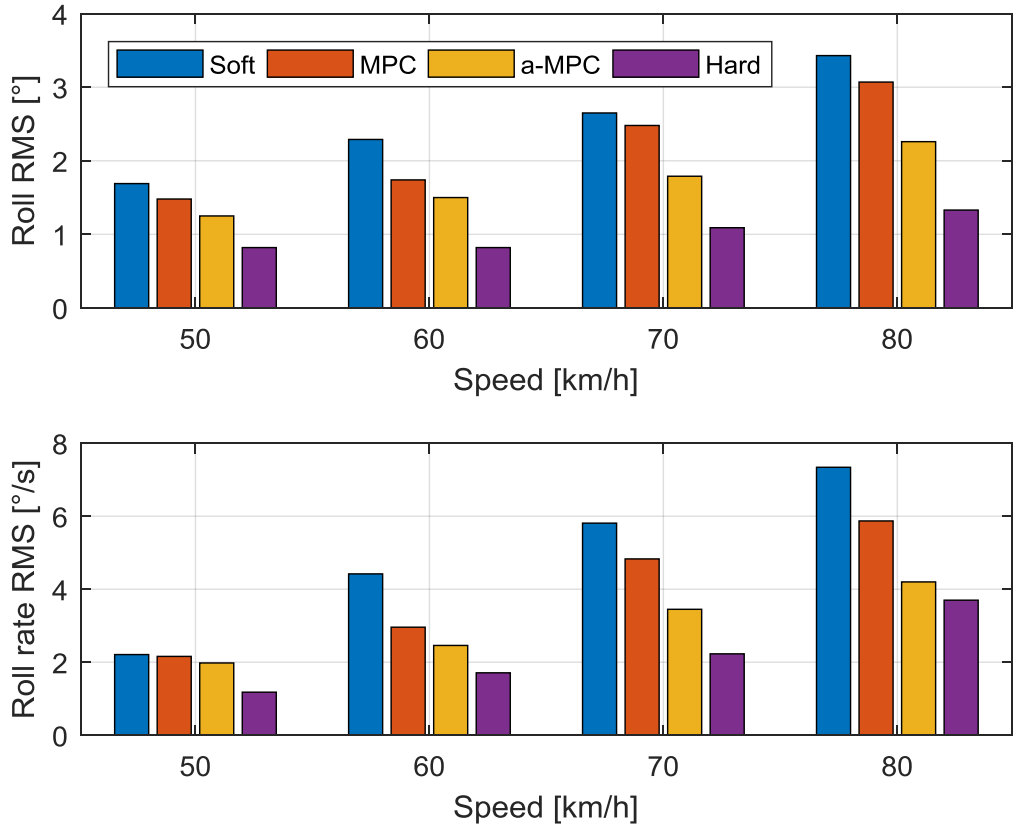

Figure 48: DLC experimental roll angle RMS and roll rate RMS comparisons for controllers

Since the vehicle had to follow the same path through the double lane change, controlled by the driver, for the different runs we can also use the roll angle vs lateral acceleration to compare the performance of the MPC and a-MPC controllers to the soft and hard suspension settings. The roll angle vs. lateral acceleration is shown in figures 49 and 50 for the MPC and a-MPC controllers respectively performing the double lane change at 70 km/h. A straight line is also plotted through the data with a regression method by making use of the minimisation of the error squared between the straight line and the roll angle vs lateral acceleration data. The gradient of the straight line gives us more insight into the resistance

to roll of the different methods. The gradients of the straight lines are reported in Table 15 for the different suspension settings and speeds.

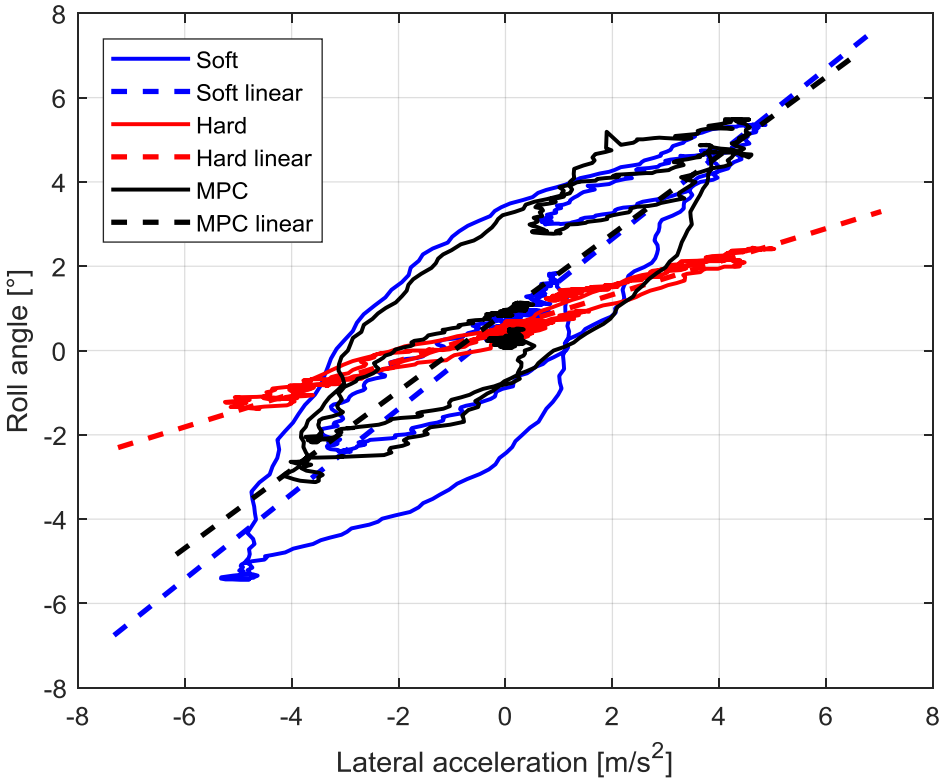

Figure 49: 70km/h DLC roll angle vs. lateral acceleration MPC controller

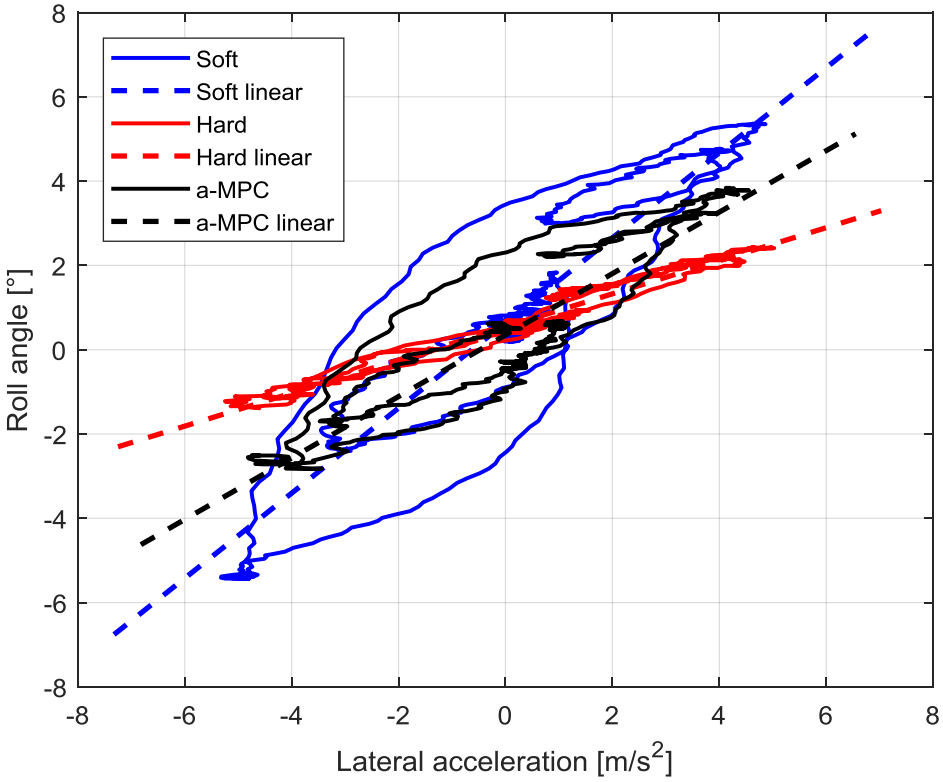

Figure 50: 70km/h DLC roll angle vs. lateral acceleration a-MPC controller

Table 15: DLC experimental roll angle vs lateral acceleration gradient comparisons for controllers

Speed [km/h]	Suspension setting	Roll angle vs lateral acceleration gradient [°/(m/s²)]
50	Soft	0.87
	Controlled MPC	0.85
	Controlled a-MPC	0.73
	Hard	0.38
60	Soft	0.95
	Controlled MPC	0.89
	Controlled a-MPC	0.72
	Hard	0.38
70	Soft	1.01
	Controlled MPC	0.93
	Controlled a-MPC	0.73
	Hard	0.39
80	Soft	1.07
	Controlled MPC	0.98
	Controlled a-MPC	0.80
	Hard	0.39

From these results, we can see that the gradient of the MPC controller is quite close to the soft suspension's gradient, with the MPC controller having a slightly smaller gradient. The a-MPC controller's gradient is significantly lower than the soft suspension's gradient. The lower the gradient the less the vehicle will roll through a handling manoeuvre, thus a good controller should have a low gradient.

As expected the a-MPC had the best improvements for both the roll angle and roll rate. The reason for this is the fact that the a-MPC controller stayed in handling mode for longer. The best situation would have been to have the suspension stay in handling mode for 100 % of the time of the handling manoeuvre. The gradient of the a-MPC controller is also smaller meaning that for the same manoeuvre the vehicle will roll less.

For the sake of comparison, a single straight line fitted through the data is used as described above to compare to the ride comfort, handling and controller test results. The actual effect that we expect from the two control methods is non-linear since the curve that is followed changes based on whether the suspension system is in the ride comfort or handling setting. Based on the suspension system switches the data points corresponding to these switches of the positive and negative lateral acceleration and roll angle is isolated from the ride comfort data points. Straight lines are fitted through the three data sets. Figures 51 and 52 shows the non-linear effect of the suspension system switches for the DLC at 70 km/h for the MPC and a-MPC controllers respectively as compared to the hard and soft suspension settings.

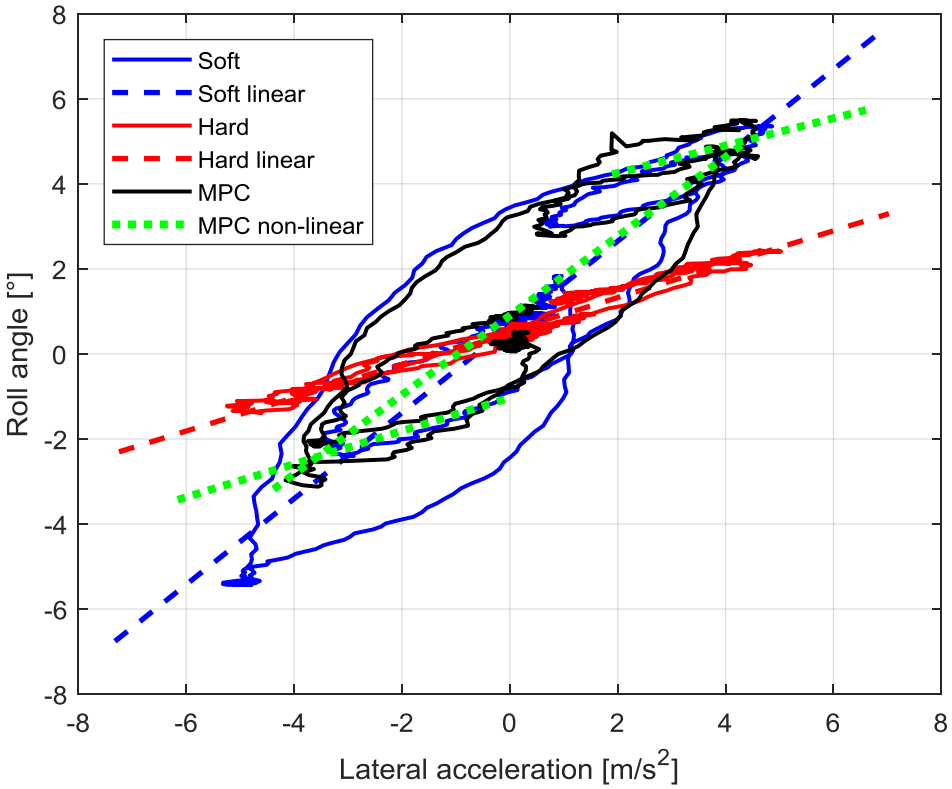

Figure 51: 70km/h DLC roll angle vs. lateral acceleration MPC controller non-linear effect

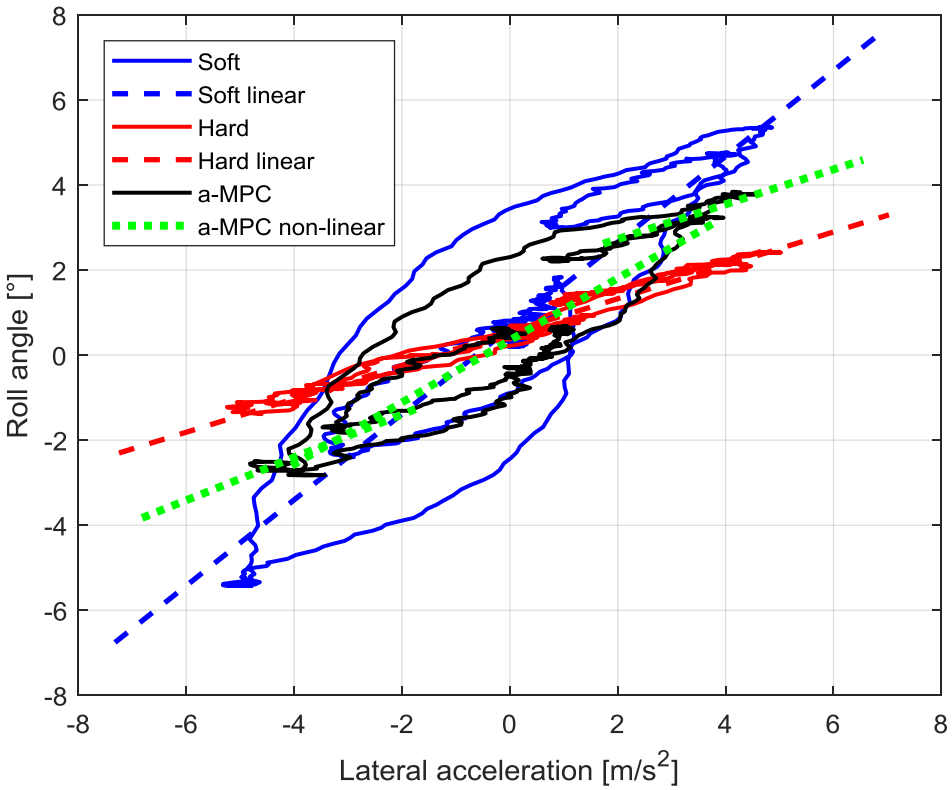

Figure 52: 70km/h DLC roll angle vs. lateral acceleration a-MPC controller non-linear effect

From figures 51 and 52 we can see that, for both the MPC and a-MPC controllers, when the suspension system switches to the handling setting at the higher roll angles and lateral accelerations the linear line's gradient is parallel to the hard suspension settings' line. For the MPC controller, the line's gradient is parallel to the soft suspension setting when the lateral acceleration and roll angles are smaller. The gradient of the a-MPC controller's line is not parallel to the soft suspension's line, for smaller lateral acceleration and roll angles, but somewhere in between the hard and soft setting.

The additional roll torque required from the MPC and a-MPC controller calculations are presented graphically in appendix F for the double lane change at the different speeds. The maximum available additional roll torque from the suspension system, the achievable additional roll torque from a continuously variable suspension system and achievable roll torque from the discrete system are presented which shows the sub-optimality of the controller described in section 4.5.

6.1.2. Dynamic handling track

For this test, the vehicle was driven around the Gerotek dynamic handling track. Each test consisted of an out-lap, a flying lap and an in-lap. The results of the flying lap are used since the start and end velocities should be similar.

In figure 53, the roll angle is shown for the different control settings. From the results, we can see that the controller does reduce the roll angle for some sections on the track, but for others, the roll angle of the controlled run is higher than the soft suspension. After further investigation, it was found that the driver of the vehicle couldn't maintain the same velocity or 'racing line' for all of the runs which resulted in the lateral acceleration of the soft suspension to be lower, which automatically would result in a lower roll angle. The velocities for the runs are shown in figure 54 and the lateral acceleration in figure 55. The roll angle vs lateral acceleration figure, with the linear line fitted through the data, is again used in figure 56 to make some sense of the roll angle propagation for the different suspension settings.

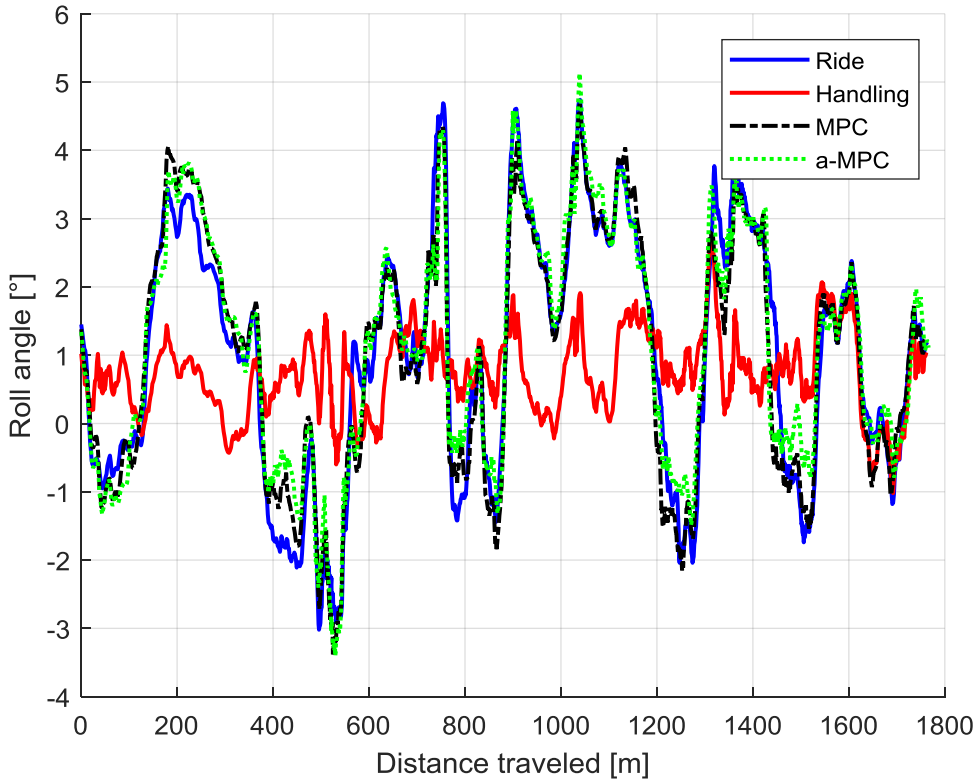

Figure 53: Dynamic handling track roll angle for different suspension settings

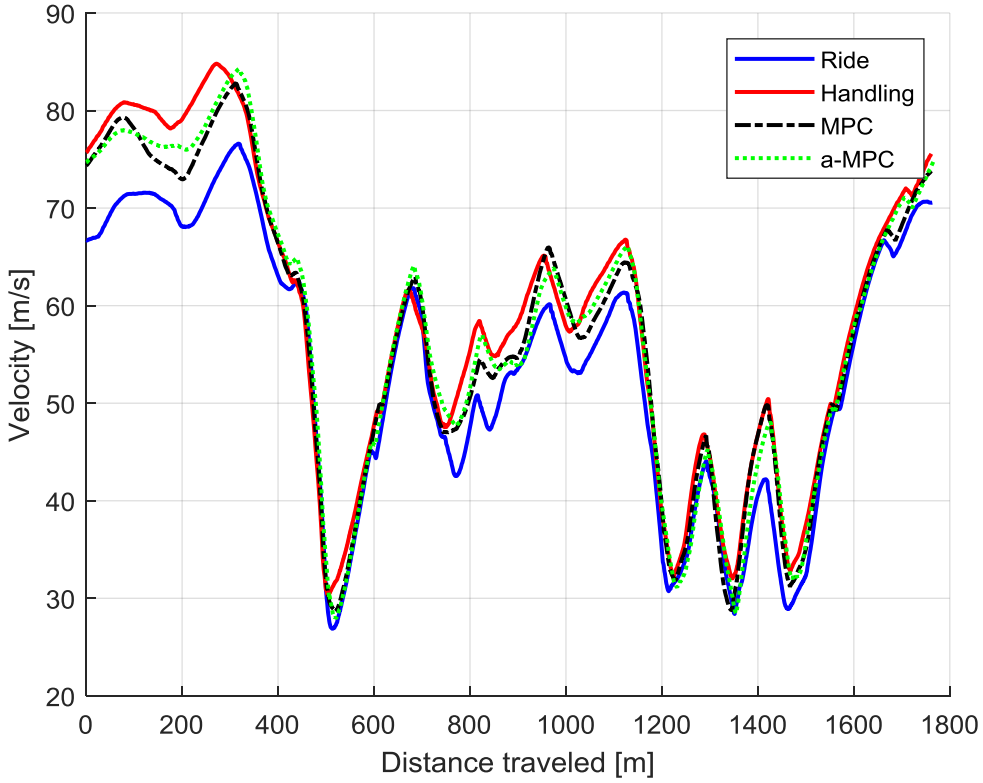

Figure 54: Dynamic handling track vehicle velocity for different suspension settings

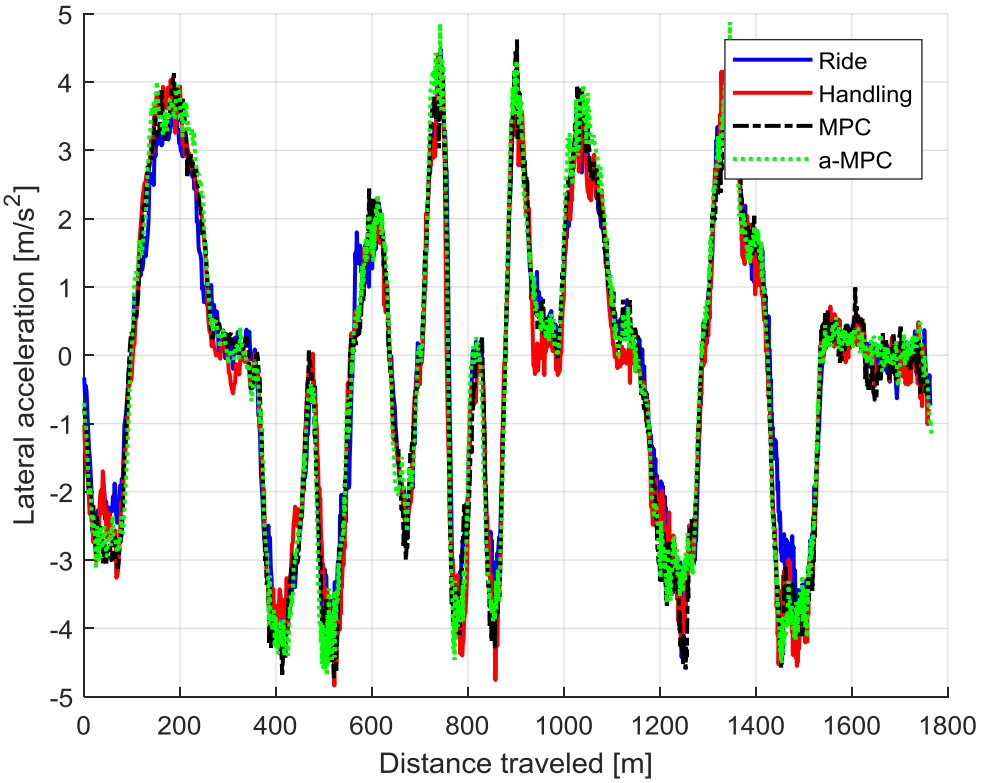

Figure 55: Dynamic handling track lateral acceleration for different suspension settings

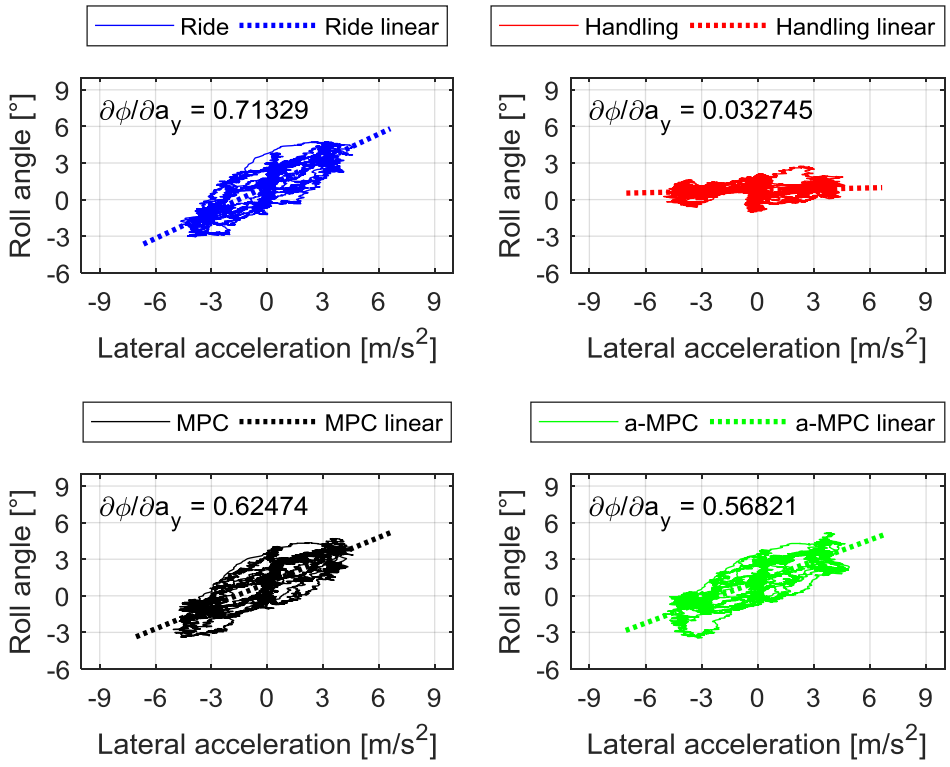

Figure 56: Dynamic handling track roll angle vs. lateral acceleration for different suspension settings

From figure 56 we can see that the two controllers do reduce the roll angle per lateral acceleration on the dynamic handling track as compared to the soft suspension if we consider the gradient of the straight lines fitted through the data points. The a-MPC controller again has the smaller gradient between the two controllers meaning that the a-MPC controller reduced the roll angle the most. The percentage of time spent in handling mode for the MPC and a-MPC runs are shown in Table 16.

Table 16: Time spent in handling on the dynamic handling track for experimental controllers

	% Time SS LF	% Time SS RF	% Time SS LR	% Time SS RR	% Time DS LF	% Time DS RF	% Time DS LR	% Time DS RR
MPC	25.2	24.2	23.9	24.1	24.7	25.4	24.6	25.2
a-MPC	31.8	31.7	29.8	31.4	32.2	32.7	32.0	32.6

Due to the speed of the vehicle not being consistent for the different runs on the track the roll angle can't be used conclusively to say that the controller performed as expected. Since the suspension switching or settings does change the handling characteristics and response of the vehicle the driver might react differently and follow a different 'racing line'. This can also contribute to the non-ideal repeatability of the tests. The effect of how the driver reacts to the change in vehicle dynamics should be investigated in the future.

6.2. Ride comfort results over rough tracks

For this section, the fidelity of the controller to not adversely affect the ride comfort is investigated. Ideally, the suspension should stay in the ride comfort mode for all of the tests performed. For the Belgian paving test, the vehicle was maintained at a constant speed of 21 km/h or 47 km/h by driving the vehicle against the engine's governor in low range 2nd gear and high range 2nd gear for the respective speeds.

6.2.1. Belgian paving tests

The vertical acceleration RRMS graphs are shown in figures 57 and 60 for the 21 km/h and 47 km/h runs over the Belgian paving track. Figures 58 and 59 shows the rollover ride comfort metric maps for the 21 km/h tests and figures 61 and 62 for the 47 km/h tests for the respective controllers.

From the results, we can see that the suspension does indeed switch over to the handling mode for brief instances. For the 47 km/h run the controller required more switches once the vehicle went onto the Belgian paving at about 10 m. Although the controller did switch we don't really see a negative impact on the RRMS figures. This might be due to the delays in the opening or closing of the valves and that the switches are of a much shorter duration than these delays.

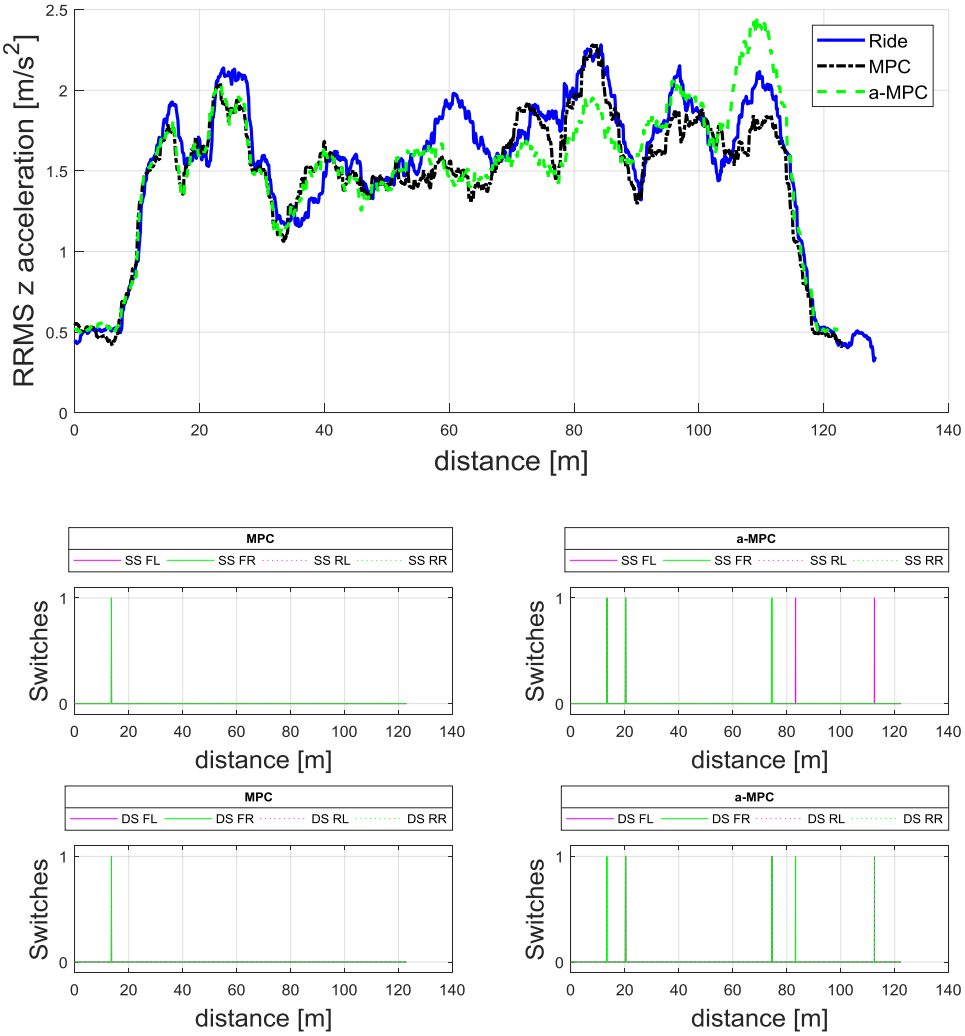

Figure 57: 21 km/h Belgian paving vertical acceleration RRMS with experimental MPC and a-MPC controllers

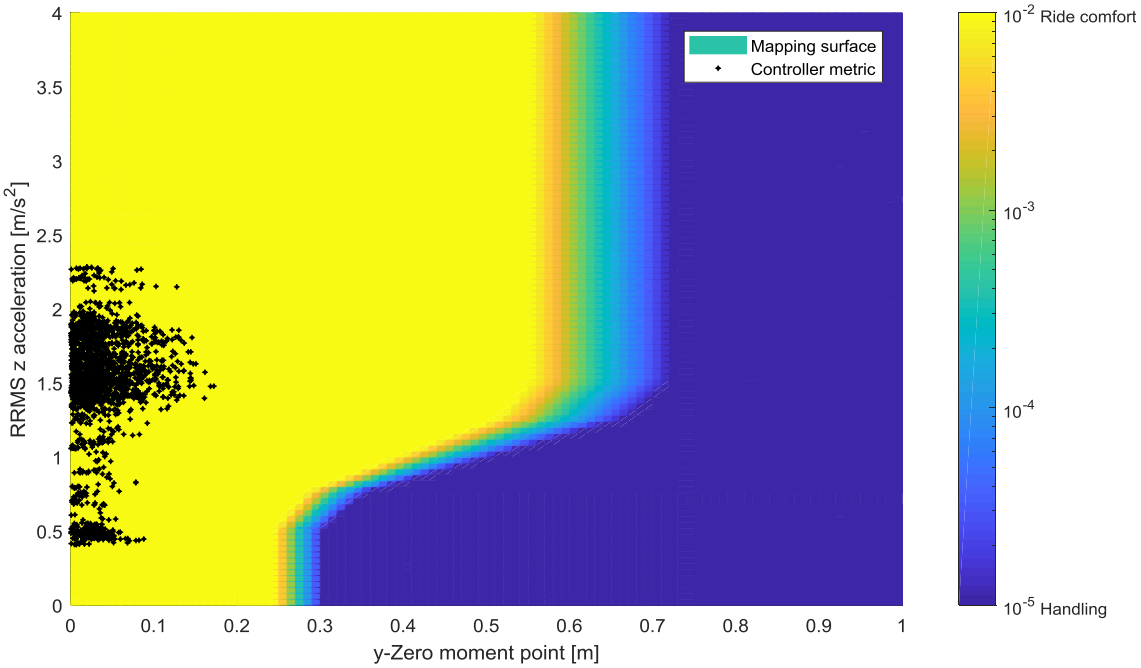

Figure 58: 21 km/h Belgian paving MPC experimental metric map

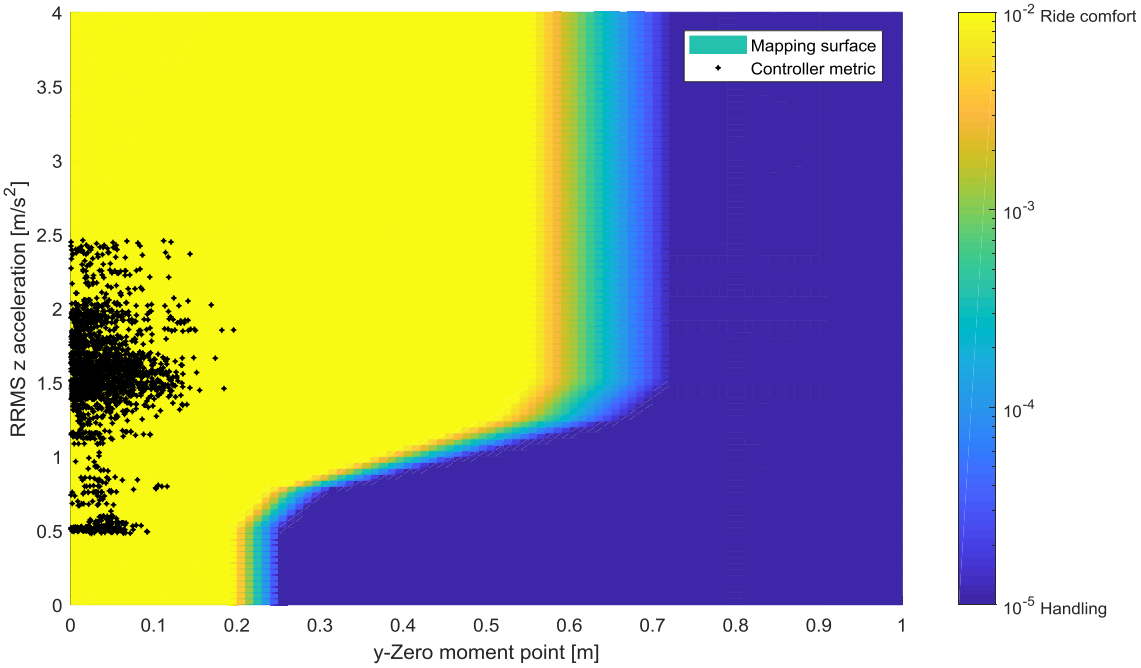

Figure 59: 21 km/h Belgian paving a-MPC experimental metric map

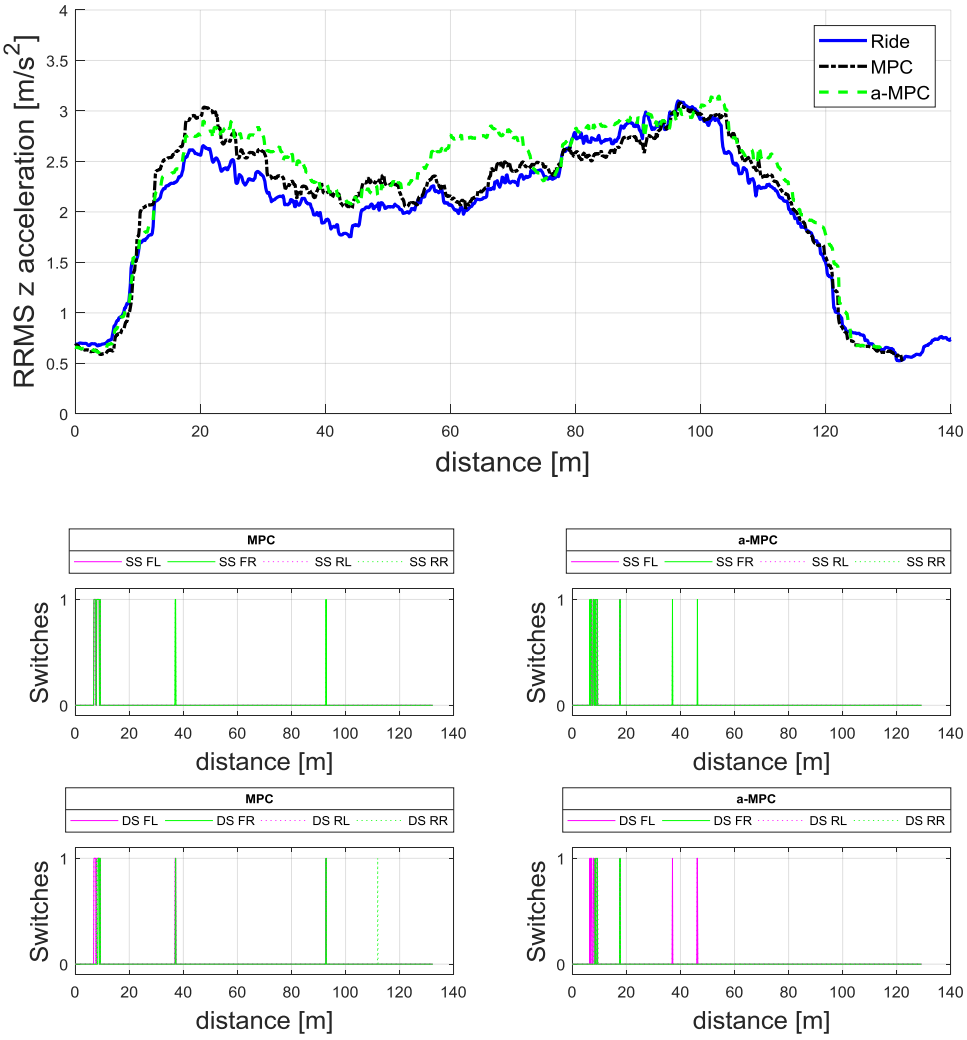

Figure 60: 47 km/h Belgian paving vertical acceleration RRMS with experimental MPC and a-MPC controllers

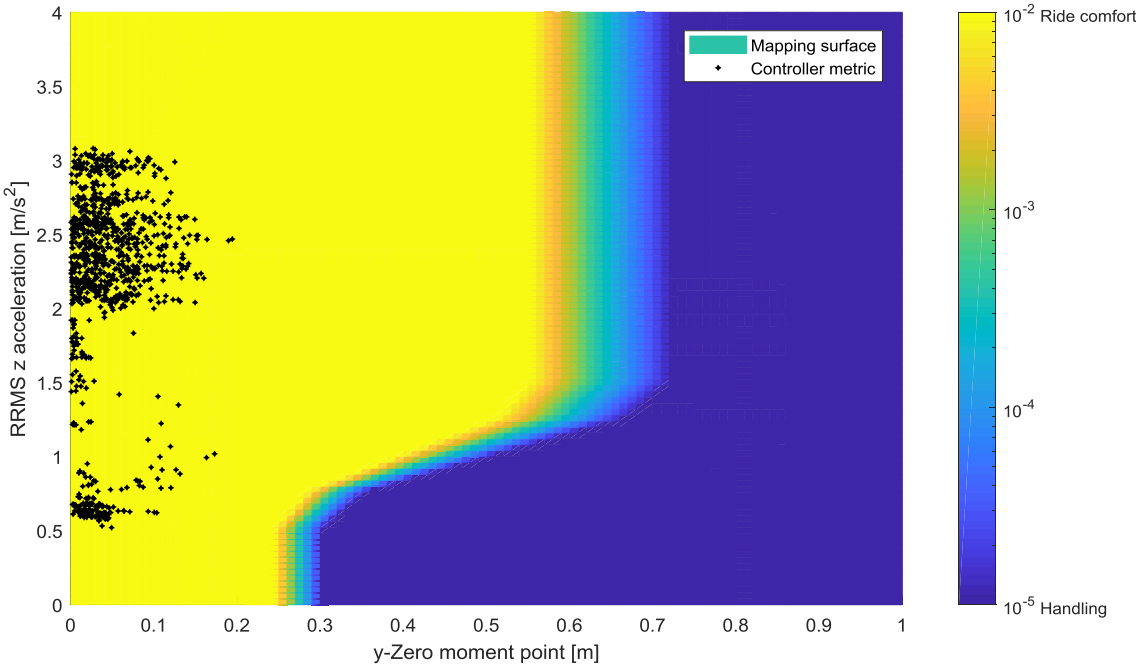

Figure 61: 47 km/h Belgian paving MPC experimental metric map

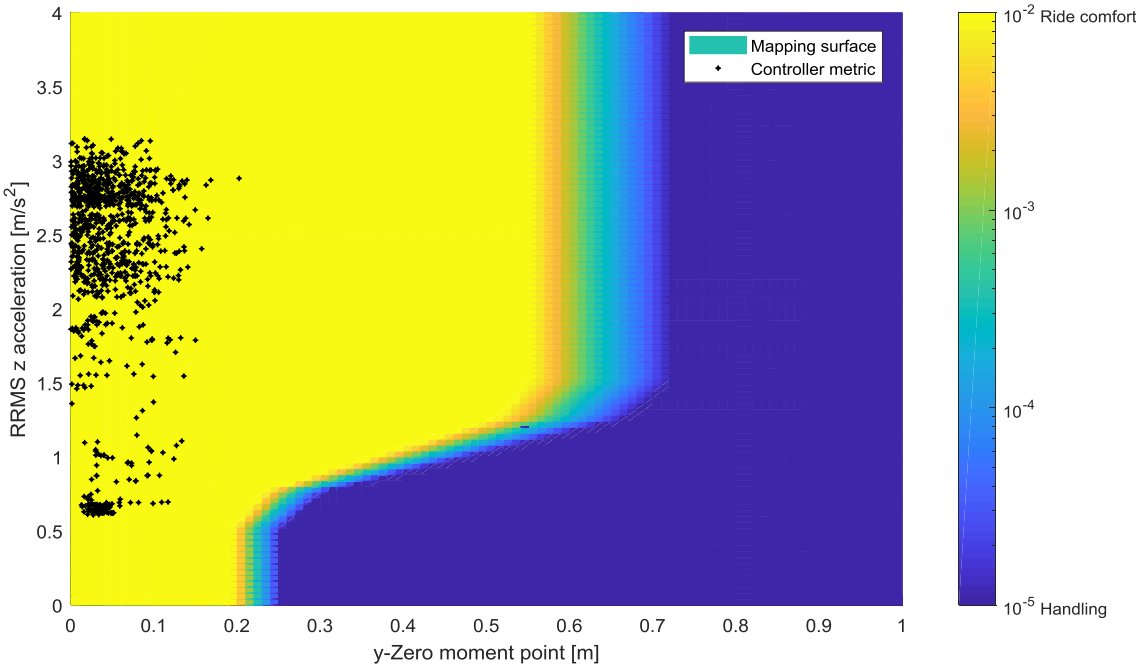

Figure 62: 47 km/h Belgian paving a-MPC experimental metric map

The percentage of time spent in the handling mode is presented in Table 17.

Table 17: Time spent in handling on Belgian paving for experimental controllers

Speed [km/h]	Controller	% Time SS LF	% Time SS RF	% Time SS LR	% Time SS RR	% Time DS LF	% Time DS RF	% Time DS LR	% Time DS RR
21	MPC	0.05	0.05	0.05	0.05	0.05	0.05	0.05	0.05
	a-MPC	0.34	0.29	0.39	0.34	0.19	0.39	0.24	0.43
47	MPC	1.46	1.76	1.56	1.95	1.76	0.68	1.95	1.17
	a-MPC	0.89	1.29	1.39	1.89	1.39	0.3	2.09	0.99

The percentage of difference in the weighted and unweighted vertical acceleration RMS between the controlled and soft suspension is shown in Table 18. The weighting was done with the BS6841 standard weighting curve for vertical accelerations.

Table 18: Percentage difference in vertical acceleration RMS values on Belgian paving experimental

Speed [km/h]	Controller	Unweighted vertical acceleration RMS [m/s²]	% difference unweighted	Weighted vertical acceleration RMS [m/s²]	% difference weighted
21	Soft	1.55		0.98	
	MPC	1.52	-2.23	0.88	-9.72
	a-MPC	1.57	1.09	0.96	-1.64
47	Soft	2.06		1.30	
	MPC	2.26	9.7	1.33	2.5
	a-MPC	2.41	16.93	1.35	3.9

From the weighted vertical accelerations, we can see that the difference between the soft and controlled runs are very small. There is a large difference in the unweighted vibrations, but it might be in a range of the vibration frequencies that the human isn't very sensitive to.

From the rollover ride comfort metric maps we can see that the suspension is in a ride comfort mode for the whole run and thus switching of the suspension shouldn't be allowed. Overall the occasions where the controller switched to the handling mode erroneously didn't influence the ride comfort over the Belgian paving significantly. There is some concern about the fact that the controller did switch over to the handling mode although the rollover and ride comfort metric found that the suspension had to stay in a ride comfort mode.

6.2.2. Left track smooth, right track Belgian paving

Runs were also made where the left track of the vehicle is driven on a smooth road and the right track on the Belgian paving at 21 km/h and 47 km/h. The running root mean square values is shown in figures 63 and 64. Seeing that the suspension system never switched to a handling mode in these runs, the differences in the figures for the soft, MPC and a-MPC can be attributed to the fact that the exact same path couldn't be followed for the runs.

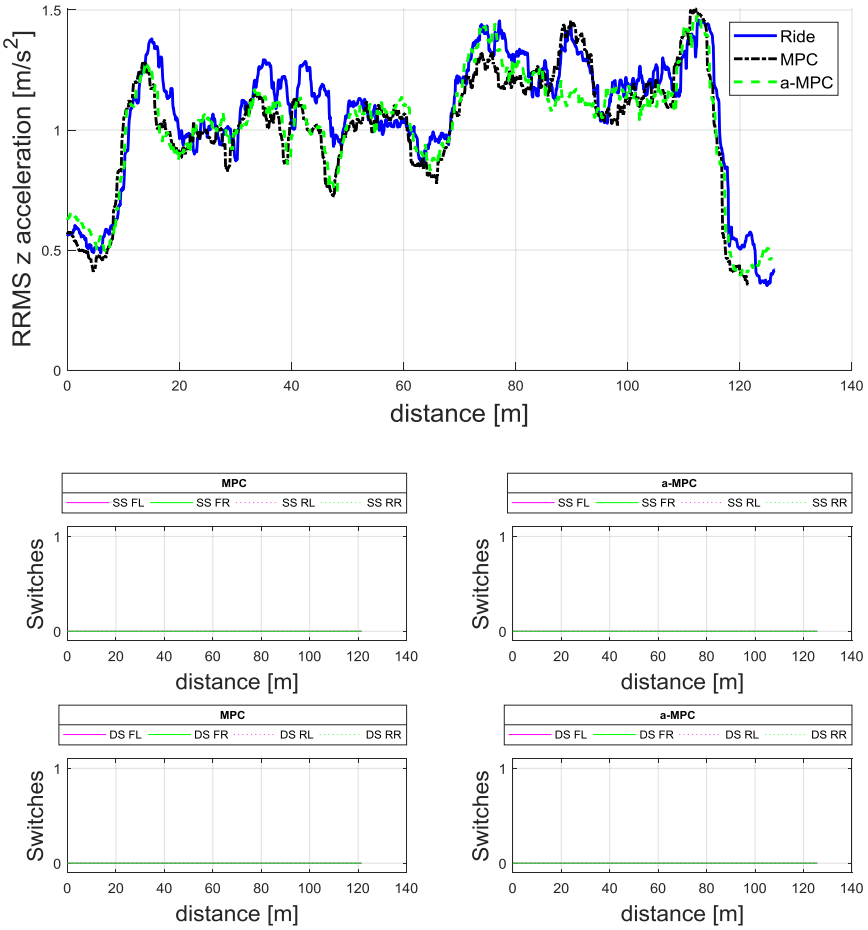

Figure 63: 21 km/h Left track smooth right track Belgian paving vertical acceleration RRMS with experimental MPC and a-MPC controllers

Table 19: Time spent in handling on half-track Belgian paving for experimental controllers

Speed [km/h]	Controller	% Time SS LF	% Time SS RF	% Time SS LR	% Time SS RR	% Time DS LF	% Time DS RF	% Time DS LR	% Time DS RR
21	MPC	0	0	0	0	0	0	0	0
	a-MPC	0	0	0	0	0	0	0	0
47	MPC	0	0	0	0	0	0	0.1	0
	a-MPC	0	0	0	0	0	0	0	0

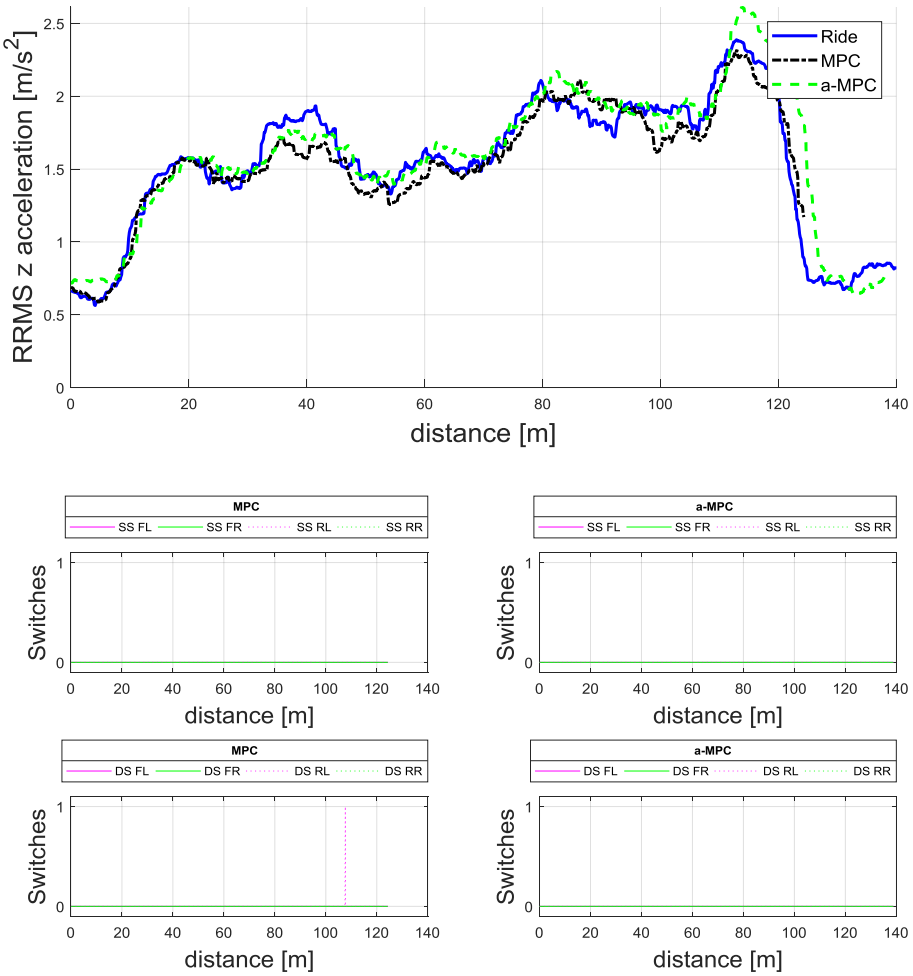

Figure 64: 47 km/h Left track smooth right track Belgian paving vertical acceleration RRMS with experimental MPC and a-MPC controllers

From figures 63 and 64 we can see that the suspension did not switch to the handling mode except for a single occasion where the left rear damper switched to high damping in the 47 km/h run with the MPC controller at about 109 m. This is in contrast with the normal Belgian paving track run where the suspension did switch more often.

6.2.3. Single lane change from Belgian paving to smooth road

A non-standardised single lane change (SLC) was performed with the vehicle driving initially on the Belgian paving and then turning right onto the smooth road. These tests were again performed at 21 km/h and 47 km/h. From this, we should see some lateral dynamics being excited, but seeing that the speed is so low and the vehicle is initially traversing the rough track the suspension should stay in ride comfort mode for most of the manoeuvre. It should be noted that the ride comfort tests weren't performed on the same day as the MPC and a-MPC tests leading to different static roll angles, which explains the dc offset from the roll angle results.

The roll angle of the vehicle is shown in figures 65 and 66 for the two different speeds. The rollover and ride comfort metric maps are shown in appendix G.

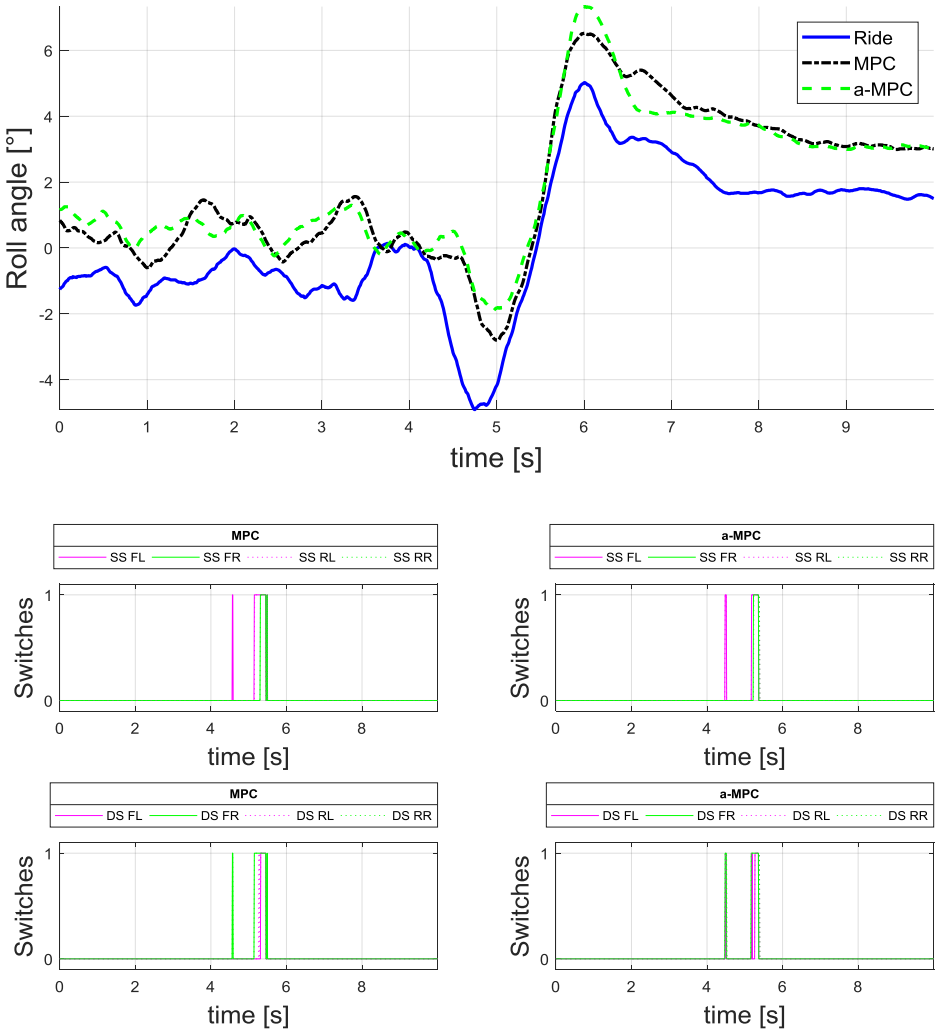

Figure 65: 21 km/h SLC from Belgian paving to smooth road roll angle with experimental MPC and a-MPC controllers

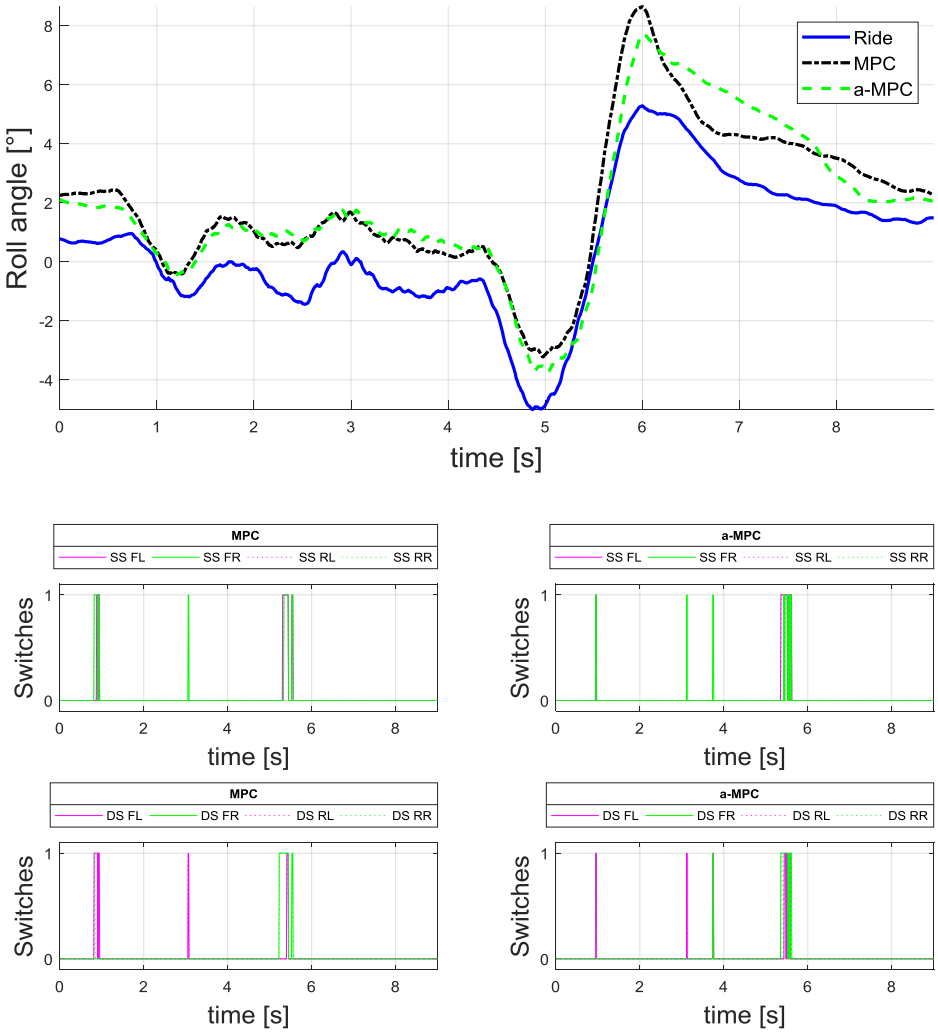

Figure 66: 47 km/h SLC from Belgian paving to smooth road roll angle with experimental MPC and a-MPC controllers

For both the speeds and controllers the suspension did indeed switch to the handling mode in the middle of the dynamic manoeuvre, although the suspension stayed in ride comfort mode for most of the time in the runs.

6.2.4. Rough track tests

The rough track at Gerotek was driven with the suspension again in soft suspension and the two controls methods. The section of the rough track that was driven included a hairpin, many road camber changes as well as dips and climbs. This road is a closer representation of what a rough off-road track would look like. The vertical running root mean square graph is shown in figure 67. Figure 68 shows the y zero moment point for the runs. The rollover and ride comfort metric maps for the two controllers are shown in figures 69 and 70.

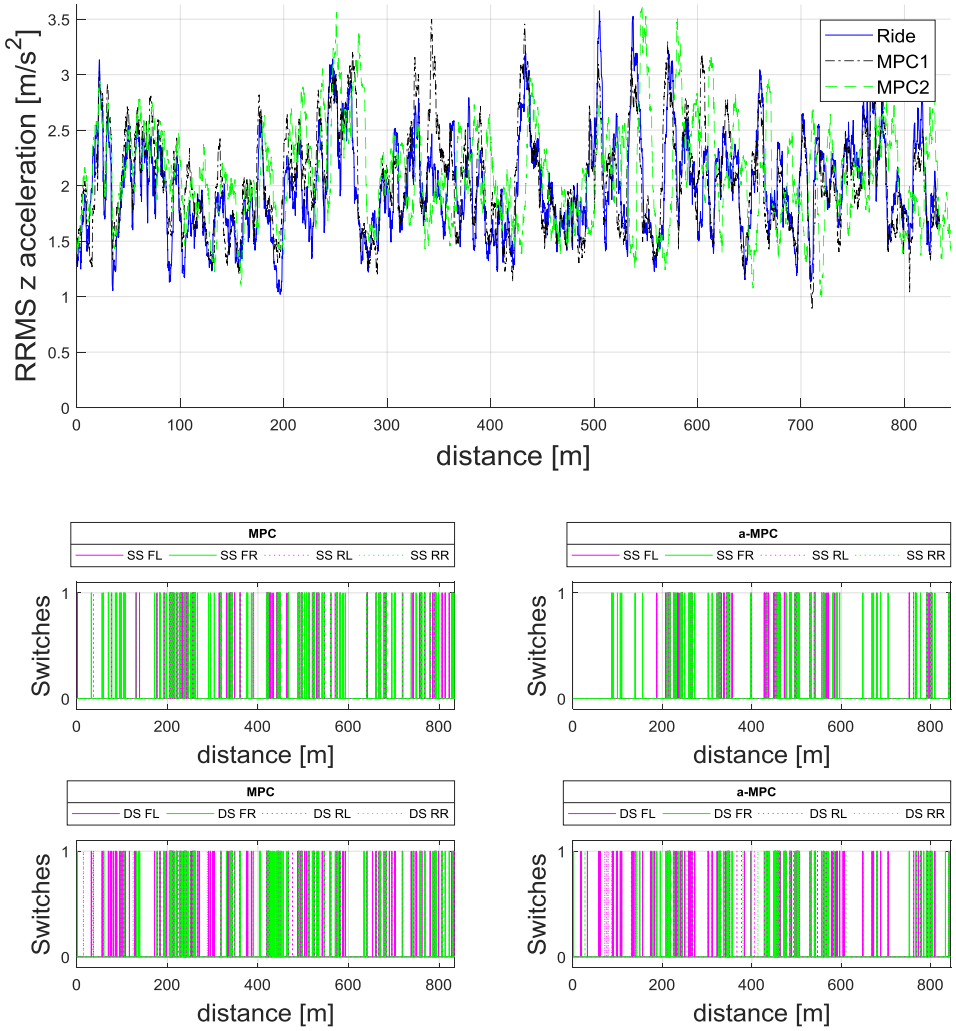

Figure 67: RRMS vertical acceleration on the rough track with MPC and a-MPC controllers

From the results, we can see that the suspension did switch many times during the runs although again the vertical acceleration running root mean square values seems the same for the soft and controlled suspension runs. We can see the peak in the y zero moment point (figure 68) where the vehicle navigated the hairpin on the rough track. From the rollover and ride comfort metric maps we can see that the controller did momentarily find the vehicle in a handling manoeuvre at the hairpin for both the controllers. In these instances, the vehicle was close to its limits seeing that the vehicle reached a ZMP value of close to 0.743 m, which is the absolute limit of the vehicle where after rollover is imminent.

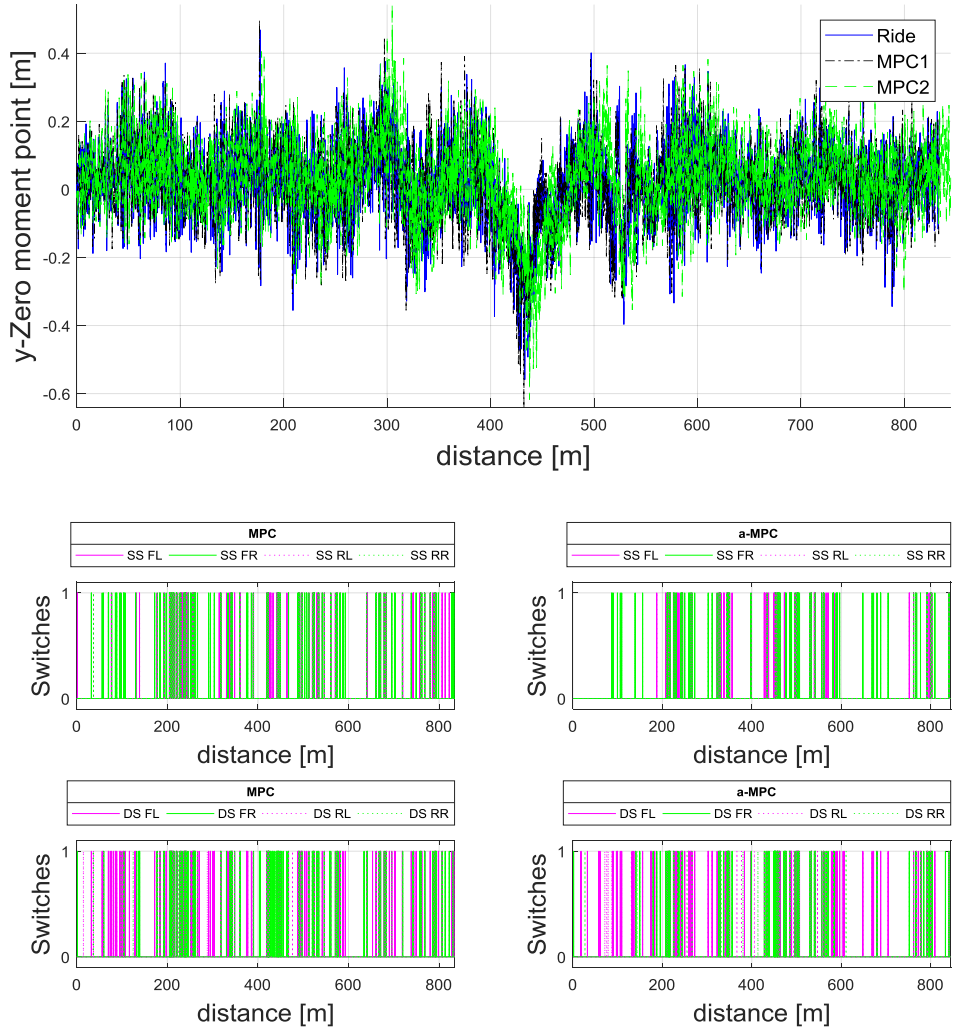

Figure 68: y-ZMP on the rough track with MPC and a-MPC controllers

The unweighted and weighted RMS vertical acceleration values of the runs are also reported in Table 20 with the time spent in the handling mode in Table 21.

Table 20: Percentage difference in vertical acceleration RMS values on rough track experimental

	Controller	Unweighted vertical acceleration RMS [m/s^2]	% difference unweighted	Weighted vertical acceleration RMS [m/s^2]	% difference weighted
Rough track	Soft	1.94		1.50	
	MPC	1.97	1.6	1.54	2.51
	a-MPC	2.07	6.59	1.66	10.56

Table 21: Time spent in handling on rough track for experimental controllers

	Controller	% Time SS LF	% Time SS RF	% Time SS LR	% Time SS RR	% Time DS LF	% Time DS RF	% Time DS LR	% Time DS RR
Rough track	MPC	2.6	3.0	2.8	3.0	3.3	2.8	4.0	3.5
	a-MPC	2.1	2.1	2.3	2.2	2.5	2.1	3.3	3.0

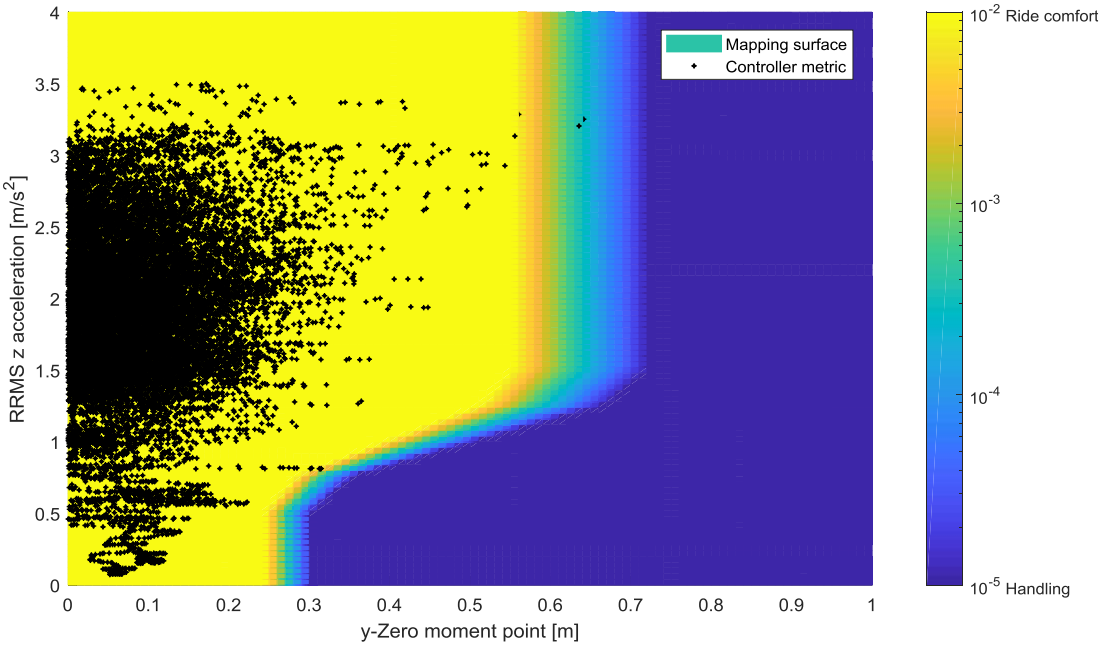

Figure 69: Rough track experimental MPC metric map

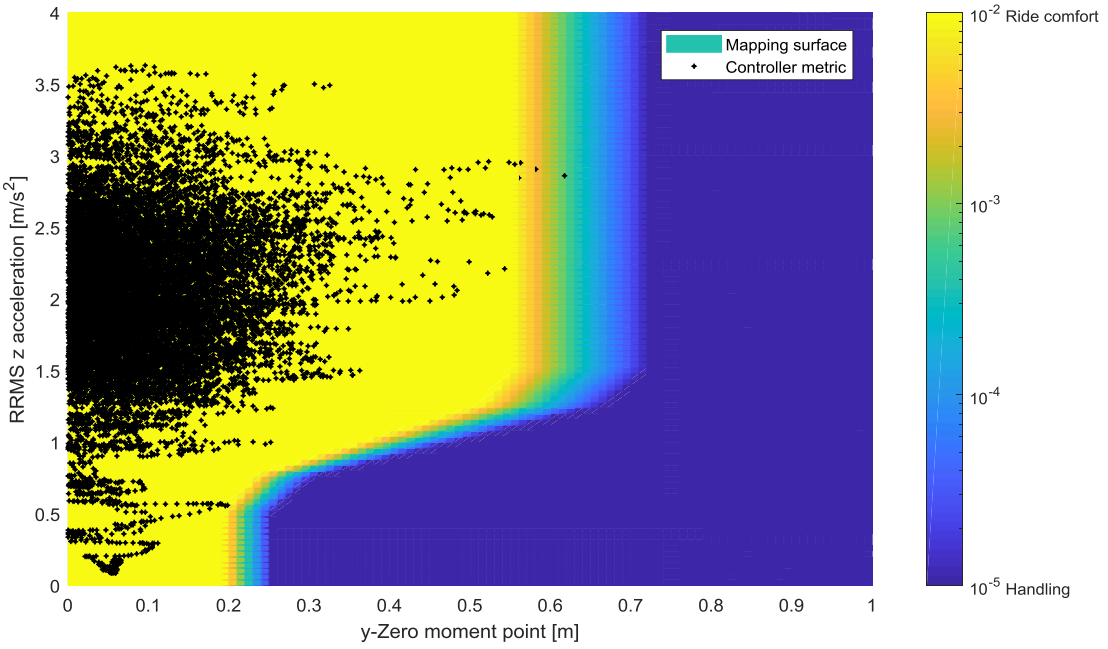

Figure 70: Rough track experimental a-MPC metric map

We can see that the ride with the a-MPC controller was more uncomfortable although in general, the controller spent less time in the handling mode as compared to the MPC controller.

6.3. Conclusion

With the controller validated through experimental work we can conclude that, for the handling test, the controller performed as expected. The more aggressive controller performed better seeing that the suspension stayed in the handling mode for longer resulting in less roll angle propagation. The MPC controller reduced the roll angle for the double lane changes by up to 24% and the roll rate by up to 33% as compared to the soft suspension. The a-MPC controller reduced the roll angle for the double lane changes by up to 34% and the roll rate by up to 44% as compared to the soft suspension. These results show the same trend which was found in the simulations although the magnitude of the improvements is smaller for the experimental work. An improvement of up to 69% reduction for the roll angle and 62% reduction in roll rate was found in the simulations, as opposed to the 34% and 44% reductions found in the experimental work for roll angle and roll rate respectively.

Further improvement of the controller for handling manoeuvres can be achieved by changing the ride comfort vs rollover metric map to switch quicker to the handling mode. After a handling manoeuvre is detected a delay can be added to the signal to delay the switch back to ride comfort mode, which might keep the suspension in handling mode for longer when manoeuvres such as the DLC is performed.

The dependability of the controller to stay in ride comfort mode when required was not good. Although the ride comfort of the vehicle is not detrimentally influenced by the unsatisfactory performance of the controller the fact that the controller did switch to the handling mode while traversing a rough road is concerning.

After post-processing the data it was found that if we consider the rollover ride comfort metric map the suspension should have stayed in the ride comfort mode but still switched to handling mode. It was found that the low cut off torque requirement of 5 Nm was too small. The additional torque required calculated from the model predictive controller, even with the ride comfort-related input weight, was frequently higher than the low cut off of 5 Nm and this resulted in the spurious switching when rough roads are driven.

In figure 71 the additional torque requirement (taken as the absolute value in the figure) of the a-MPC is plotted with a horizontal line representing the low cut of torque value of 5 Nm for the 21 km/h Belgian paving experimental results, as well as the collective spring setting suspension switches.

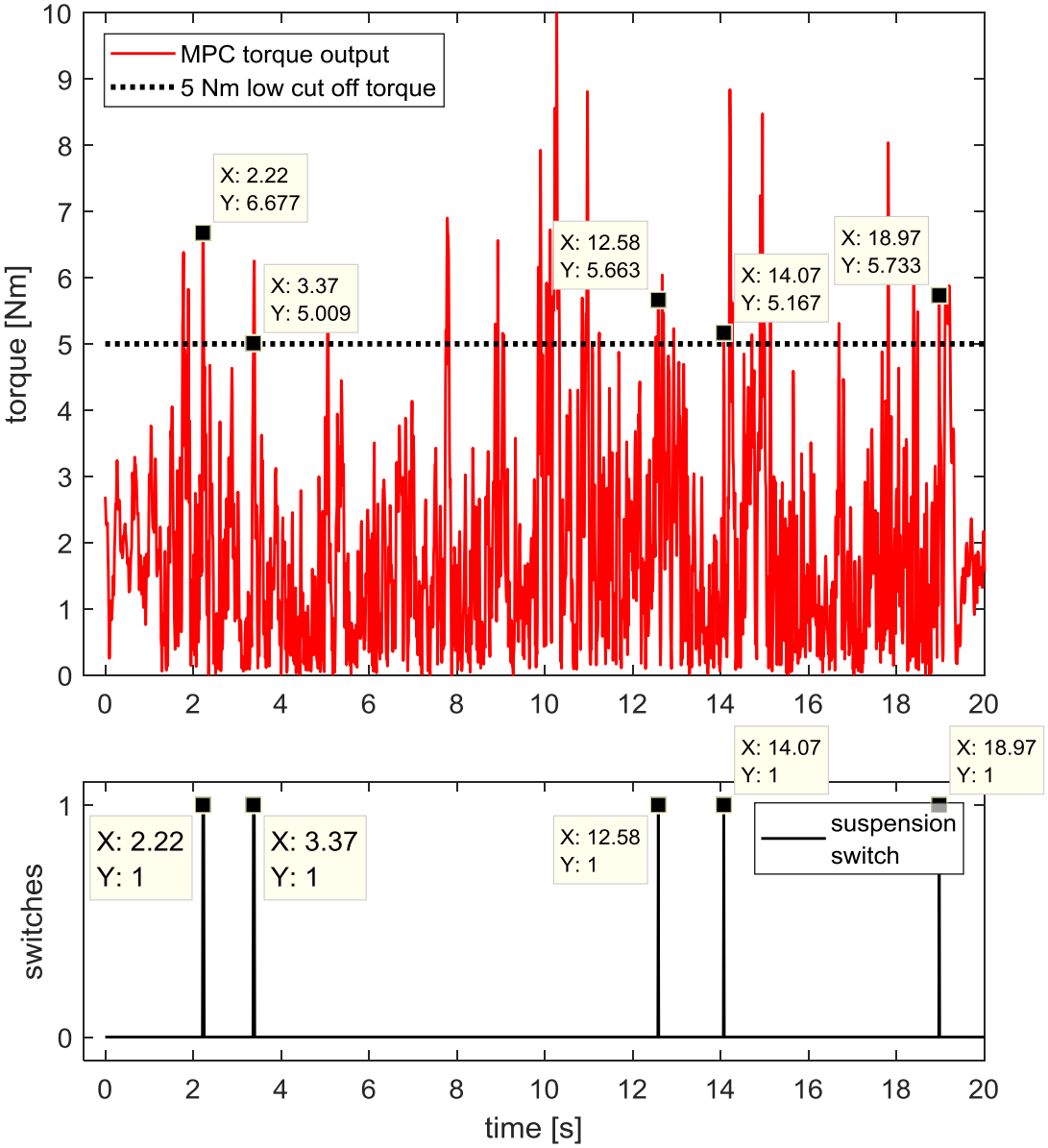

Figure 71: low cut off torque controller issue

In figure 71 we can see that the suspension switches correspond to locations on the MPC torque output where the torque is above 5 Nm. There are other locations where the torque output is higher than the 5 Nm cut off value where the suspension did not switch to the handling mode. This can be attributed to the spring stiffness or damper setting being below the buffer value used in the relays in the Simulink model as described in section 4.6, thus the suspension member's spring or damper setting never had to change.

The reason that the controller's switching to a handling mode didn't influence the weighted and unweighted vertical acceleration RMS values too much might be due to the delays of the physical valves on the suspension struts, seeing that most of the switches to handling mode happened for about a sample time of 10 ms and the response of the valves are at best 50 ms.

Development of an improved controller shall thus be investigated to perform even better in handling manoeuvres while addressing the problems found when traversing rough roads.

7. Final conclusion and Recommendations

For this study, the ride comfort and handling compromise were circumvented through the use of a semi-active suspension system controlled by a model predictive controller. The controller was created in such a way that the roll dynamics of the vehicle is captured and the roll angle and roll rate regulated towards the origin through the smart distribution of the roll torque necessary to make the vehicle stable and safe. A combined rollover and ride comfort metric were used to steer the controller towards the desired output based on the vehicle's current states. The discrete suspension damper and spring settings were varied to reduce the vehicle roll angle in the case of a handling or emergency manoeuvre while keeping the vehicle comfortable on rough roads.

The controller performed well in the handling manoeuvres reducing the roll angle of the vehicle by up to 34% as compared to the soft suspension setting. On the rough roads, the controller did not perform that well seeing that the controller occasionally switched the suspension to a handling mode when in fact the system should have stayed in a ride comfort mode. The low cut off torque requirement set in the controller was found to be the problem. If the low cut off torque requirement can be set to a higher numeric value the system might perform better over rough roads. Although the controller did switch to the handling mode in the ride comfort experiments the vehicle's vertical acceleration RMS values weren't significantly different to the ride mode values, presumably because of the relatively slow response time of the suspension valves.

7.1. Recommendations

There is definite potential for further development of the controller. The pitfalls identified for the ride comfort experiments is the largest aspect of the controller that can be improved, while some minor changes in the handling aspect of the controller may also be achievable.

7.1.1. Ride comfort improvements

The low cut off torque requirement of the controller was found to be the major problem with the ride comfort aspect of the controller. The cut of torque value can either be increased significantly to circumvent this issue or overwritten completely if the rollover ride comfort metric sees that the vehicle is traversing a rough track and the suspension should stay in ride comfort mode.

7.1.2. Handling improvements

One method to improve the handling of the vehicle is to study the rollover ride comfort maps carefully from the experimental results and reshape the surface which was used in this study to help the controller switch quicker to a handling mode.

Given that the ride comfort improvements makes the controller absolutely robust against all scenarios and guaranteeing that the suspension won't switch to the handling mode at all if the rollover ride comfort metric deems the suspension should stay in ride comfort mode we

can also add a delay in switching back to ride comfort mode if the suspension switches to handling mode. This will increase the time spent in handling mode of the controller, which will improve the handling of the vehicle, but it will also remove any chattering that the controller might experience.

By adding an additional actuator such as an active anti-roll bar to the front and/or rear of the vehicle the required additional roll torque requested from the MPC can be achieved, which currently can't be reached due to the neglected physical suspension system constraints in the formulation of the controller. This could, in theory, bring the controller and the response of the vehicle closer to the optimal controlled setup.

7.1.3. General improvements

The controller can be extended to incorporate the yaw plane, pitch plane, longitudinal and lateral dynamics to make an even more complex controller. By using these extra states the controller can be extended to control the longitudinal dynamics of the vehicle such as braking and accelerating, as well as other combinations such as combined braking and turning. The applicability of the x-location of the zero moment point can also be investigated for possible use as a metric or constraint.

The model predictive controller can be changed from making use of a linear time-invariant system to a non-linear system to improve the accuracy of the model used in the control. For this study the external disturbances considered in the controller were assumed to be constant throughout the preview horizon, thus some form of a preview model for these disturbances might improve the accuracy of the model further and lead to more accurate control efforts.

Additional state and input constraints can also be incorporated to capture the true vehicle better. The steering angle and longitudinal velocity can be used combined with the rollover and ride comfort metric map to make better decisions about the input biasing of the controller.

References

- Al-Holou, N., Bajwa, A. & Joo, D.-S., 1993. COMPUTER CONTROLLED INDIVIDUAL SEMI-ACTIVE SUSPENSION SYSTEM. *IEEE,* pp. 208-211.
- Armscor, 2016. *Gerotek Test Facilities.* [Online]
  Available at: http://www.armscor.co.za/?page_id=3967
  [Accessed October 2018].
- Bakker, E., Pacejka, H. B. & Linder, L., 1989. A new tire model with an application in vehicle dynamics studies. *SAE,* Volume 890087, pp. 101-113.
- Bernard, J., Shannan, J. & Vanderploeg, M., 1989. Vehicle Rollover on Smooth Surfaces. *SAE Technical Paper,* Issue 891991.
- Borrelli, F., Bemporad, A. & Morari, M., 2017. *Predictive Control for linear and hybrid systems.* California: UC Berkeley.
- Bosch, H.-R. B., Hamersma, H. A. & Els, P. S., 2016. Parameterisation, validation and implementation of an all-terrain SUV FTire tyre model. *Journal of Terramechanics,* 67(10), pp. 11-23.
- Botha, T. R., 2011. *High speed autonomous off-road vehicle steering, Unpublished Masters degree thesis.* [Online]
  Available at: http://hdl.handle.net/2263/29665
  [Accessed 2018].
- Brezas, P., Smith, M. C. & Hoult, W., 2015. A clipped-optimal control algorithm for semi-active vehicle suspensions: Theory and experimental evaluation. *Automatica,* Volume 53, pp. 188-194.
- British Standards Institution, 1987. *BS 6841 British Standard Guide to Measurement and evaluation of human exposure to whole-body mechanical vibration and repeated shock,* s.l.: British Standards Institution.
- Canale, M., Milanese, M. & Novara, C., 2006. Semi-Active Suspension Control Using "Fast" Model-Predictive Techniques. *IEEE Transactions on Control Systems Technology,* 14(6), pp. 1034-1046.
- Carlson, C. R. & Gerdes, J. C., 2003. Optimal rollover prevention with steer by wire and differential braking. *ASME IMECE,* 72(1), pp. 345-354.
- Chu, D. et al., 2015. Smooth Sliding Mode Control for Vehicle Rollover Prevention Using Active Antiroll Suspension. *Mathematical Problems in Engineering,* Volume 2015, pp. 1-8.
- Consumer Reports, 2014. *Consumer Reports.* [Online]
  Available at: https://www.consumerreports.org/cro/2012/02/rollover-101/index.htm
  [Accessed 23 July 2017].
- Consumer Reports, 2017. *Consumer Reports.* [Online]
  Available at: https://www.consumerreports.org/car-safety/cars-with-advanced-safety-systems/
  [Accessed 19 September 2017].
- cosin scientific software, 2018. *FTire.* [Online]
  Available at: https://www.cosin.eu/products/ftire/
  [Accessed October 2018].
- Cronje, P. H., 2008. *Improving Off-Road Vehicle Handling Using an active Anti-Roll Bar, Unpublished Masters degree Thesis.* [Online]

Available at: https://UnivofPretoria.on.worldcat.org/oclc/956376208
[Accessed 2018].

- Das, N., Suresh, B. & Wambold, J., 1993. Estimation of Dynamic Rollover Threshold of Commercial Vehicles Using Low Speed Experimental Data. *SAE Technical Paper 932949,* Issue 932949.
- dSPACE, 2018. *MicroAutoBox II.* [Online]
Available at:
https://www.dspace.com/en/inc/home/products/hw/micautob/microautobox2.cfm
[Accessed 2018].
- Els, P. S., 2005. The applicability of ride comfort standards to off-road vehicles. *Journal of Terramechanics,* 42(1), p. 47–64.
- Els, P. S., 2006. *The ride comfort vs. handling compromise for off-road vehicles, Unpublished PhD thesis.* [Online]
Available at: https://UnivofPretoria.on.worldcat.org/oclc/724424371
[Accessed 2017].
- Fergani, S., Sename, O. & Dugard, L., 2016. An LPV/H∞ Integrated Vehicle Dynamic Controller. *IEEE TRANSACTIONS ON VEHICULAR TECHNOLOGY,* 64(4), pp. 1880-1889.
- Gillespie, T., 1992. *Fundamentals of Vehicle Dynamics.* 1st ed. Warrendale: Society of Automotive Engineers.
- Göhrle, C., Wagner, A., Schindler, A. & Sawodny, O., 2012. *Active suspension controller using MPC based on a full-car model with preview information.* Montreal, 2012 American Control Conference (ACC).
- Hamersma, H. A., 2014. *Longitudinal vehicle dynamics control for improved vehicle safety, Unpublished Masters degree thesis.* [Online]
Available at: http://hdl.handle.net/2263/40829
[Accessed 2018].
- Hamersma, H. A. & Els, P. S., 2014. Improving the braking performance of a vehicle with ABS and a semi-active suspension system on a rough road. *Journal of Terramechanics,* 56(12), pp. 91-101.
- International Organisation for Standardisation, 1997. *Mechanical vibration and shock – Evaluation of human exposure to whole-body vibration, Part 1: General requirements, ISO 2631-1,* s.l.: International Organisation for Standardisation.
- International Organisation for Standardisation, 1999. *ISO3888-1, Passenger cars, Test track for a severe lane-change manoeuvre-Part 1: Double lane change,* s.l.: International Organisation for Standardisation.
- Ivanov, V., Augsburg, K. & Savitski , D., 2012. *TORQUE VECTORING FOR IMPROVING THE MOBILITY OF ALL-TERRAIN ELECTRIC VEHICLES.* Pretoria, International Society for Terrain-Vehicle Systems.
- Kim, J., Chung, W. K., Youm, Y. & Lee, B., 2002. *Real-time ZMP Compensation Method using Null Motion for Mobile Manipulators.* Whasington DC, IEEE International Conference on Robotics and Automation.
- Kolansky , J. J. & Sandu, C., 2013. Real-Time Parameter Estimation Study for Inertia Properties of Ground Vehicles. *Archive of Mechanical Engineering,* 60(1), pp. 7-21.
- Lapapong, S. & Brennan, S., 2010. *Terrain-Aware Rollover Prediction for Ground Vehicles Using the Zero-Moment Point Method.* Baltimore, American Control Conference, pp. 1501-1507.

- Marine, M., Wirth, J. & Thomas, T., 1999. Characteristics of On-Road Rollovers. *SAE Technical Paper,* Issue 99-01-0122.
- MathWorks, 2018. *Matlab and Simulink.* [Online]
  Available at: https://www.mathworks.com/products/matlab.html
  [Accessed October 2018].
- McCarthy, N., 2015. *Forbes.* [Online]
  Available at: https://www.forbes.com/sites/niallmccarthy/2015/08/24/the-top-selling-points-for-american-car-buyers-infographic/#57ccf17413b2
  [Accessed 23 July 2017].
- MSC Software, 2018. *Adams.* [Online]
  Available at: http://www.mscsoftware.com/product/adams
  [Accessed October 2018].
- Nguyen, M. Q., Canale, M., Sename, O. & Dugard, L., 2016. *A Model Predictive approach for semi active suspension control problem of a full car.* Las Vegas, 55th IEEE Conference on Decision and Control.
- NHTSA, 2017. *Traffic Safety Facts,* Washington DC: NHTSA.
- PC/104 Consortium, 2018. *PC/104.* [Online]
  Available at: https://pc104.org
  [Accessed 14 July 2018].
- Phanomchoeng, G. & Rajamani, R., 2012. *Prediction and Prevention of Tripped Rollovers,* Minnesota: Intelligent Transportation Systems Institute Centre for Transportation Studies.
- Pradko, F. & Lee, R., 1966. *Vibration comfort criteria. SAE Technical Paper 660139,* Warrendale: Society of Automotive Engineers.
- Rakheja, S. & Piche, A., 1990. Development of Directional Stability Criteria for an Early Warning Safety Device. *SAE Technical Paper,* Issue 902265.
- Sammier, D., Sename, O. & Dugard, L., 2003. Skyhook and H8 Control of Semi-active Suspensions: Some Practical Aspects. *Vehicle System Dynamics,* 39(4), pp. 279-308.
- Sharp, R. S. & Peng, H., 2011. Vehicle dynamics applications of optimal control. *Vehicle System Dynamics,* 49(7), pp. 1073-1111.
- Shtessel, Y., Edwards, C., Fridman, L. & Levant, A., 2014. Introduction: Intuitive Theory of Sliding Mode Control. In: Springer, ed. *Sliding Mode Control and Observation.* New York: Birkhäuser, New York, NY, pp. 1-42.
- Strauss, R., 2016. *Braking based integrated rollover prevention and yaw control for an off-road vehicle, Unpublished Master degree thesis.* [Online]
  Available at: http://hdl.handle.net/2263/61339
  [Accessed 2018].
- Strydom, A., 2013. *Controllable Suspension Design Using Magnetorheological Fluid, Unpublished Masters degree Thesis.* [Online]
  Available at: https://UnivofPretoria.on.worldcat.org/oclc/961195893
  [Accessed 2017].
- Thoresson, M. J., 2003. *Mathematical optimisation of the suspension system of an off-road vehicle for ride comfort and handling, Unpublished Master degree thesis.* [Online]
  Available at: http://hdl.handle.net/2263/29489
  [Accessed 2018].

- Thoresson, M. . J., 2007. *Efficient Gradient-Based Optimisation of Suspension Characteristics of an Off-Road Vehicle, Unpublished PhD thesis.* [Online] Available at: https://UnivofPretoria.on.worldcat.org/oclc/727339370 [Accessed 2018].
- Uys, P. E., Els, P. S. & Thoresson, M. J., 2006. Criteria for handling measurement. *Journal of Terramechanics,* 43(1), pp. 43-67.
- Uys, P. E., Thoresson, M. J. & Els, P. S., 2007. Suspension settings for optimal ride comfort of off-road vehicles traveling on roads with different roughness and speeds. *Journal of Terramechanics,* 44(2), pp. 163-175.
- Van Der Westhuizen, S. F. & Els, P. S., 2015. Comparison of different gas models to calculate the spring force of a hydropneumatic suspension. *Journal of Terramechanics,* Volume 57, pp. 41-59.
- van Zanten, A., 2000. Bosch ESP Systems: 5 years of Experience. *SAE Technical Paper,* Issue 2000-01-1633.
- VBOX automotive, 2018. *VBOX Inertial Measurement Unit.* [Online] Available at: https://www.vboxautomotive.co.uk/index.php/en/products/modules [Accessed 2018].
- VBOX automotive, 2018. *VBox 3i.* [Online] Available at: https://vboxautomotive.co.uk/index.php/en/products/data-loggers [Accessed 2018].
- Wielenga, T. & Chace, M., 2000. A study in rollover prevention using anti-rollover braking. *SAE Technical Paper,* Issue 2000-01-1642.
- Yoon, J., Kim, D. & Yi, K., 2007. Design of a rollover index-based vehicle stability control scheme. *Vehicle System Dynamics,* 45(5), pp. 459-475.

Appendix A: Yaw plane cornering equation derivation

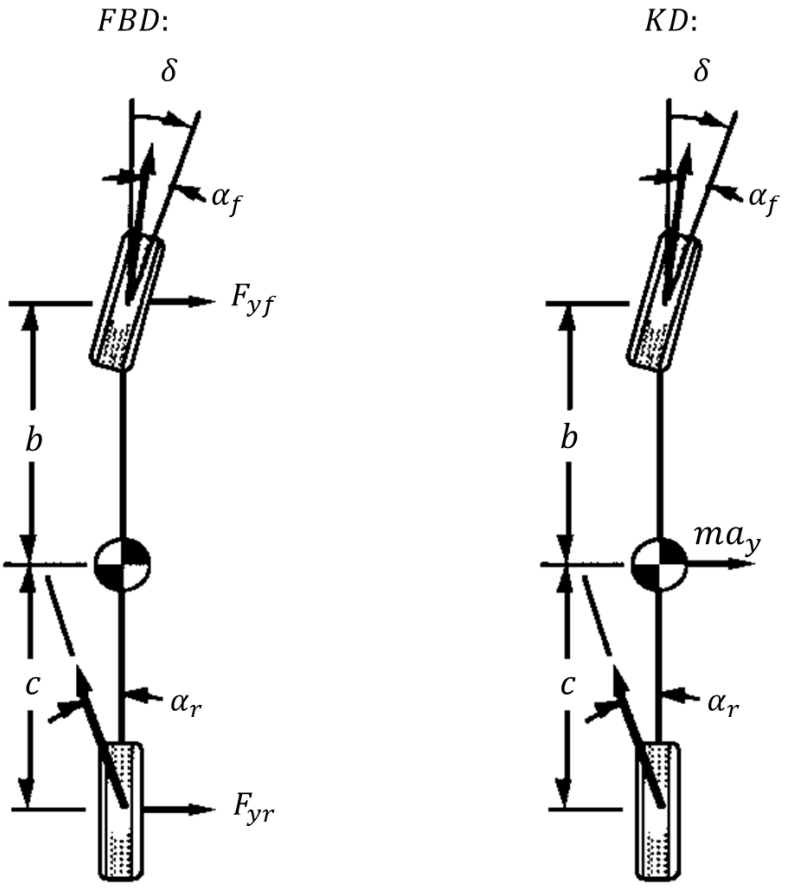

Figure 72: Yaw-plane model

For the bicycle model, the front and rear linear tyre lateral forces are given by equations A1 and A2.

$$F_{yf} = C_{\alpha f}\alpha_f \quad [A1]$$

$$F_{yr} = C_{\alpha r}\alpha_r \quad [A2]$$

The cornering equation is developed by applying Newton's second law in the lateral direction:

$$\Sigma F_y = ma_y \quad [A3]$$

$$F_{yf} + F_{yr} \approx m\frac{V^2}{R} \quad [A4]$$

Taking the sum of moments about the CG of the vehicle results in:

$$F_{yf}b - F_{yr}c = 0 \quad [A5]$$

Assumptions:

3. Small-angle assumption
    a. $sin\gamma = \gamma$
    b. $cos\gamma = 1$
4. Steady-state behaviour
    a. Vehicle speed and yaw rate is constant

With substitution and rearrangement, we get

$$\alpha_r = \frac{W_r V^2}{g C_{\alpha r} R} \quad [A6]$$

and

$$\alpha_f = \frac{W_f V^2}{g C_{\alpha f} R} \quad [A7]$$

Analysing the Bicycle model in figure 2 gives:

$$\delta = \frac{L}{R} + \alpha_f - \alpha_r \quad [A8]$$

Thus by substituting equation A6 and equation A7 we find:

$$\delta = \frac{L}{R} + \left(\frac{W_f}{C_{\alpha f}} - \frac{W_r}{C_{\alpha r}}\right)\frac{V^2}{gR} \quad [A9]$$

Appendix B: Simulation DLC metric maps

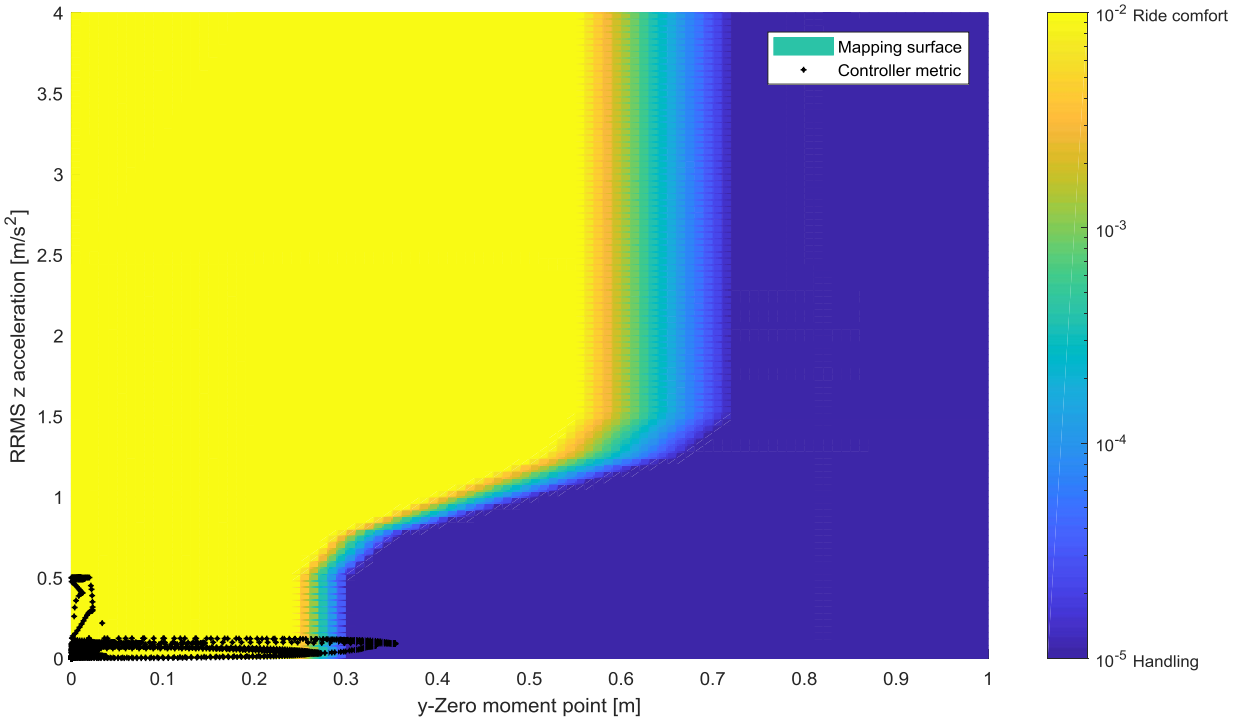

Figure 73: 50 km/h DLC simulation metric map

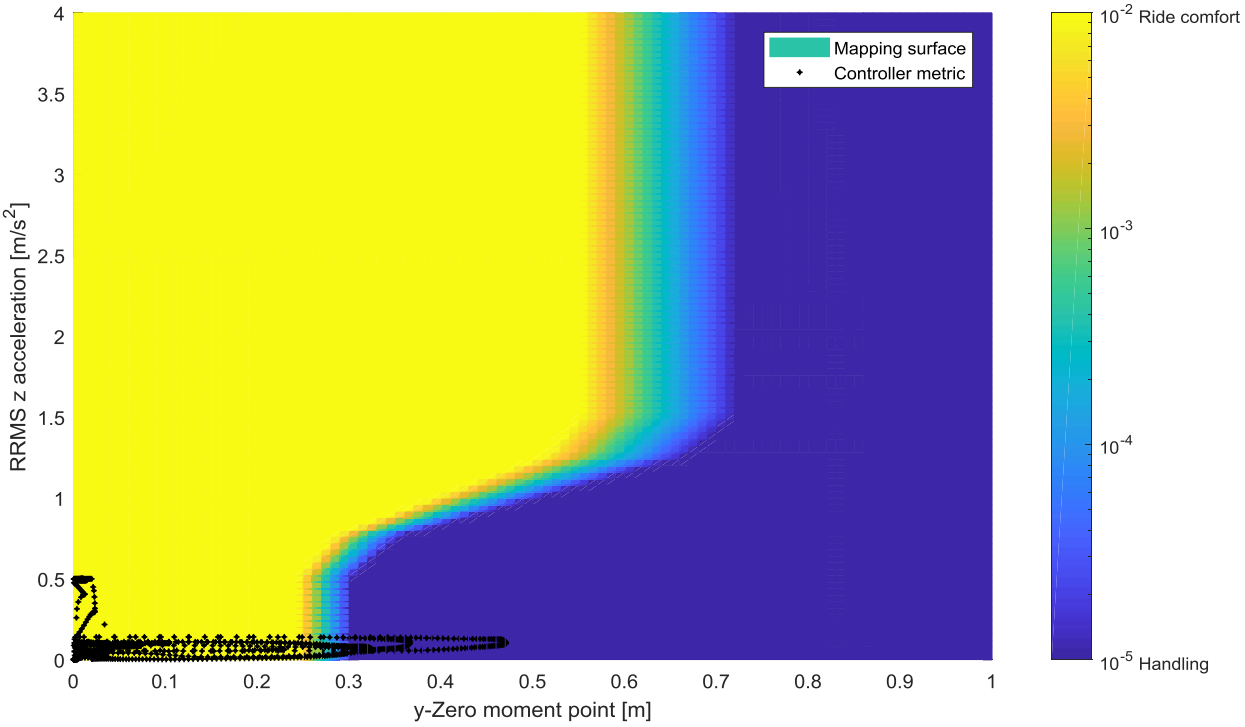

Figure 74: 60 km/h DLC simulation metric map

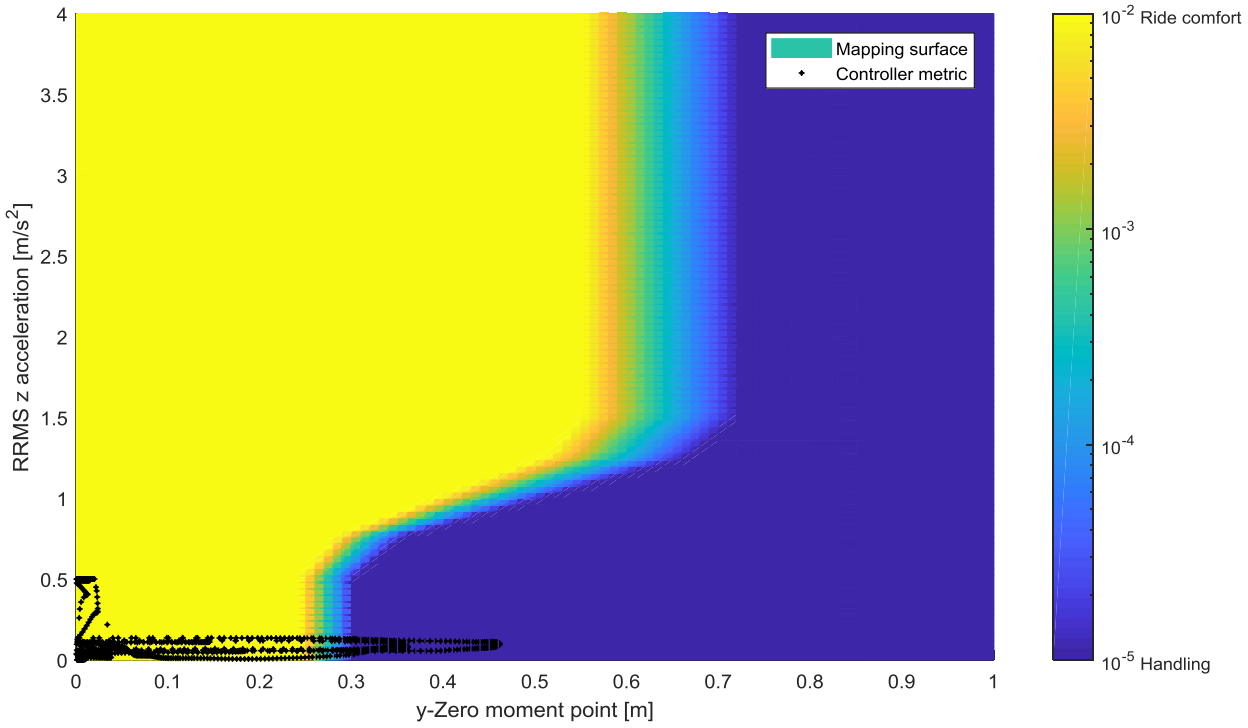

Figure 75: 70 km/h DLC simulation metric map

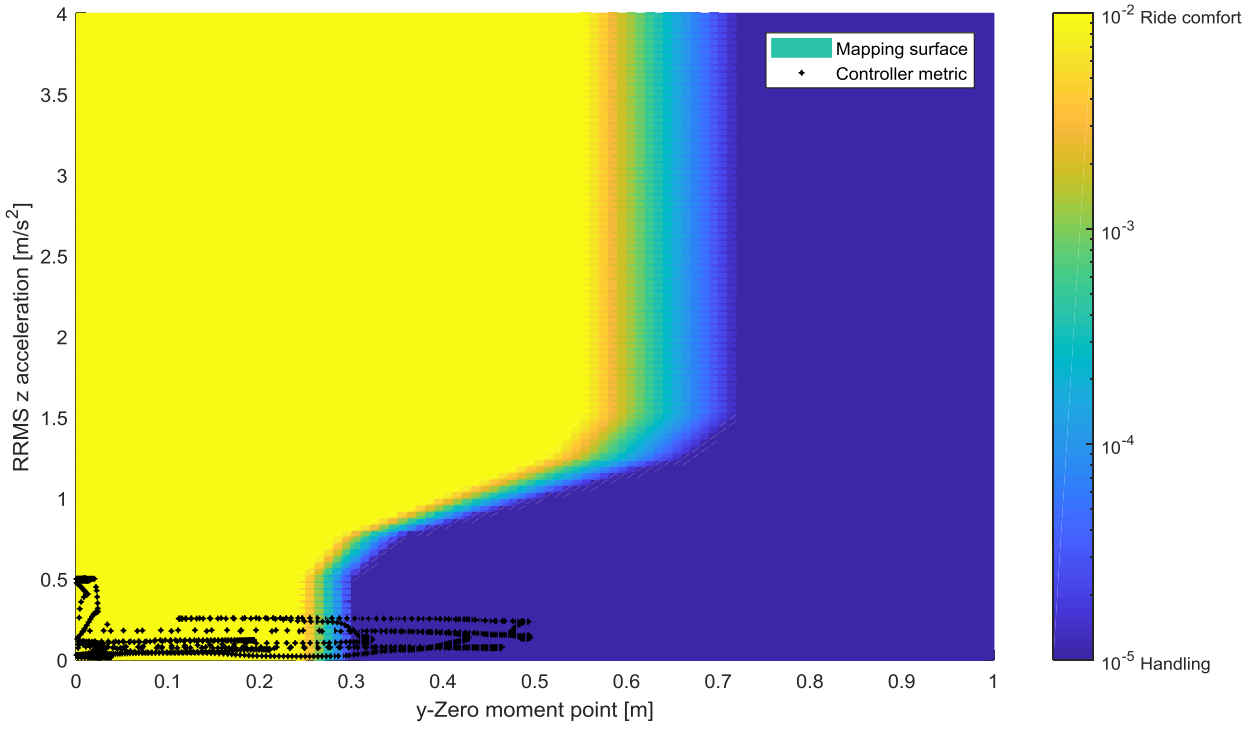

Figure 76: 80 km/h DLC simulation metric map

Appendix C: Additional roll torque requirements simulation

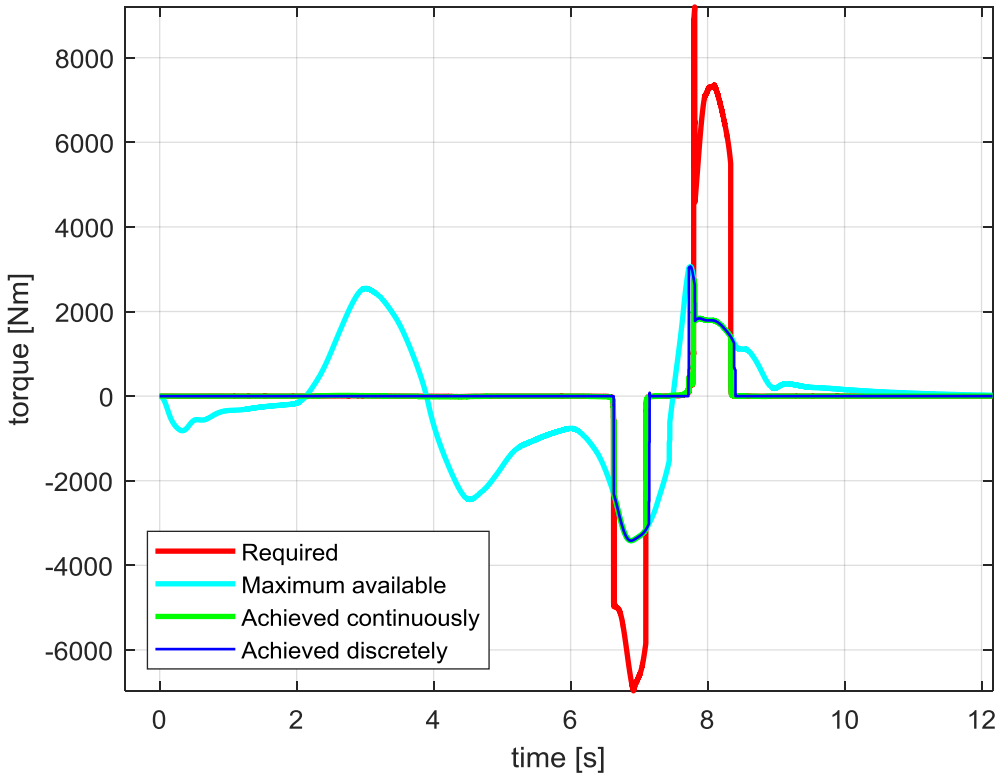

Figure 77: DLC roll torque 50 km/h simulation

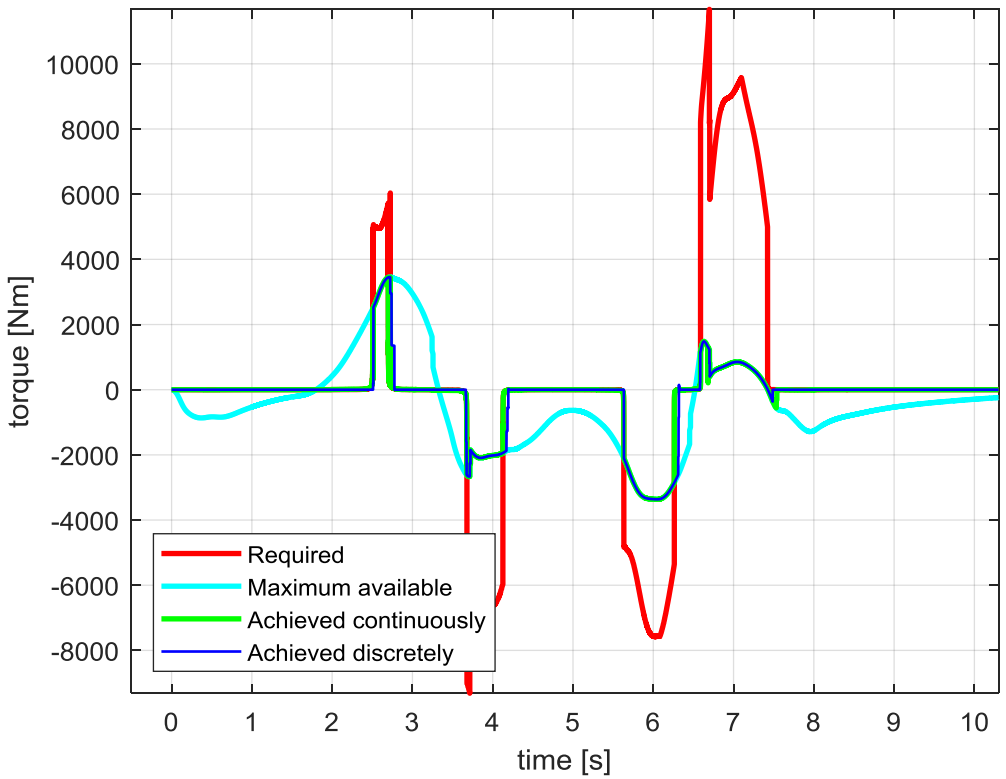

Figure 78: DLC roll torque 60 km/h simulation

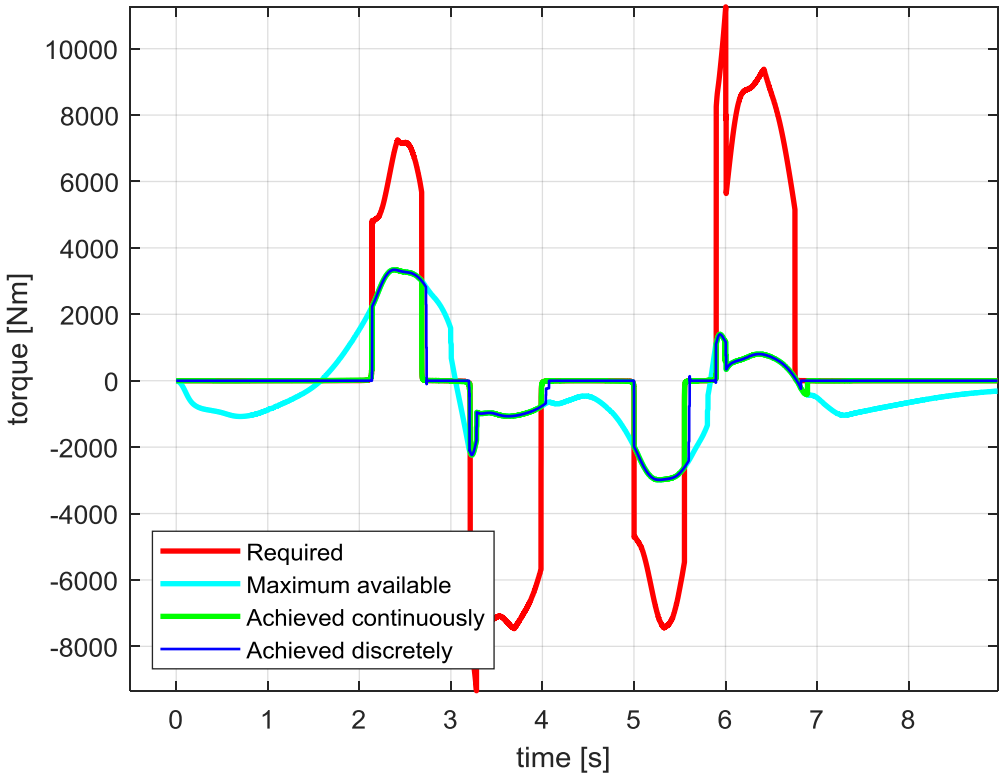

Figure 79: DLC roll torque 70 km/h simulation

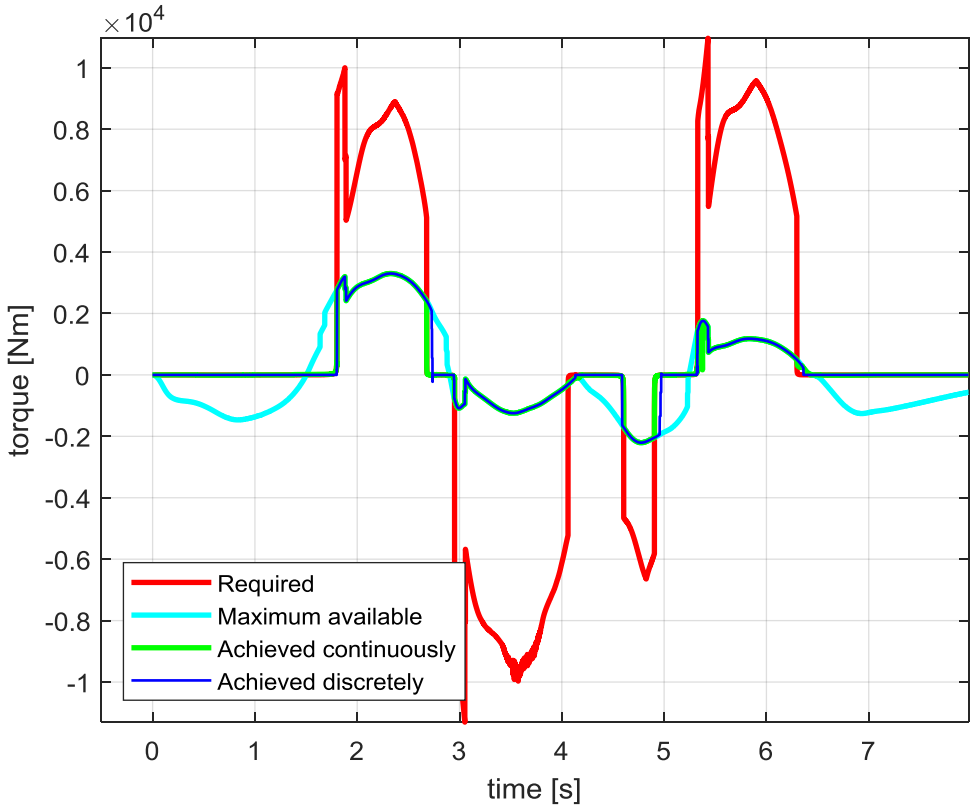

Figure 80: DLC roll torque 80 km/h simulation

Appendix D: MPC vs RRMS strategy simulation

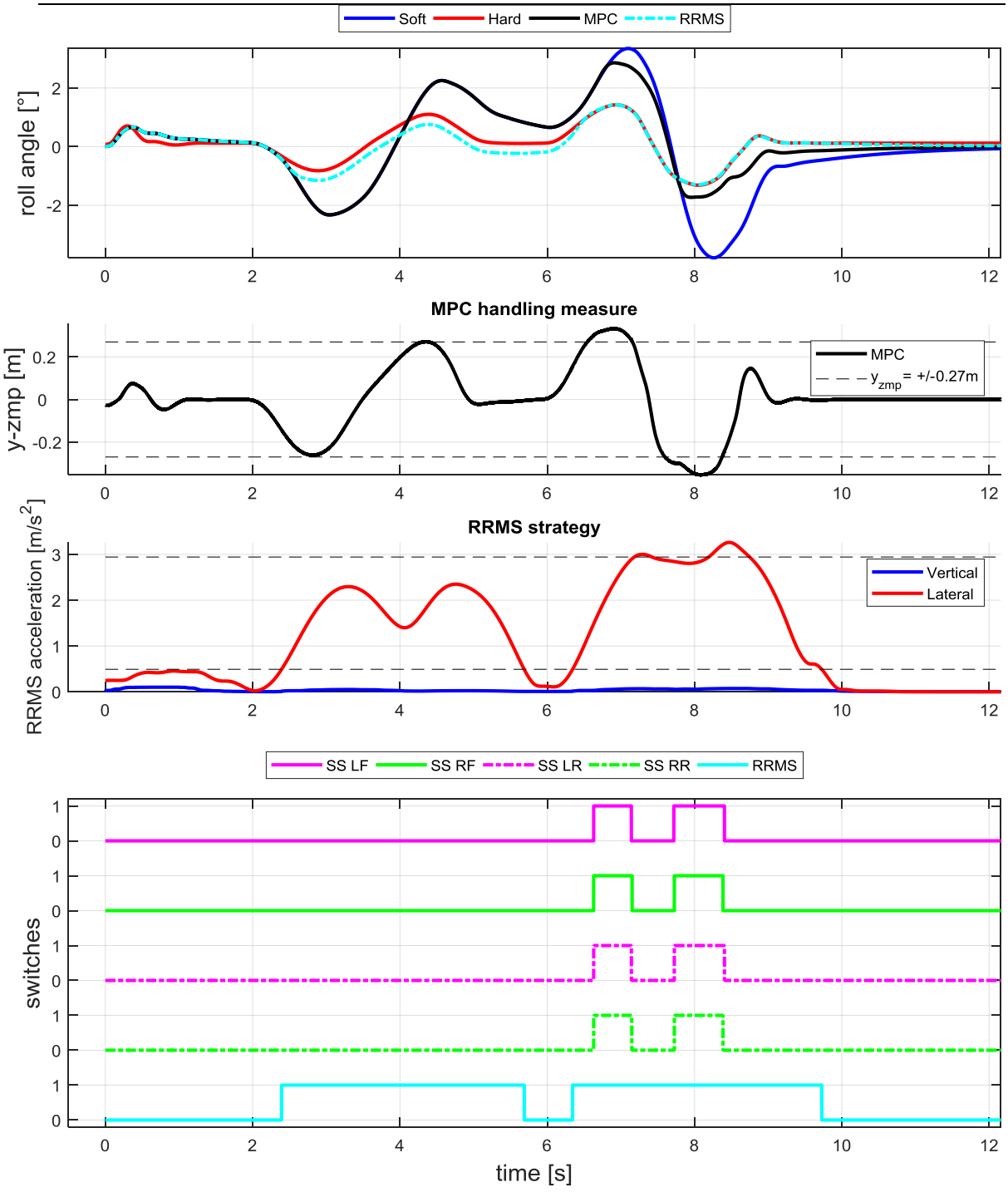

Figure 81: MPC vs baseline RRMS 50 km/h DLC handling comparison

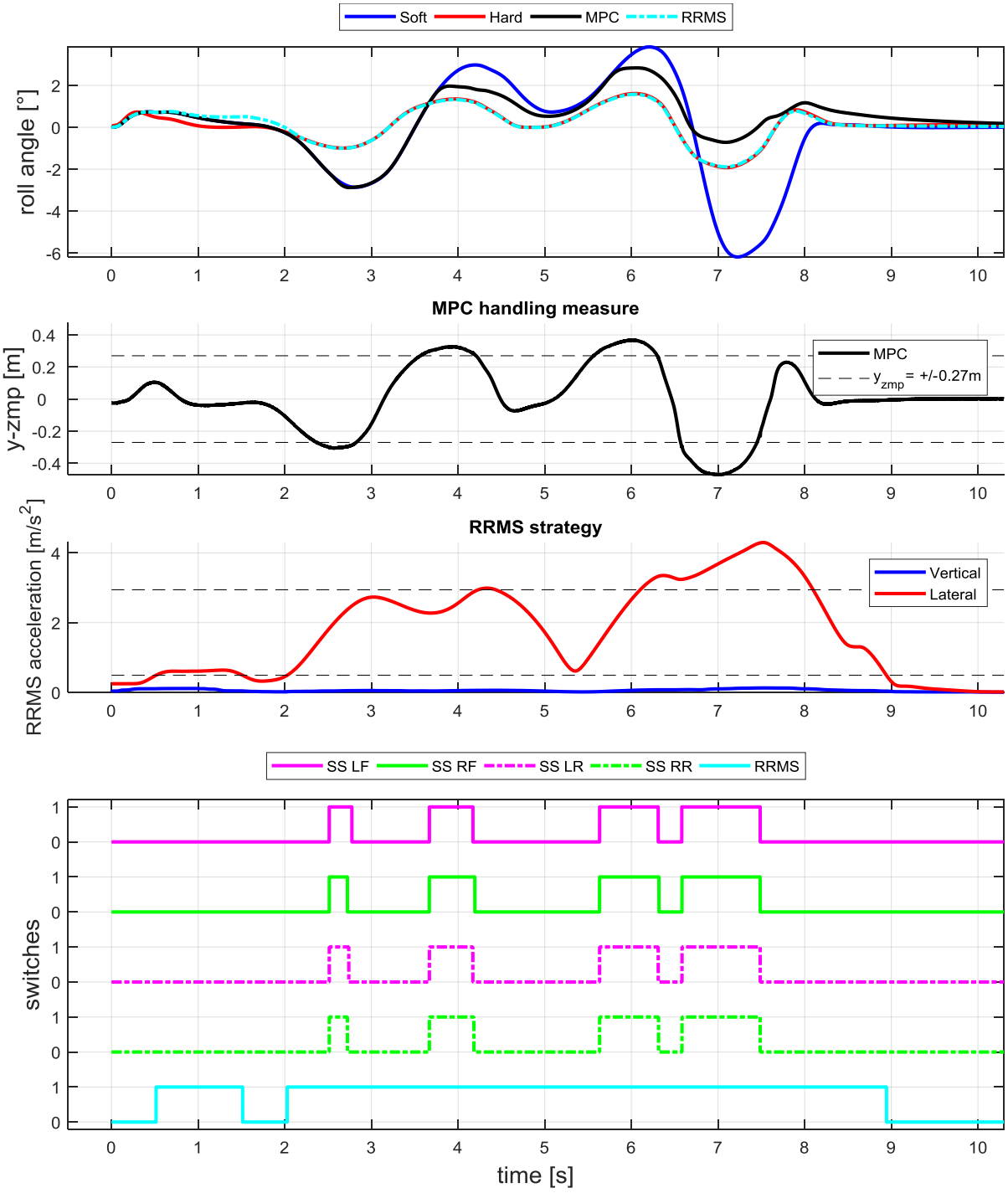

Figure 82: MPC vs baseline RRMS 60 km/h DLC handling comparison

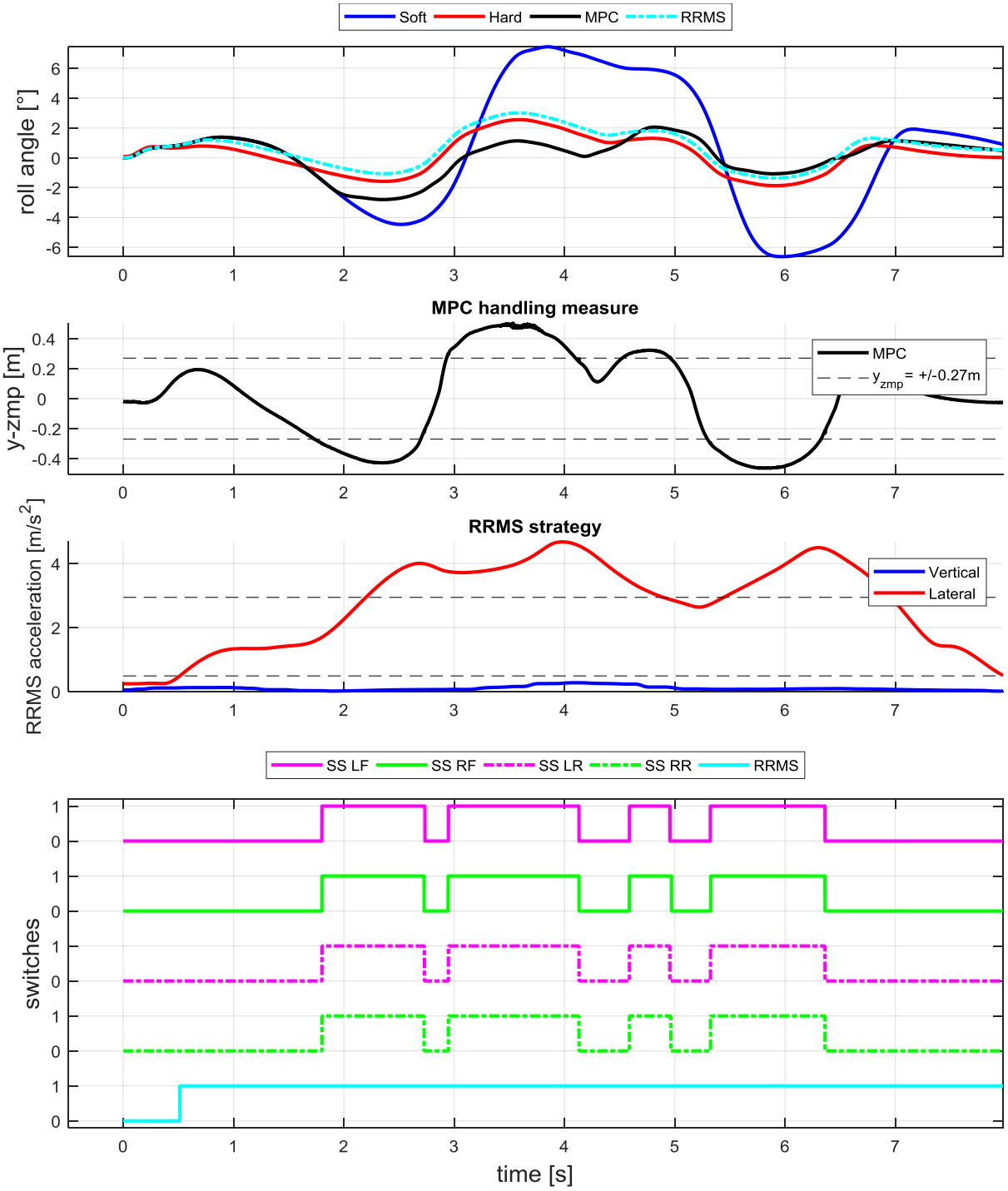

Figure 83: MPC vs baseline RRMS 80 km/h DLC handling comparison

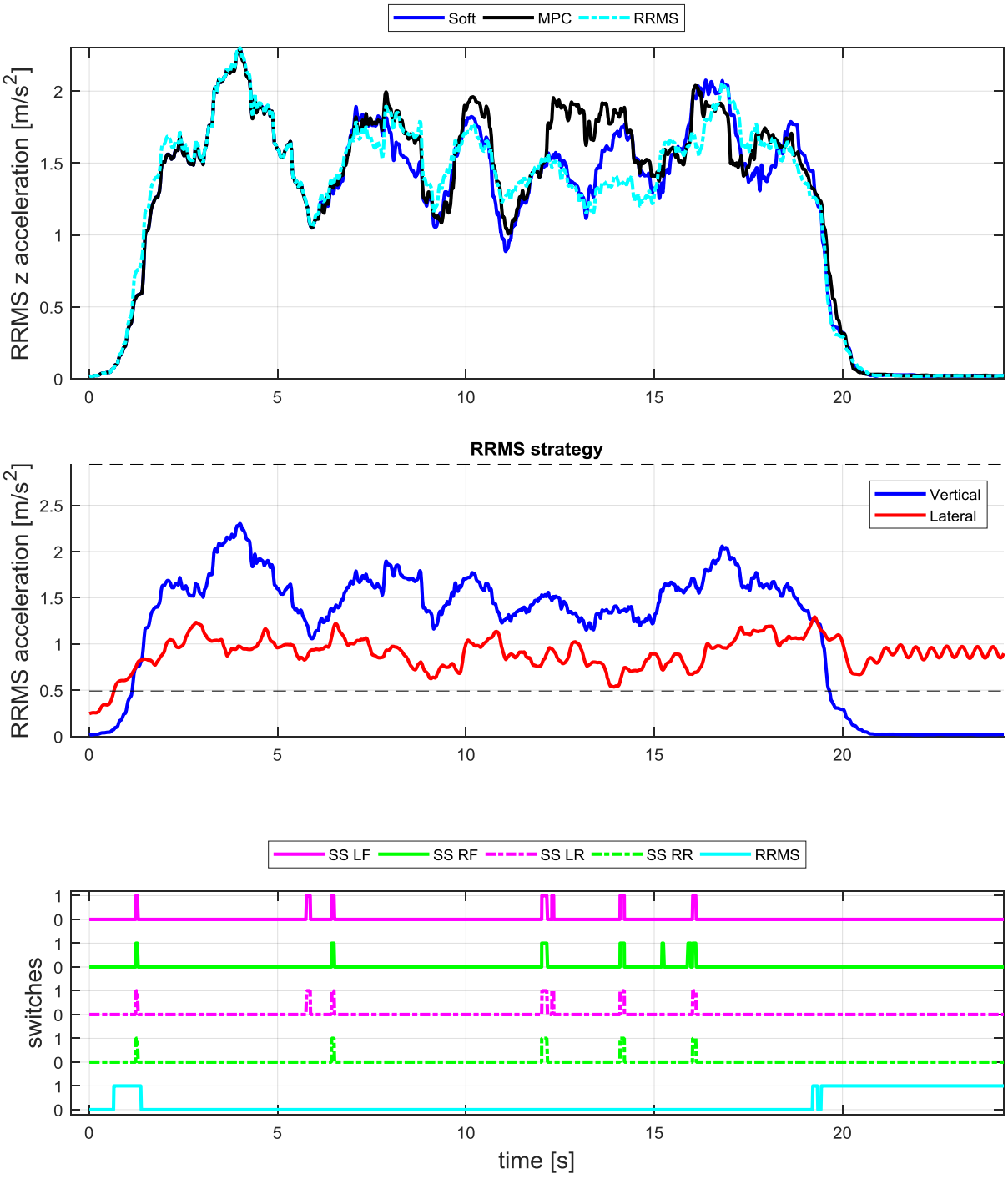

Figure 84: MPC vs baseline RRMS 21 km/h Belgian paving ride comfort comparison

Appendix E: Experimental DLC metric maps

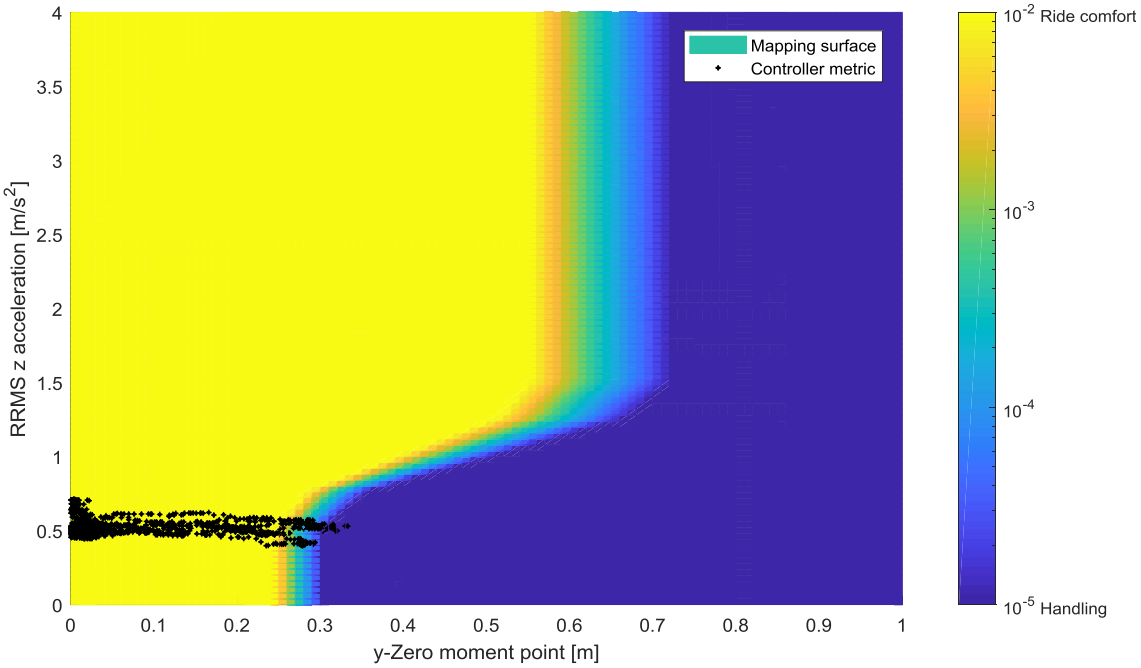

Figure 85: 50 km/h DLC MPC experimental metric map

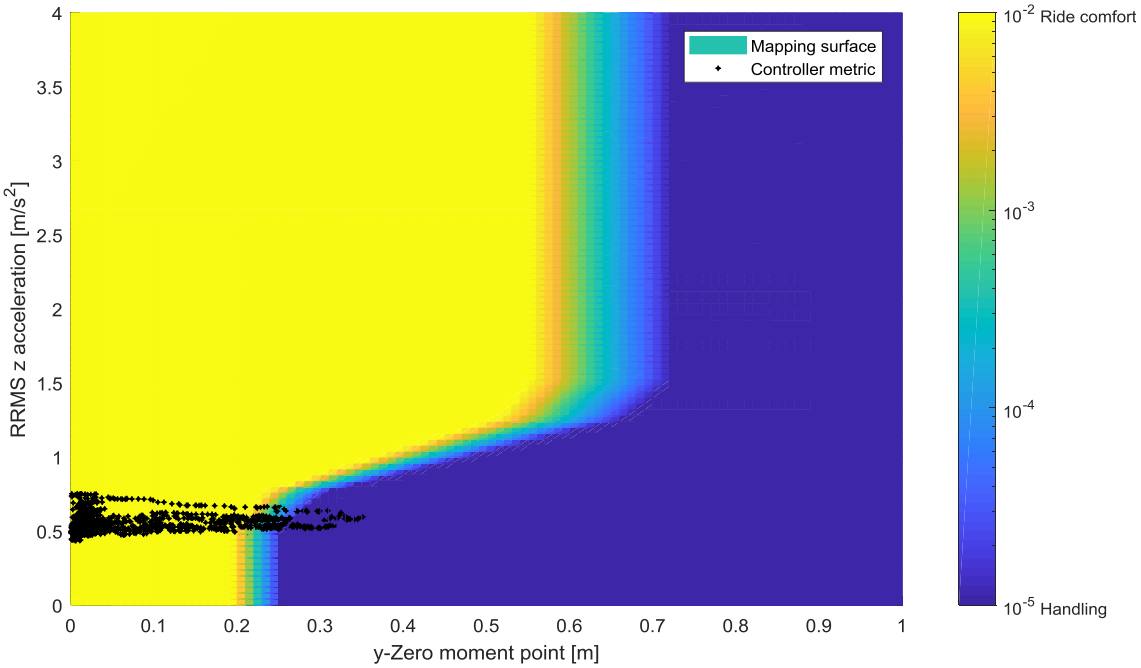

Figure 86: 50 km/h DLC a-MPC experimental metric map

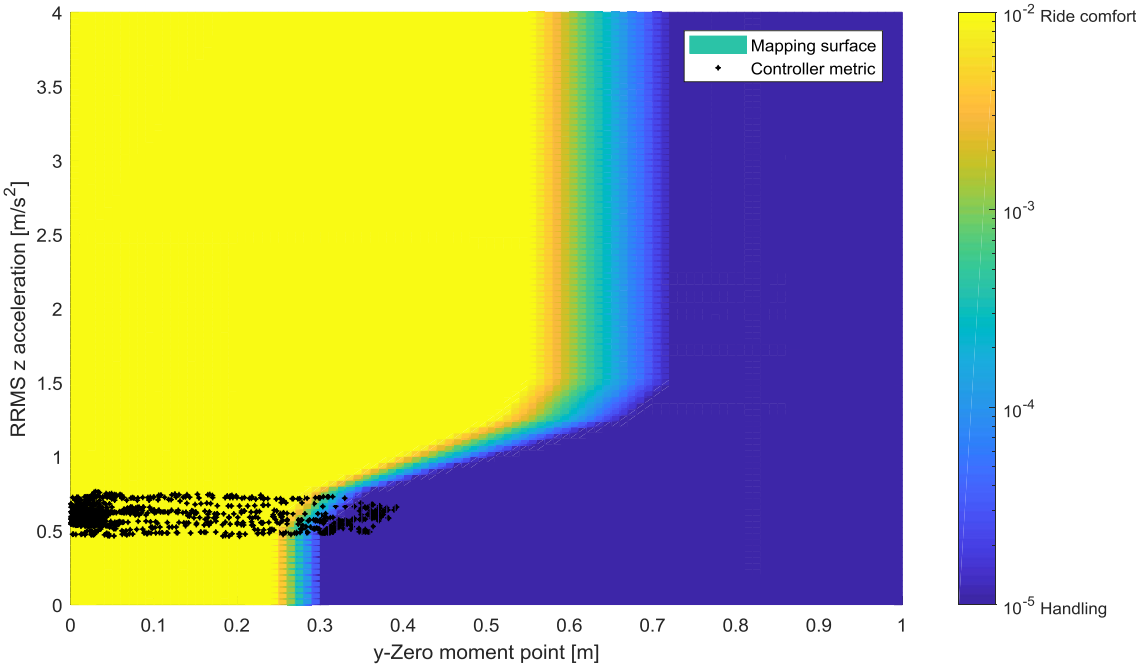

Figure 87: 60 km/h DLC MPC experimental metric map

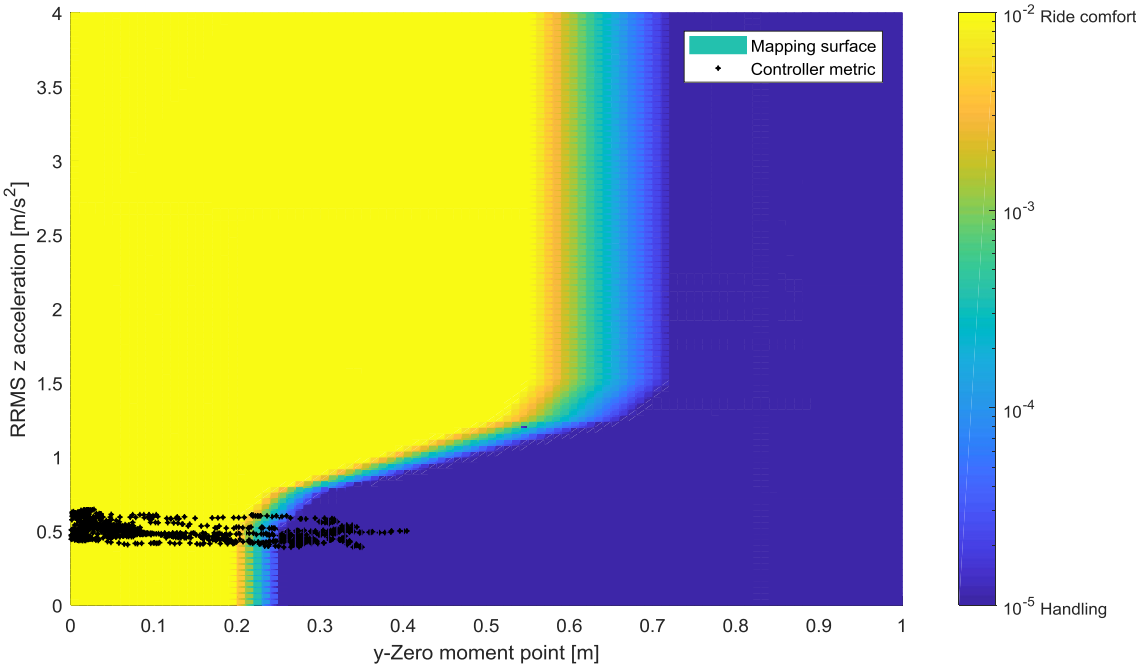

Figure 88: 60 km/h DLC a-MPC experimental metric map

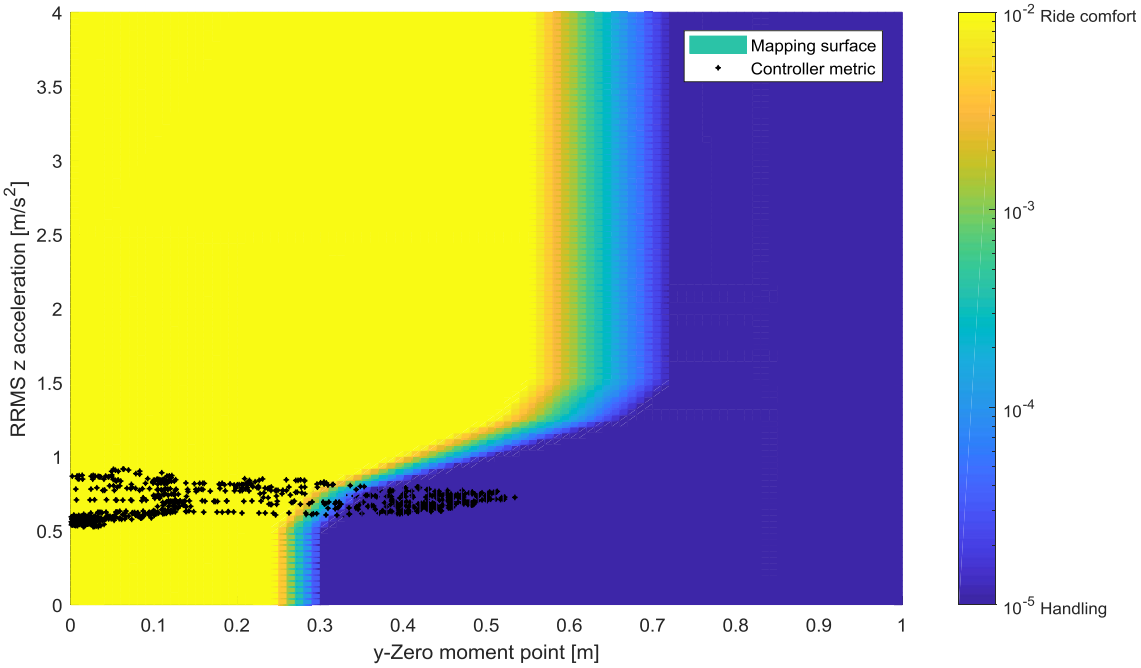

Figure 89: 80 km/h DLC MPC experimental metric map

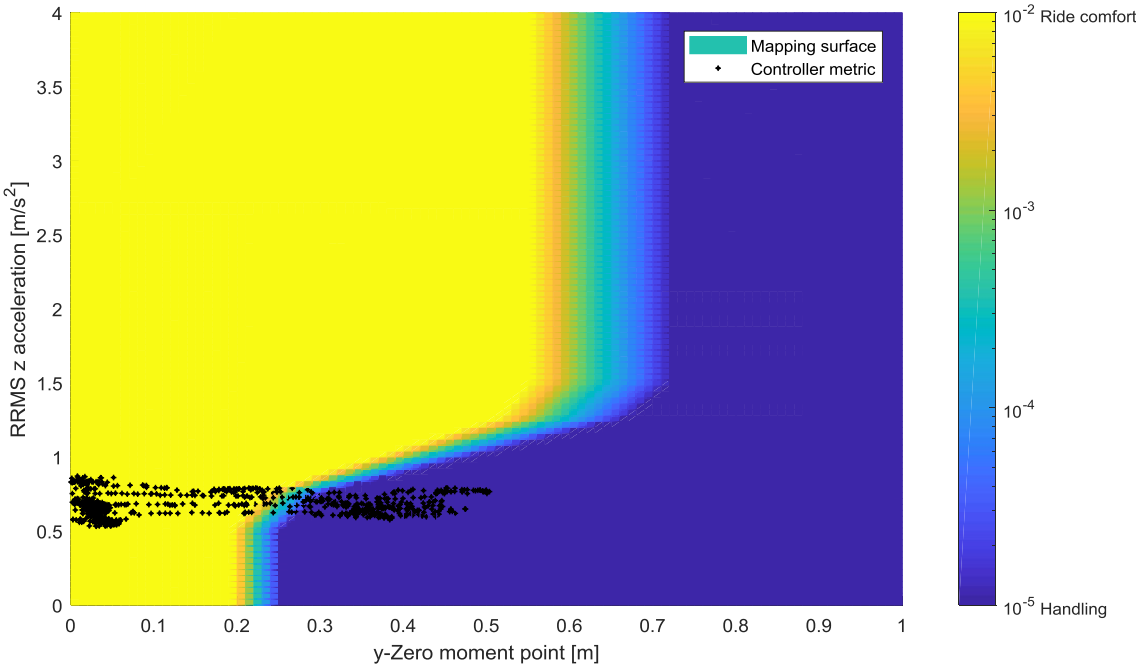

Figure 90: 80 km/h DLC a-MPC experimental metric map

Appendix F: Additional roll torque requirements experimental

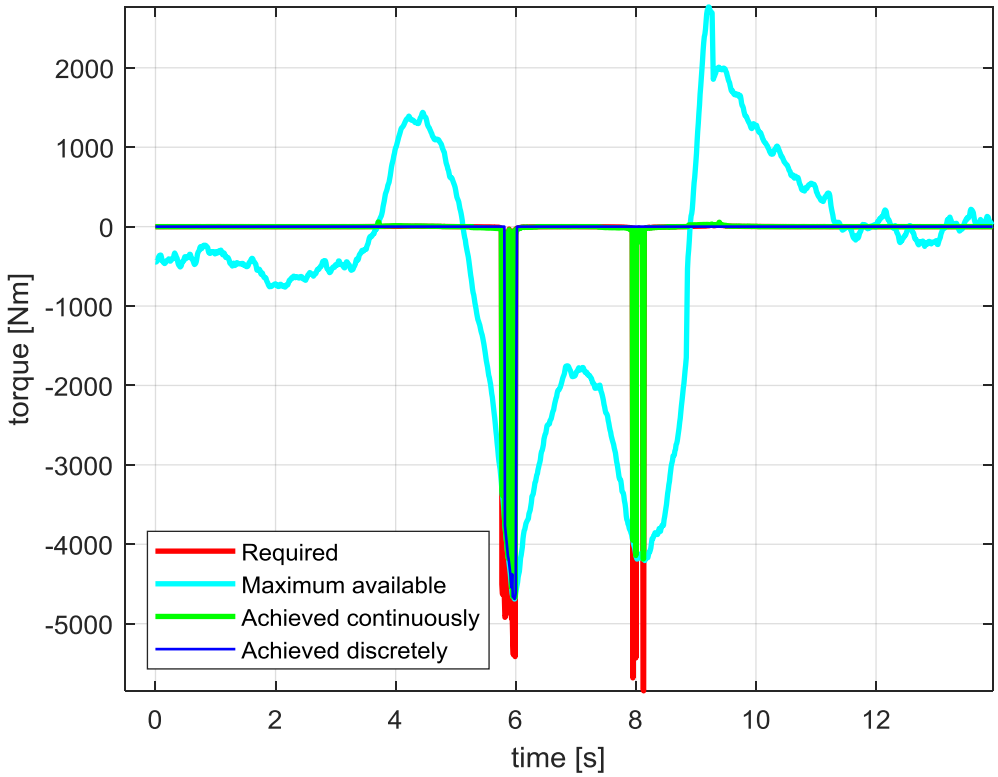

Figure 91: DLC MPC roll torque 50 km/h experimental

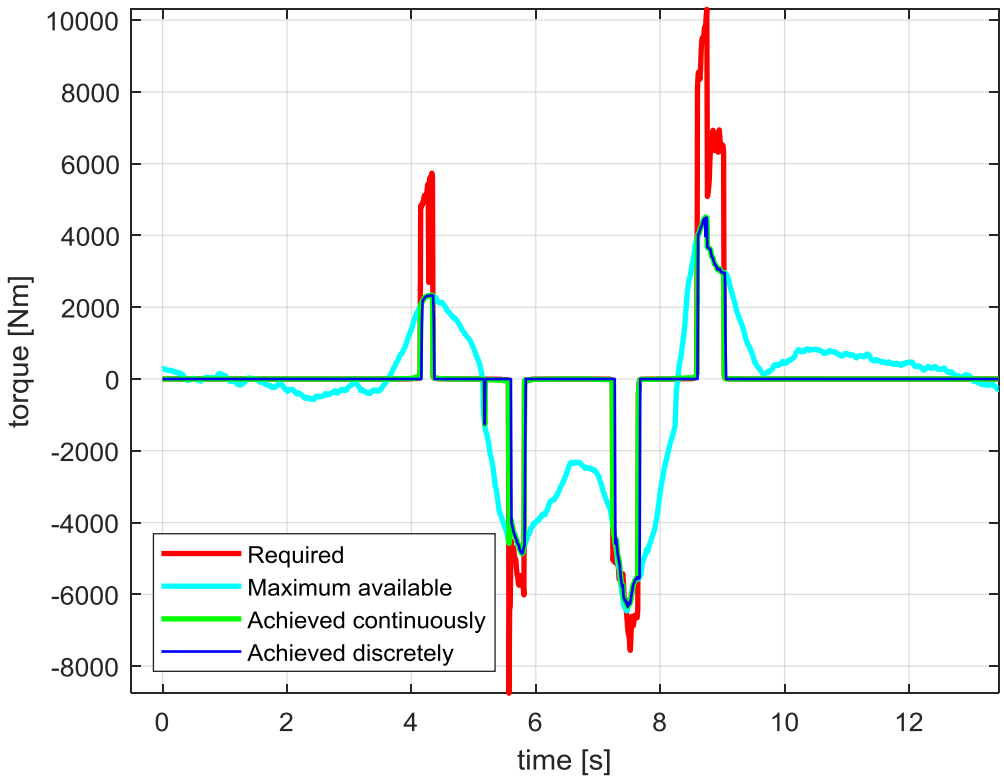

Figure 92: DLC MPC roll torque 60 km/h experimental

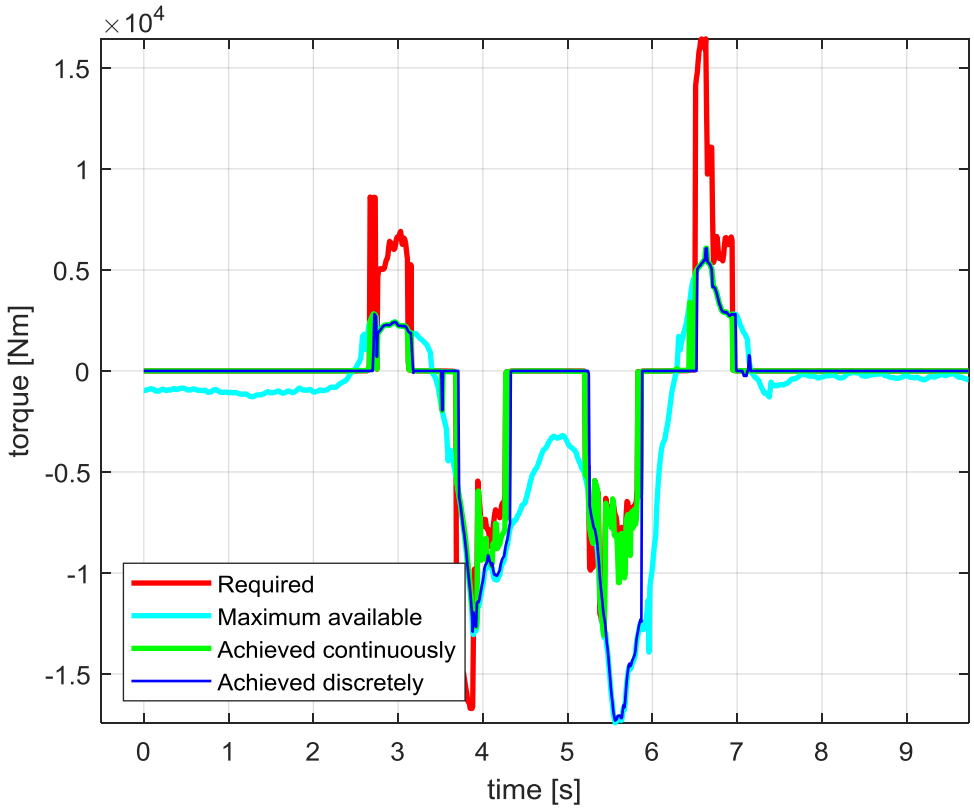

Figure 93: DLC MPC roll torque 70 km/h experimental

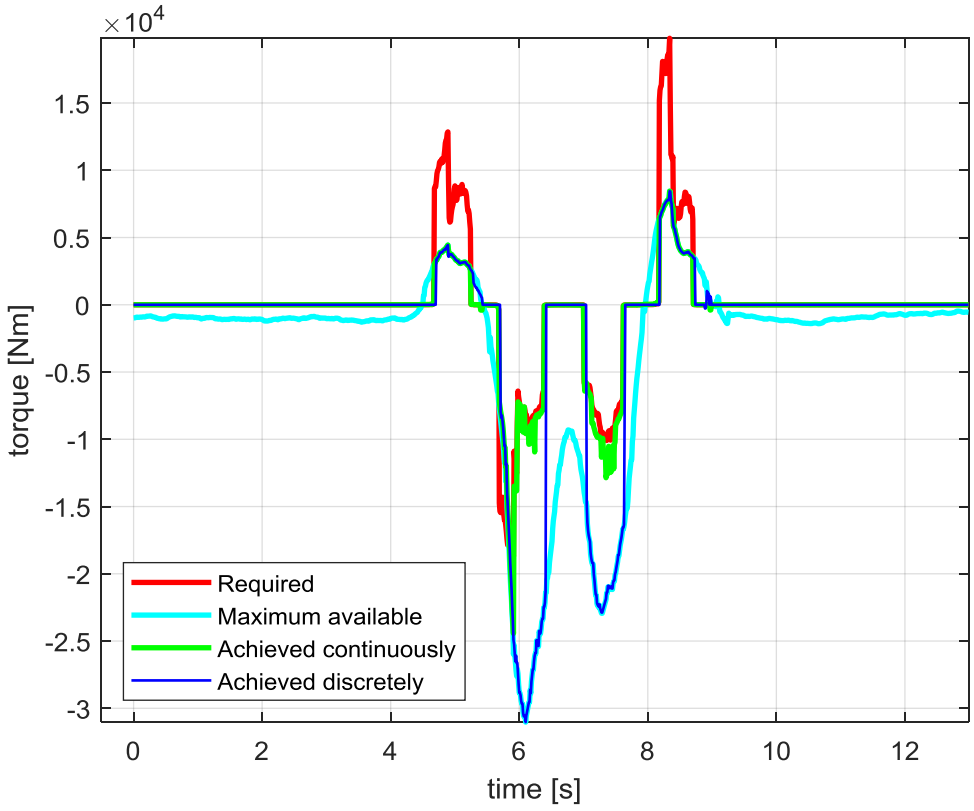

Figure 94: DLC MPC roll torque 80 km/h experimental

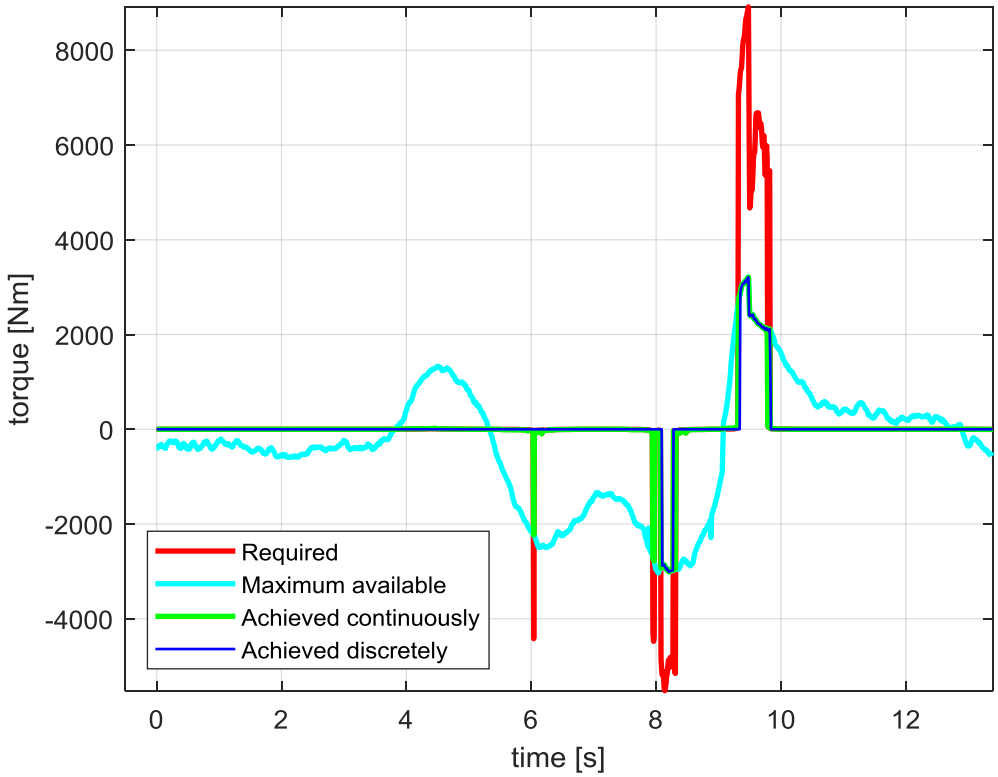

Figure 95: DLC a-MPC roll torque 50 km/h experimental

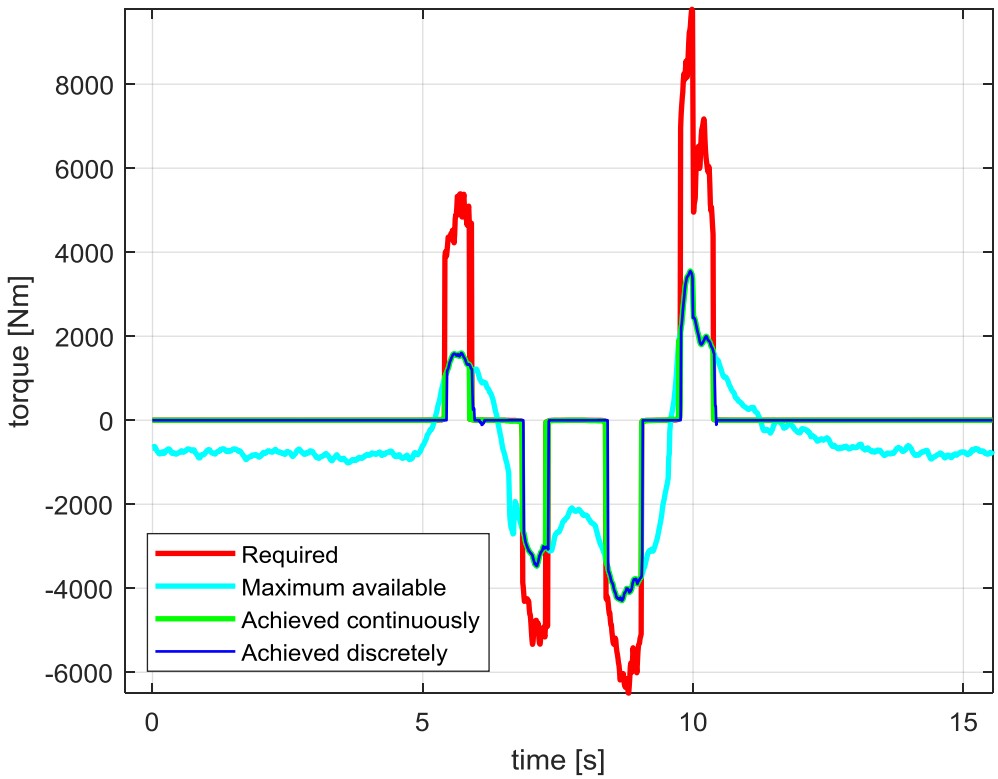

Figure 96: DLC a-MPC roll torque 60 km/h experimental

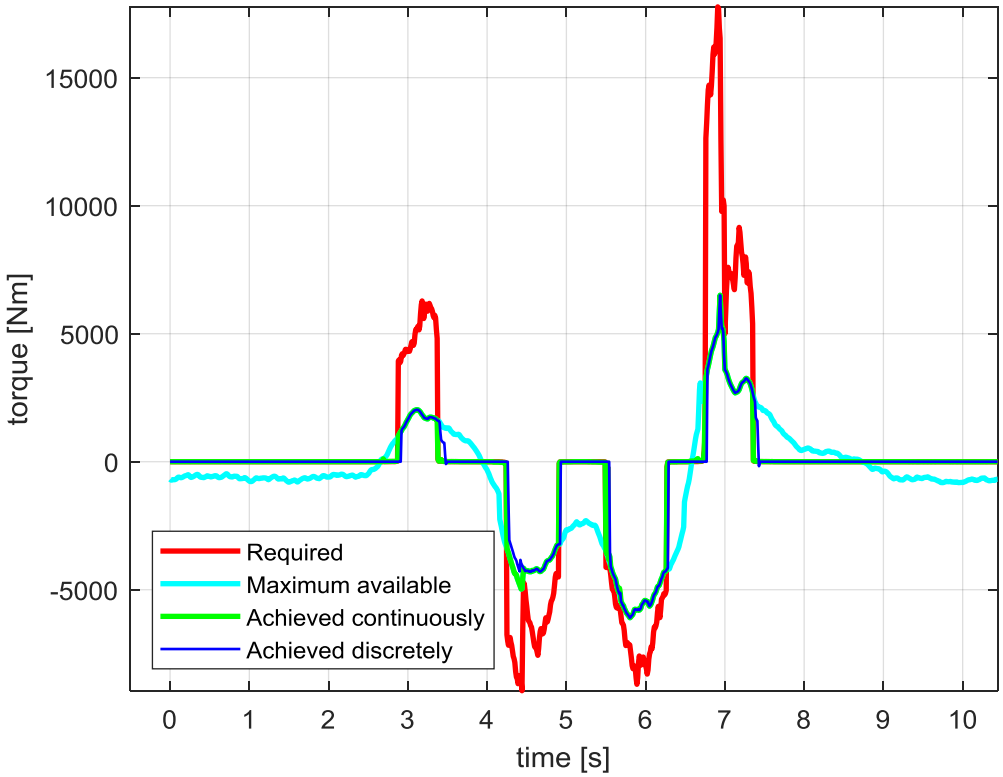

Figure 97: DLC a-MPC roll torque 70 km/h experimental

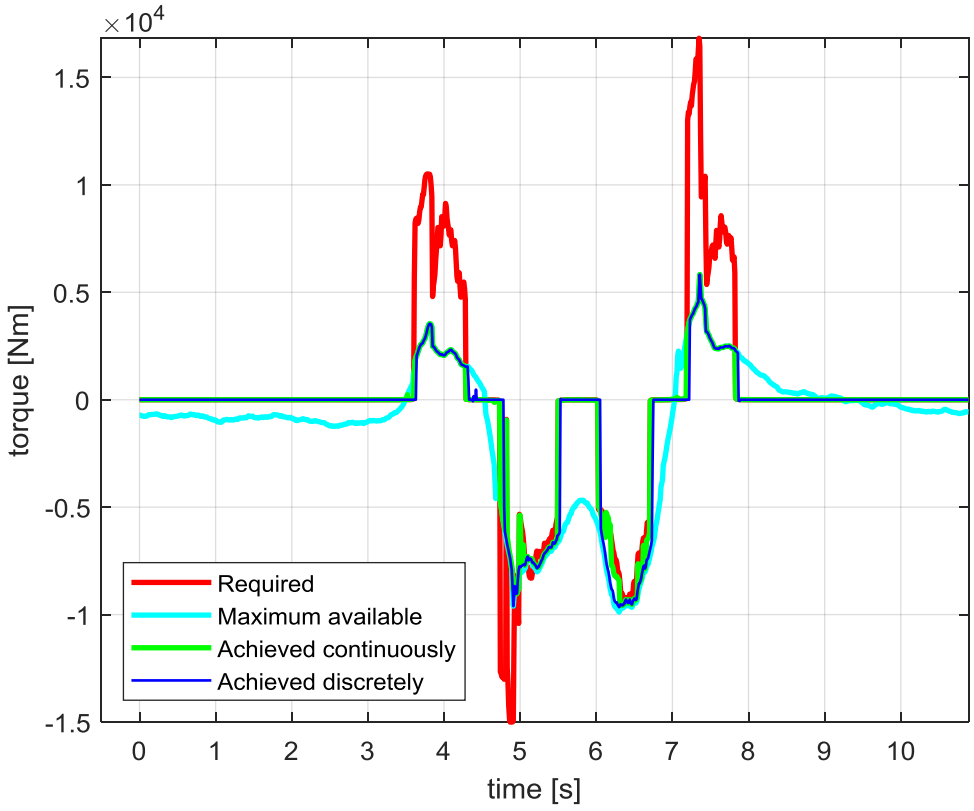

Figure 98: DLC a-MPC roll torque 80 km/h experimental

Appendix G: Experimental rough road metric maps

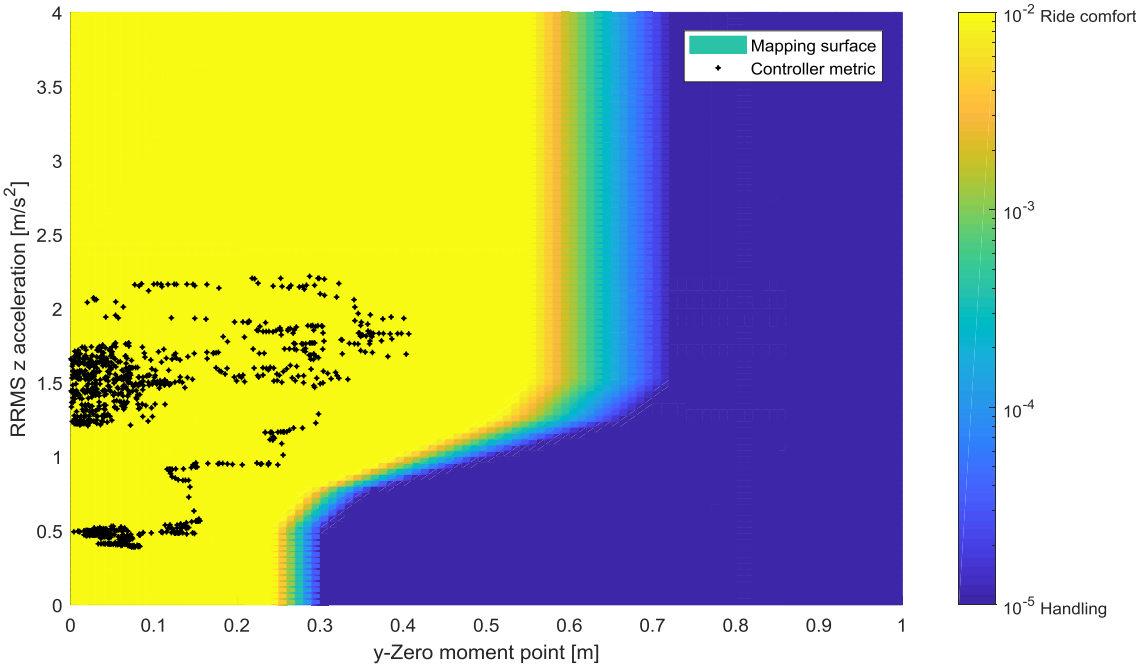

Figure 99: 21 km/h SLC MPC experimental metric map

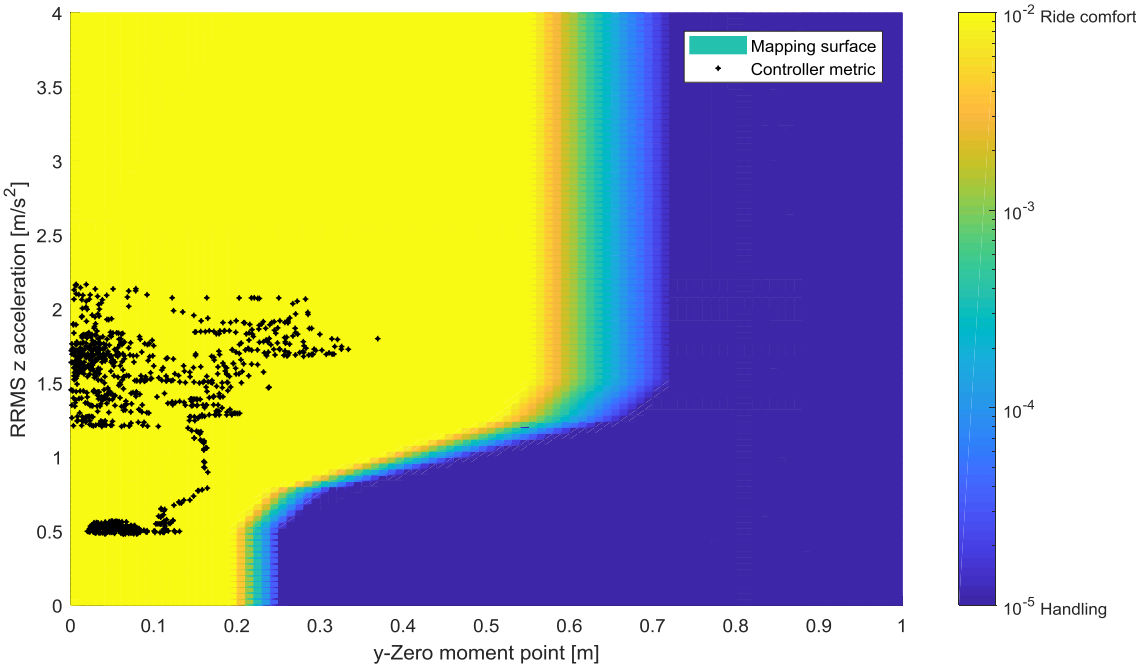

Figure 100: 21 km/h SLC a-MPC experimental metric map

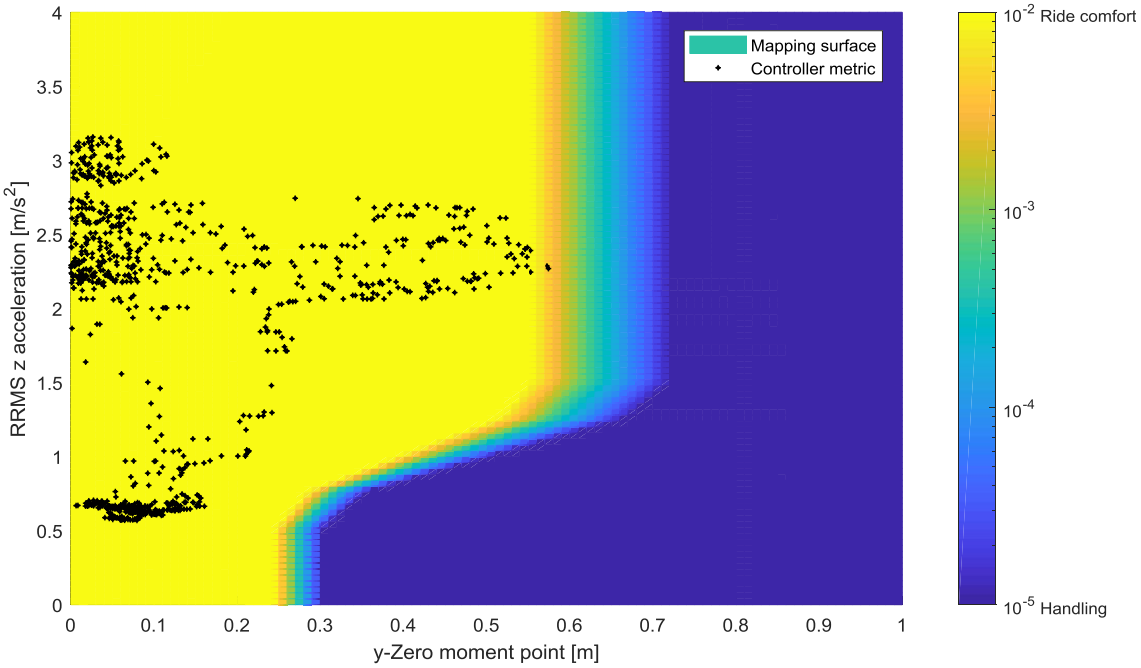

Figure 101: 47 km/h SLC MPC experimental metric map

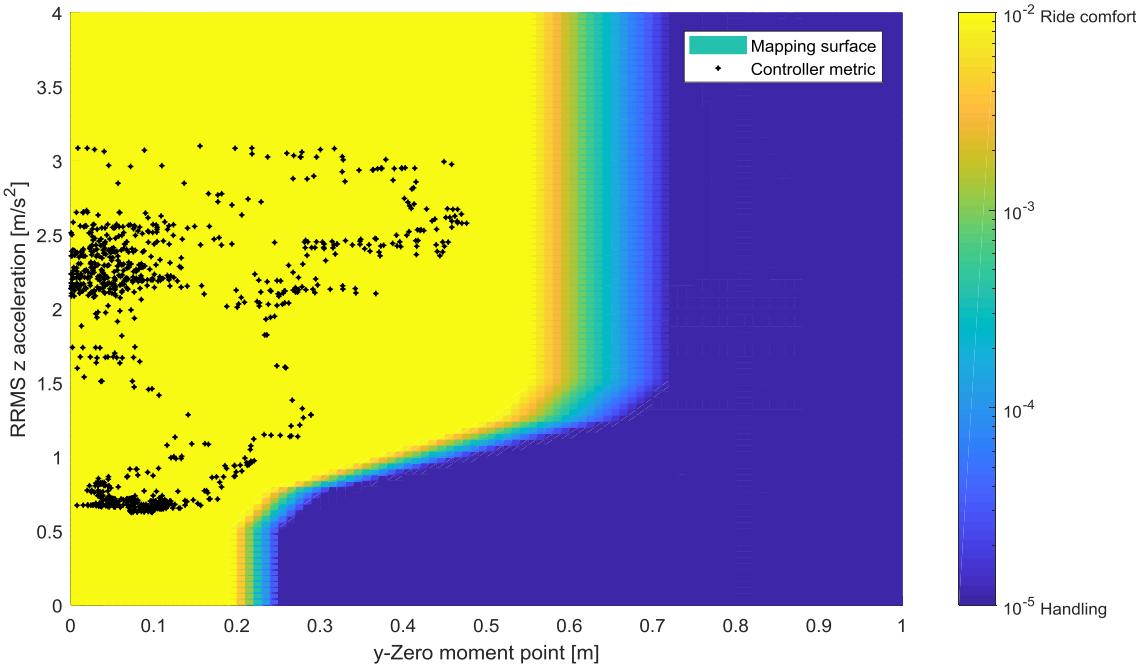

Figure 102: 47 km/h SLC a-MPC experimental metric map